THE APPLICATION OF PROTON INDUCED CHARACTERISTIC X-RAYS TO RADIOGRAPHY AND FLUORESCENCE ANALYSIS

BY

MAZIN FADHEL MAHROK, B.Sc. M.Sc.

A thesis submitted to the University of Aston in Birmingham for the degree of Doctor of Philosophy.

May, 1983.

Dedicated To My Wife,

May 1983.

THE UNIVERSITY OF ASTON IN BIRMINGHAM

THE APPLICATION OF PROTON INDUCED CHARACTERISTIC X-RAYS TO RADIOGRAPHY AND FLUORESCENCE ANALYSIS

Submitted for the Degree of PhD

Mazin Fadhel Mahrok May, 1983

SUMMARY

This work investigates the feasibility of employing proton induced X-rays for radiography and fluorescence analysis. High purity characteristic X-rays, produced by bombarding metallic targets with 2.6 MeV protons, were used either to take radiographs or to fluoresce biomedical samples.

High contrast has been obtained by using characteristic Ag X-rays for radiographing Cd and Mo foils placed adjacently. A comparison of this contrast with the low contrast obtainable using different energy characteristic radiation or broad X-ray spectra was made. A radiography table containing parameters for the range of perspex thickness that can be radiographed using these X-rays is presented.

A water-cooled rotary anode chamber has been constructed allowing manual or remote positioning of metallic targets of Ag, Mo, Zr, Cu, Fe and Ti at 45° with respect to the incident proton beam. Specimens to be analysed were sandwiched between two pieces of Kimfoil and mounted in standard 35 mm slide mounts. The fluorescent X-rays from specimens were detected with a standard Si(Li) detector coupled to a multichannel analyser. Fluorescent K X-ray yields from thin calibration foils of KCl, Ti, Mn, Co, Cu, Ge, Y and Mo were employed to calibrate the system. Repeated measurements on these calibrators and using thin Ti wire as X-ray beam monitor verified the system reproducibility.

A system detection limit of $(10^{-6}-10^{-8})$ g.cm^{-2} has been obtained for elements with Z numbers between 22 and 39, present in a 30 mg.cm^{-2} biological matrix irradiated for 20 minutes. The accuracy of the system has been evaluated by comparing the measured elemental concentration of NBS bovine liver with the certified values.

The versatility of this technique was demonstrated by analysing blood samples and hair samples of hyperactive children.

Suggestions for improving the analytical capabilities of the present system are discussed.

Key words: PIXE, Monoenergetic X-rays, Radiography, XRF, Trace element analysis.

ACKNOWLEDGEMENTS

I would like to express my great appreciation to my academic supervisor, Dr.D.Crumpton for his guidance, encouragement and assistance shown throughout this work. His invaluable help and enthusiasm is deeply acknowledged. Dr.P.E.Francois, my associate supervisor, is thanked for the many helpful discussions and suggestions. Special thanks are due to Professor S.E.Hunt for his support of this work.

The Birmingham Radiation Centre staff are thanked for their assistance with the experimental work.

I am very grateful to the members of the Physics Department Workshop. Members of PIXE group, especially Mr.J.Phull and Mr.R.Sokhi, are thanked for their companionship and assistance.

Mrs.A.Howell is thanked for her accurate typing of this thesis.

A special thanks is given to my wife, Viviane, for her patience and understanding and also to my daughter Runa for being a source of pleasure to me. My deepest gratitude must go to my father, brothers and sister for their many years of encouragement and support.

Finally, I would like to thank the University of Mosul in Iraq for providing me with leave of study throughout the period of this work.

Mazin Fadhel Mahrok

LIST OF CONTENTS

LIST OF FIGURES

LIST OF TABLES

CHAPTER ONE

INTRODUCTION

Since their discovery by W-K.Rontgen in 1895, X-rays have played a substantial role in many fields. Soon after their discovery, it was realised that X-rays could be used to produce an image of the internal structures of the human body. A high degree of activity was devoted to understand and apply this phenomenon. Consequently, the well known technique of radiography was developed. X-rays have made an important contribution to the solution of many industrial, medical and environmental problems. A number of major techniques based on the properties of X-rays have been established. Among these are; diagnostic and therapeutic X-rays in medicine and biology, industrial radiography, X-ray crystallography and electron probe microanalysis. Two important analytical techniques that have been developed over the years are radiography and X-ray fluorescence (XRF) analysis. X-ray radiography today is employed in many fields. The literature is replete with publications on radiography using X-rays. A number of recent publications are concerned with new developments and advances in industrial radiography, of note are those of Smith (1980) and Stewart (1982). Fewell and Shuping (1978) and Beaman and Lillicrap (1982) deal with X-rays in medical mammography. X-ray fluorescence analysis is described in a review article by Goulding and Jaklevic (1973) and Owers and Shalgosky (1974). Another major analytical technique which has emerged during the past decade is

Proton Induced X-Ray Emission (PIXE). The capabilities and limitation of PIXE analysis and its application to a multielemental trace analysis and a wide variety of analytical problems has been reviewed in detail by Folkmann (1975), Johansson and Johansson (1976) and more recently by Khan and Crumpton (1981).

In radiography, a broad spectrum of X-rays is usually used to project the internal structure of an object onto an external recording medium. The low energy photons in such a spectrum are normally filtered out. The use of monoenergetic X-rays in radiography is preferred for certain applications because the broad spectrum of X-rays are absorbed differently in a particular feature in the radiographed object causing a reduction in the radiographic contrast and possible loss of image details. In addition, the lower energy photons of the filtered spectrum may not contribute to the radiographic image as they are absorbed even in the transparent parts of the radiographed object. A further disadvantage is that low energy photons increase the object dose causing more radiation damage. The need to obtain high contrast in radiography initiated interest in the use of monoenergetic X-rays as described by Clark and Shafer (1941) and Dick and Motz (1981). Elemental analysis also becomes possible if two pictures are taken one on each side of an absorption edge of an element in a biological object and then compared, Spiller (1980).

X-ray fluorescence analysis is now widely accepted as a highly versatile and potentially accurate method for elemental analysis. Excitation of fluorescent X-rays in specimens by a continuous spectra has been used by many authors including Gilfrich and Birks (1968). However, it is recognized that polyenergetic X-rays generated by a conventional X-ray tube are not ideal for use as primary radiation since their scatter from the specimen causes excessive background and unfavourable detection limits, Cooper (1973). An appreciation of the importance of monoenergetic X-rays for analytical purposes has led many authors including Porter (1973), Standzenieks et al (1978), Giauque et al (1979), Toribara et al (1982) and Sood et al (1983) to employ monoenergetic X-rays. Sources of monoenergetic X-rays are usually X-ray tube spectra modified by suitable filters, Jaklevic et al (1972) and Kieser and Mulligan (1976), or secondary targets, Walter et al (1974) and Jaklevic and Thompson (1982). Other sources of monoenergetic radiation are the direct use of radioactive materials, Birks (1969), or their indirect use by exciting spectra from secondary targets, Bador et al (1979). The common factor in all the above mentioned sources of monoenergetic radiation is the presence of a considerable amount of bremsstrahlung impurity in the exciting beam. For example, in the spectrum of a molybdenum transmission X-ray tube operated at 42 kV the ratio of the number of photons in the K_α and K_β lines to the total number of bremsstrahlung continuum is 9 : 1, Giauque et al (1973). This ratio is only 2.6 : 1

for Cu, Motz et al (1971), and was found to be in the range 5.7-9 : 1 using an X-ray generator and a series of secondary targets, Hoffman and Phelps (1974). The bremsstrahlung impurity accompanying the primary X-ray beam imposes limitations on the maximum contrast that can be achieved in radiography and on the sensitivity of detecting small quantities of elements in a specimen when such radiation is used for XRF analysis. A minimum detection limit of only 10 ppm was reported by Christensen et al (1980) for nearly all the elements between Ti and Cd possibly because of the presence of the twice-scattered high intensity bremsstrahlung radiation.

The availability of charged particle accelerators opens up the opportunity of establishing analytical techniques based on the high purity monoenergetic X-ray beams that can be obtained from targets bombarded by 600 keV to 3 MeV protons. The ratio of the K_α and K_β radiation to the total number of bremsstrahlung radiation is at least 20 : 1 for 2.6 MeV protons incident on a Mo target. Such a high purity monoenergetic X-ray beam should permit much better analysis as compared to the use of an X-ray beam which has a much higher bremsstrahlung content. The utilization of a number of these high purity monoenergetic X-rays in sequence can be used beneficially to minimize enhancement effects as well as providing an optimum excitation energy for specific elements.

The first to employ monoenergetic X-rays induced by protons

for radiography were Cookson et al (1972) and more recently Mahrok et al (1981). The application of these X-rays for elemental analysis have been described by Lin et al (1978) and more recently by Gihwala et al (1982).

The increasing importance of determining trace elements in biomedical materials has led to the publication of many analytical methods. Most of these involve the excitation of the specimen by some kind of radiation, but little emphasis has been placed on the use of monoenergetic radiation induced by protons as the exciting source.

The present work attempts to evaluate the accelerator based technique of using high purity monoenergetic X-rays induced by protons. The production of characteristic X-rays and background radiation are discussed in chapter 2. Also in this chapter the X-ray interaction processes with matter are described.

The merits of applying monoenergetic X-rays induced by protons as compared to a broad X-ray spectrum in radiography is evaluated experimentally and theoretically in chapter 3. The capabilities and limitations concerning the use of such X-rays for radiography are discussed, and a radiography data table providing information about the range of perspex thickness that can be radiographed using these X-rays is calculated.

In chapter 4, the excitation of fluorescent X-rays from specimens for analysis using different modes of photon excitation is described. The utilization of the characteristic X-rays induced by protons for solving a complicated problem in the analytical work is discussed in detail. A water-cooled rotary anode chamber capable of mounting six targets has been constructed with the associated sample compartments and Si(Li) detector mounting. The system as developed in chapter 4 has been calibrated on a theoretical and experimental basis in chapter 5. The overall accuracy of the system has been tested by comparing the analysis data obtained for the SRM-1577 bovine liver with the NBS certified values. Factors affecting the sensitivity and system reproducibility are also discussed in chapter 5.

Chapter 6 is concerned with sample preparation, corrections for X-ray attenuation in samples and some blood and hair applications. In the diagnosis of abnormalities, clinical chemists need trace elements analysis of samples that can be easily obtained from patients, such as blood and hair, and for this reason the technique has been applied to blood analysis. The versatility of this technique has been further demonstrated by analysing hair samples from hyperactive children. Finally conclusions and suggestions for improvements are given in chapter 7.

CHAPTER TWO

THEORY OF CHARGED PARTICLE INDUCED X-RAY EMISSION AND X-RAY INTERACTION PROCESSES

2.1 PARTICLE INDUCED X-RAYS

The ionization of atoms by the removal of one or more electrons from the inner-shells is followed either by the production of characteristic X-ray lines, or by Auger electrons, except in very light atoms. An inner-shell vacancy may be created by charged particle bombardment, using electrons, protons or heavier ions or by photons.

Atomic electrons are removed by incident charged particles as a result of Coulomb interaction. Characteristic X-rays of the bombarded atom may be produced when the vacancy in the inner-shell is filled by an electron transition from an outer-shell. The energy of the X-ray photons is given by $E_x = h\nu$ and is equal to the energy difference between the level of the vacancy (E_1) and that of the electron (E_2) filling that vacancy:

$$E_x = E_2 - E_1 \qquad (2.1)$$

The vacancy created in the outer-shell due to the electron transition, is filled by a second electron transition and so forth until the electron configuration of the ground state atom is reproduced. Transitions to the K-shell result in emission of X-ray lines which are

called the K-series. Transitions to the L-shell from outer shell result in the L-series and so on. X-rays emitted from the L-K transitions are known as K_α lines and those emitted as a result of the M-K transitions are called K_β lines. A complete energy diagram, showing the origin of X-ray lines and all possible transitions for all elements up to Z = 92 is reproduced from Valkovic (1975) and shown in Figure (2.1).

Energies of X-ray lines and their relative intensities are characteristic of the atom from which they are emitted, and it is this property of the emitted X-rays which has made the identification and subsequent quantification of an element in a sample by X-ray emission analysis feasible.

Moseley's law states that the frequencies of corresponding X-ray spectral lines, such as K_α, may be represented by an equation of the form:

$$\sqrt{\nu} = a(Z - b) \qquad (2.2)$$

where a and b depend on the particular line and Z is the atomic number of the element.

According to Bohr model, each atomic shell is characterised by a principal quantum number n and has an energy given by the Bohr formula:

$$h\nu = \frac{me^4}{8\varepsilon_o^2 h^2 n^2} Z^2 \qquad (2.3)$$

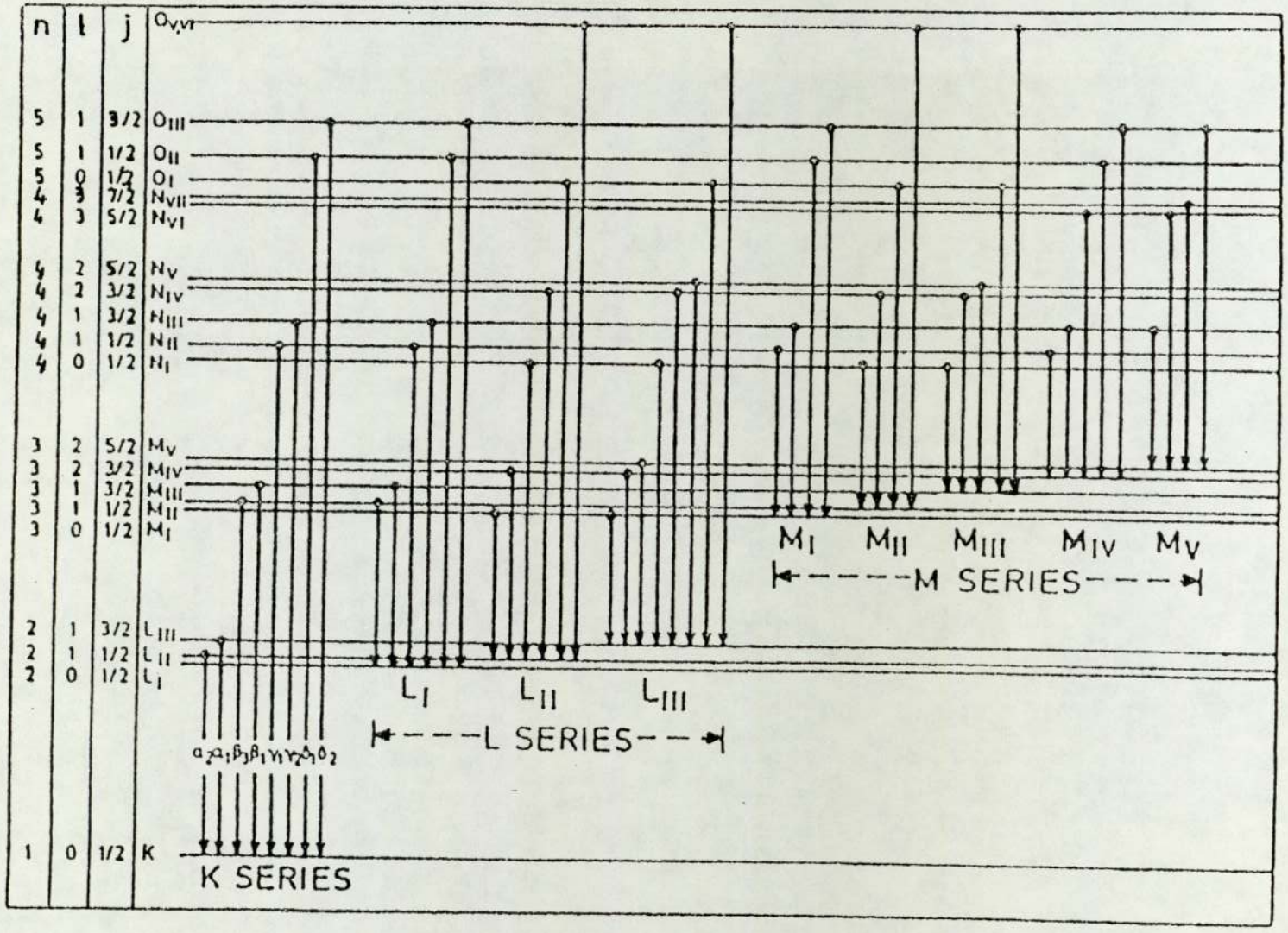

Figure 2.1 Complete energy-level diagram and possible transitions up to the element Z = 92 (from Valkovic, 1975).

where ε_o is the permittivity of free space and h is Planck's constant. Due to the electrons in the inner shell, the screening of the nuclear charge must be accounted for. In the case of the electron transition, replacing Z with (Z - b) in equation (2.3) where b is a nuclear screening constant gives:

$$h\nu = \frac{me^4}{8\varepsilon_o^2 h^2}\left(\frac{1}{n_1^2} - \frac{1}{n_2^2}\right)(Z - b)^2 \qquad (2.4)$$

where n_1 and n_2 represent the principal quantum numbers for two shells. Equation (2.4) agrees generally with Moseley's law.

2.2 INNER-SHELL IONIZATION BY PROTONS

The important quantity, following the ionization process, for radiography or X-ray fluorescence analysis, is the X-ray production cross section. This is a measure of the probability that exposure of a target atom to the proton beam will result in the emission of a radiative characteristic X-rays. These X-rays are to a good approximation isotropically distributed, Folkmann et al (1974). The isotropic emission of characteristic X-rays induced by protons is also verified experimentally by Lewis et al (1972). These X-rays are unique for each element and form the basis for selecting particular energy for radiography or X-ray fluorescence analysis work.

Several theoretical models describing the inner shell ionization by charged particles have been developed.

These are the Plane Wave Born Approximation PWBA of Merzbacher and Lewis (1958), Garcia semi-classical Binary Encounter Approximation BEA of Garcia (1970 a,b) and the Semi-Classical Approximation SCA of Bang et al (1959).

These models make the assumption that the production of an inner shell vacancy occurs as a result of an interaction of the nucleus of the incident charged particle with the bound electron.

In the PWBA the incident and the inelastically scattered particles are described by a plane wave. The vacancy is produced by the Coulomb interaction between the bound electron and the incident proton.

The BEA considers that the direct energy exchange between the incident charged particle and the bound electron is the dominant interaction producing the transition. Garcia et al (1973) pointed out that the binary encounter model offers a scaling law for the cross sections which is composed of only the electron binding energy and particle energy. A universal curve is thus derived when:

$$\frac{U_i^2(Z)\sigma_i}{Z} \text{ is plotted against } \frac{E_p}{\lambda U_i(Z)}$$

where U_i is the electron binding energy, E_p the particle energy and σ_i the ionization cross section for K and L shell and λ the ratio of the particle mass to the electron mass.

The SCA holds for low velocity projectiles and makes use of an impact parameters to deal with the Coulomb deflection of the incident projectile.

In principle, experimental cross sections can be used to test the validity of a given theory. It has been shown by Madison and Merzbacher (1975), that the BEA can be obtained from the PWBA theory by suitable choice of the representation of the emitted electron. But BEA fails at low impact velocities especially when it is applied to the ionization of specific subshells.

A theoretical account of these models has been discussed by Garcia et al (1973), Madison et al (1975) and Hansteen et al (1973, 1975). The cross section is described by all the theories as increasing with the energy of bombarding particles in the 1-4 MeV energy range, as reported by Bearse et al (1973), Garcia (1970 a) and Khandelwale et al (1969).

The K shell ionization cross section is proportional to the fourth power of the proton energy and is inversely proportional to U_K^6 where U_K is the binding energy of the electron in the K shell. Also U_K is proportional to Z^2, the effective atomic number, thus the ionization cross section is proportional to Z^{-12}, Merzbacher and Lewis (1958). Hence:

$$\sigma_K \propto \frac{E_p^4}{Z^{12}}$$

or $$\sigma_K \propto \frac{E_p^4}{U_K^6}$$

therefore $$\sigma_K U_K^2 \propto \left(\frac{E_p}{U_K}\right)^4$$

$\sigma_K U_K^2$ is usually plotted as a function of $(E_p/U_K)^4$ and these should define a universal function, BEA of Garcia et al (1973).

For a given proton energy, the cross section for X-ray production is a continuous and smoothly varying function of atomic number.

The Perturbed Stationary State PSS theory is essentially second order correction to the PWBA theory. Brandt and Lapicki (1979) accounted for the discrepancies between experimental L shell cross sections and the PWBA by the CPSSR theory provided the projectile-target atomic number ratio $(Z_1/Z_2) \leqslant 0.3$. This approach incorporates the Coulomb deflection of the incident particle by the target atoms, the increase in electron binding energy for small impact parameters, the polarization of the electron shell for large impact parameters, and the relativistic effects on the target electron. Brown et al (1982) obtained measurements of the K shell ionization cross section which are in agreement within 3% of the theoretical predictions of the CPSSR theory.

2.3 INTERACTION OF X-RAYS WITH MATTER

For the energy region employed in radiography and X-ray fluorescence analysis, there are three main modes through which X-rays interact with matter, i.e. photoelectric absorption, coherent scattering and Compton scattering.

(a) The Photoelectric Effect

This type of interaction is important in the energy region 1-100 keV and it is most likely to occur when the photon energy hν is slightly greater than the binding energy of the electrons in one of the inner shells:

$$h\nu = W + \tfrac{1}{2}mv^2$$

Photon energy = Binding energy + Kinetic energy of photo-electron

when a K electron has been ejected, the vacancy in the K-shell is immediately filled by an electron moving in from one of the outer shells. During the transition the energy difference between the shells involved may be radiated as an X-ray photon known as a fluorescent or characteristic X-ray. Thus photoelectric absorption gives rise to two kinds of secondary radiation: photoelectrons and characteristic X-rays.

Photoelectric absorption decreases with increasing photon energy, corresponding to the physical notion that there is a decreasing probability of the electron being found in a field sufficiently strong for the resonance to take place, Grodstein (1957).

If the photon energy is above the K edge energy, then the K shell makes the greatest contribution to the photoelectric absorption, followed by the L,M,N shells etc., in decreasing order of importance. If the photon energy is less than the binding energy of the K shell, ejection of the K electrons is no longer possible, and only the L,M, etc. shells can interact in this way.

The photoelectric cross-section varies approximately as E^{-3} and Z^{5}. At low Z it varies as $E^{-3.5}$. Figure (2.2) from Dyson (1973), illustrates these variations.

Absorption Edges: The minimum photon energy that can expel an electron from a given level in an atom of a given element is known as the absorption edge of that level of that element. The sudden changes in the absorption of radiation occur at photon energy equal to the binding energies of different shells.

Only photons having energies equal to or greater than that of an absorption edge can excite the associated lines. An element is relatively transparent to its own spectral lines, Bertin (1978).

The absorption edge jump ratio J and the jump difference d are measures of that portion of the total absorbed X-radiation that is absorbed by a specified atomic energy level. For example, K and L_{111} jump ratios are defined by:

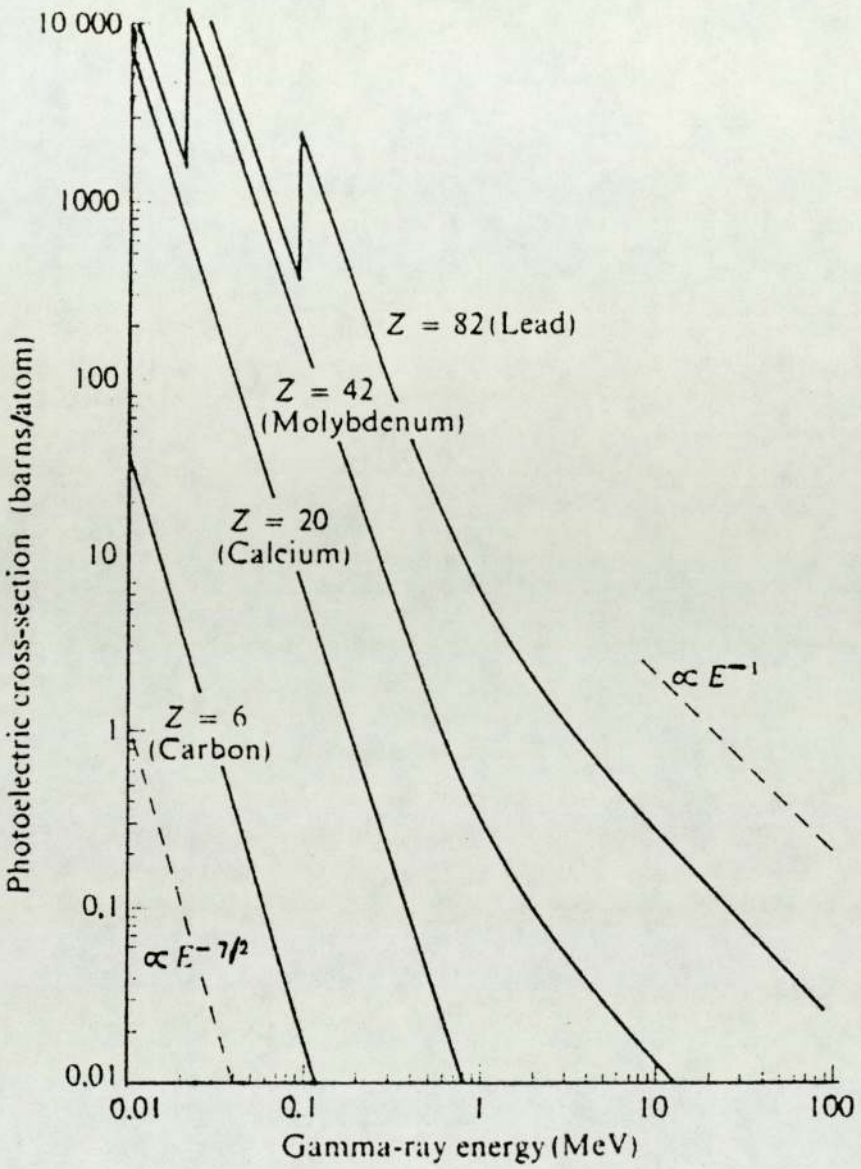

Figure (2.2) Photoelectric cross-section as a function of photon energy. The dotted lines have slopes corresponding to E^{-1} and $E^{-7/2}$ laws. (From Dyson 1973).

$$J_K = \frac{(\mu/\rho)_K + (\mu/\rho)_{L_1} + (\mu/\rho)_{L_{11}} + \ldots\ldots}{(\mu/\rho)_{L_1} + (\mu/\rho)_{L_{11}} + \ldots\ldots} \quad (2.5)$$

$$J_{L_{111}} = \frac{(\mu/\rho)_{L_{111}} + (\mu/\rho)_{M_1} + (\mu/\rho)_{M_{11}} + \ldots\ldots}{(\mu/\rho)_{M_1} + (\mu/\rho)_{M_{11}} + \ldots\ldots} \quad (2.6)$$

K and L_{111} jump differences are defined by the difference between the numerator and denominator in the respective equations. More simply:

$$J = (\mu/\rho)_H \,/\, (\mu/\rho)_L \quad (2.7)$$

$$d = (\mu/\rho)_H - (\mu/\rho)_L \quad (2.8)$$

where H and L refer, respectively to the high and low energy sides of the edge, that is, the top and bottom, or maximum and minimum values of (μ/ρ). The actual fraction of the total number of photoionization that occurs in the K shell, for example, is given by:

$$\left[(\mu/\rho)_H - (\mu/\rho)_L\right] / (\mu/\rho)_H = 1-(1/J_K) = (J_K-1) / J_K \quad (2.9)$$

Figure (2.3) from Bertin (1975) shows various absorption edge jump ratios J and differences d as a function of atomic number. Use is made of J in Chapter 5.

Experimental values of the jump ratio for some elements have been reported by a number of authors including Hopkins (1959) and Boster and Edwards (1968), and for others were determined from the experimental data near absorption edges. Values for all elements may be found from the equation given by Veigele (1973) which was

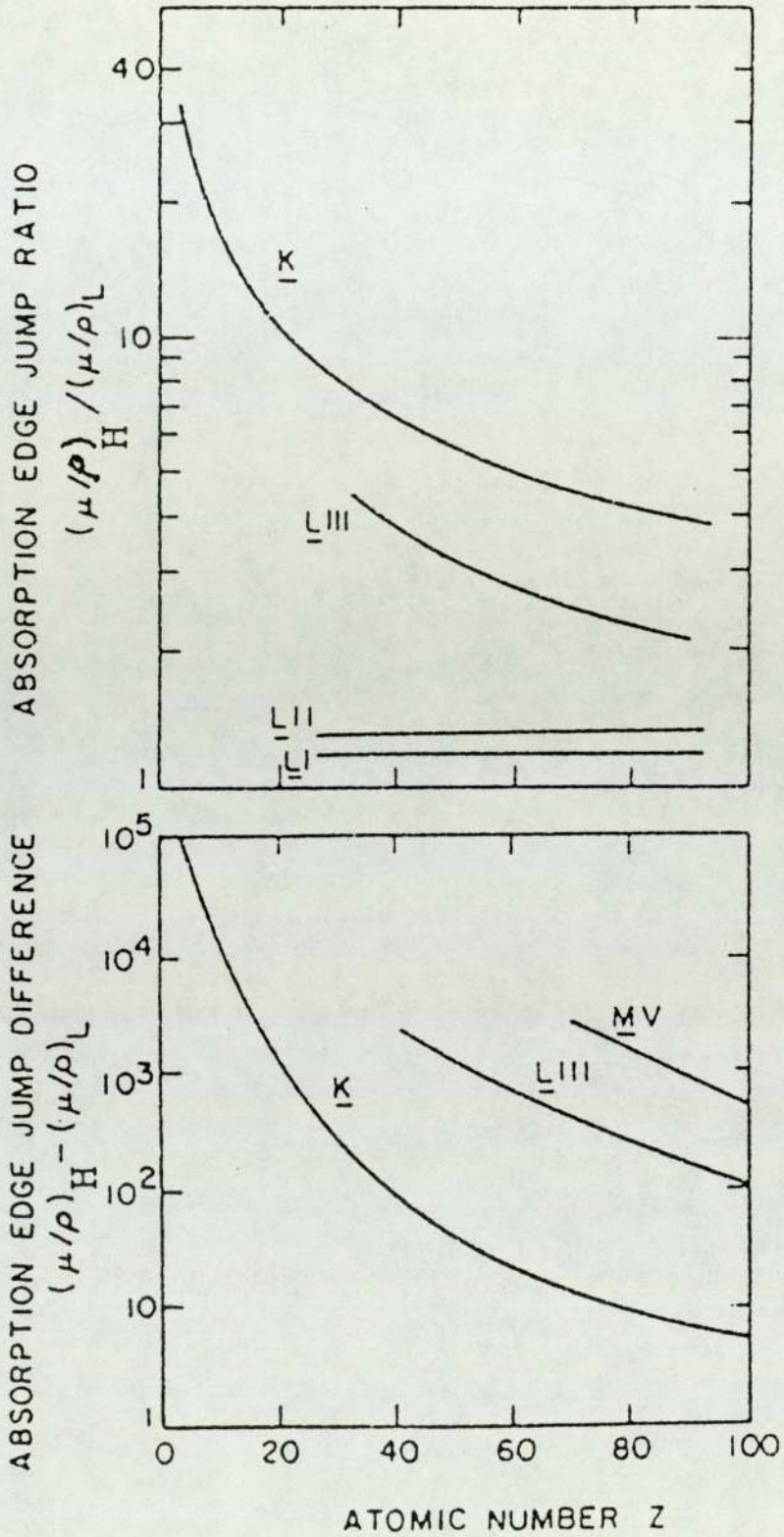

Figure (2.3) Absorption edge jump ratio and differences versus atomic number. (From Bertin, 1975)

fitted to the plot of the experimental jump ratios for K versus 1/Z:

$$J_K = \frac{125}{Z} + 3.5 \qquad (2.10)$$

(b) Coherent Scattering

In this process the incident photon is deflected without losing any energy. X-rays passing close to an atom cause bound electrons to vibrate at a frequency equal to that of the incident photon, provided that electrons do not get enough energy to be ejected. These vibrating electrons in turn emit X-rays of this same frequency but in all directions.

Coherent scattering is important with low energy radiation, and because it involves bound electrons it occurs more in higher atomic number materials.

(c) Compton Scattering

In Compton scattering the incident photon interacts with a free electron, which is in the outer orbit of the atom. The incident photon is scattered with less energy. The recoil electron receives the amount of energy that is lost by the incident photon:

$$h\nu - h\nu' = T$$

where $h\nu$ and $h\nu'$ are the energies of the incident and scattered photon respectively, T is the kinetic energy of the ejected electron. The Compton cross section is

inversely proportional to the photon energy.

The detection of the inelastically scattered photon in the experimental analysis (see Chapter 5) imposes certain considerations relating to excitation mode, sensitivity and detection limit.

The energy of scattered photon is evaluated by applying the laws of conservation of energies and momentum:

$$h\nu' = \frac{h\nu}{1 + \frac{h\nu}{m_o c^2}(1 - \cos\theta)} \qquad (2.11)$$

where m_o is the rest mass of electron and θ is the angle between unscattered and scattered photon. It is seen from equation (2.11) that the energy of scattered photon decreases with scatter angle, with maximum shift for 180^o scatter (backscatter). Equation (2.11) can be written in the form:

$$\lambda' - \lambda = \frac{h}{m_o c}(1 - \cos\theta) \qquad (2.12)$$

where $h/m_o c$ is the Compton wavelength and is equal to 2.426×10^{-12} m. The change in wavelength is thus independent of the incident photon energy and of scatter, but it is dependent on angle.

Total mass attenuation coefficient may be obtained from the compilation of Hubbell (1969), Storm and Israel (1970), Veigele (1973) and Millar and Greening (1974).

2.4 INNER-SHELL FLUORESCENCE YIELD

The emission of fluorescent photons follows the ionization of atoms by photons or protons. When a vacancy in the K shell is filled by an electron transition from an outer shell, either K X-rays or K Auger electrons may be emitted. The K-shell fluorescence yield, ω_K, is defined as the fraction of K shell vacancies that are filled through a radiative transition, i.e. $\omega_K = N_K/N_i$ where initial vacancies are created in N_i atoms and N_K of those atoms emit X-rays. Correspondingly, the Auger yield a_K, is defined as the fraction of such vacancies filled through a radiationless transition. Thus:

$$\omega_K + a_K = 1 \qquad (2.13)$$

The fluorescence yields for other shells will not be considered as K shell fluorescence yield has mainly been employed in this study. However for other shells, the primary vacancy in a certain subshell may change to another subshell of lower energy within the same shell due to Coster-Kronig transitions and the situation becomes more complex. Consequently, care must be taken in formulating proper definitions of the quantities that are measured, and in interpreting experimental results in a manner that is consistent with these definitions. In their review article, Fink et al (1966) gave consistent definitions of fluorescence yields for the three L subshells.

The fluorescence yield is an increasing function of atomic number Z. For example, ω_K = 0.219 for T_i and 0.764 for M_o. A detailed discussion of the fluorescence yield and Coster-Kronig transitions may be obtained from Bambynek et al (1972), which also summarizes fluorescence yield experimental data up to July 1971.

Recently, Krause (1979) has calculated K and L shell fluorescence yields and presented tables and graphs. Figure (2.4) from his paper illustrates K shell fluorescence and Auger yield versus atomic number. His tabulations are more comprehensive than those of Bambynek et al (1972) since they cover the range Z = 5 to 110. The difference between these results and those of Bambynek et al (1972) is insignificant for most of the elements. For example there is no difference for Ca, the difference for Br is 0.6% while for V is 10%. The fluorescence values of Bambynek et al (1972) are adopted throughout the work because these are fitted values to the most reliable experimental data, and cover the range Z = 14 to 92.

2.4.1 Auger Effect

The energy gained by the atom when an inner shell vacancy is filled by an electron from an outer shell may be emitted as an electron rather than a photon. This electron is known as an Auger electron. For an atom in which an initial K shell vacancy is filled by an L electron, the result of the Auger effect is a doubly

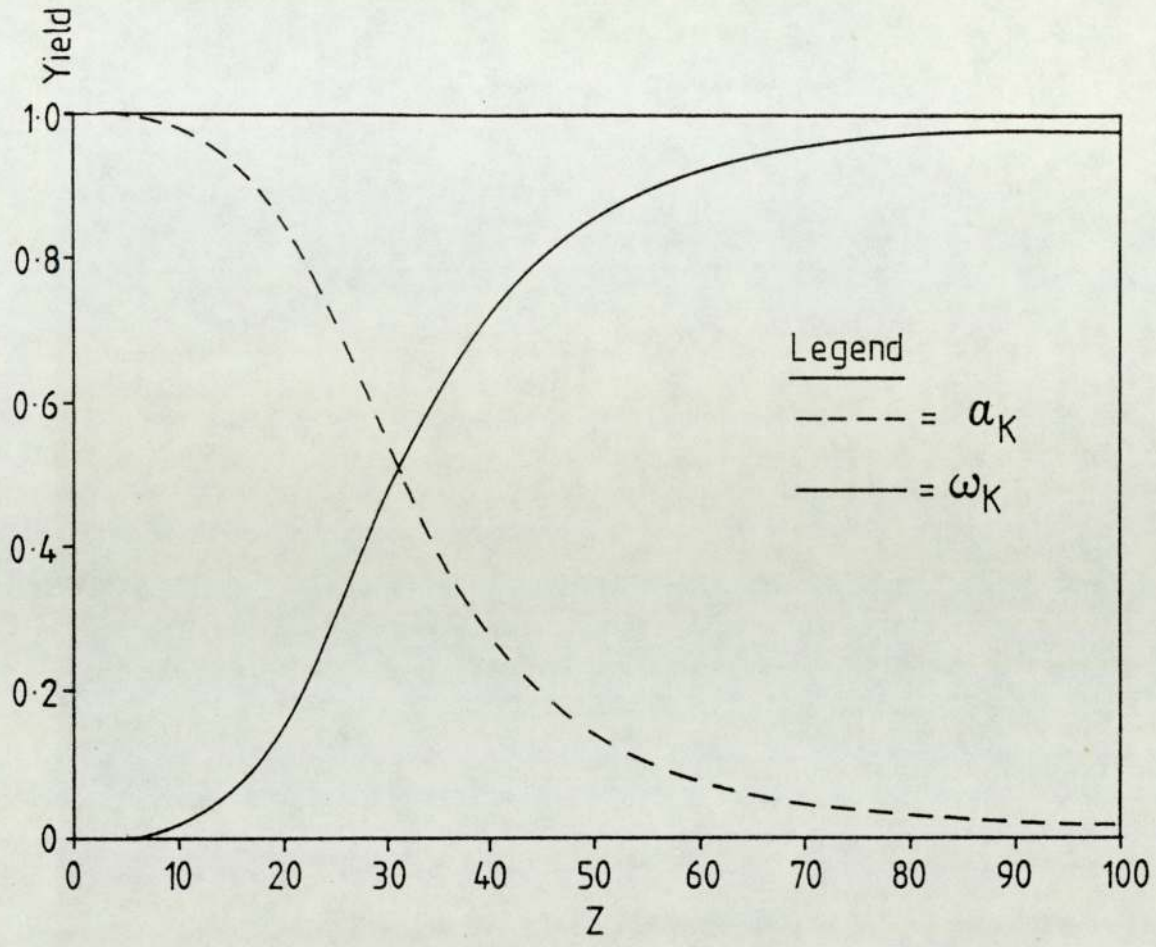

Figure (2.4) K-shell fluorescence and Auger yield versus atomic number. The values are calculated by Krause (1979).

ionized atom having two vacancies, the one created by filling of the initial vacancy and the one resulted from the ejected Auger electron. The Auger electron emerges with an energy equal to the energy difference between the energy released due to the initial electron transition and the binding energy of the Auger electron. Burhop (1972) has reviewed the Auger effect in detail.

Lander (1953) was the first to suggest the use of Auger electrons for surface analysis. Recent developments in Auger electron spectroscopy have led to its emergence as an effective tool in the investigation of solid surfaces. Carlson (1975) discussed the use of Auger electrons in the study of spectra of gases and in the elemental analysis on surfaces of solids.

2.4.2 Coster-Kronig Transitions

These transitions are between the subshells of an atomic shell having the same principal quantum number. A primary vacancy created in one of the subshells could move to another subshell of lower energy before the vacancy is filled by another transition. The primary vacancy is redistributed within a shell as a result of these subshell transitions, Chattarji (1976).

2.5 BACKGROUND RADIATION INDUCED BY PROTONS

This background radiation is associated with the characteristic X-rays used for either radiography or X-ray fluorescence analysis. The characteristic X-rays

obtained from targets bombarded by protons are superimposed on a continuous background of electromagnetic radiation. The level of this background radiation affects the purity of the characteristic radiation used for analysis. However, this level depends on the target composition and thickness, in addition to the projectiles and their energies. The intensity of this background radiation is lower than that encountered by electron bombardment or associated with the monoenergetic radiation from radioactive sources. This background radiation is mainly caused by the acceleration of charged particles in a close encounter with a nucleus and by the deceleration of the secondary electrons of the target in the Coulomb field of the target atom. Since the intensity of the bremsstrahlung is proportional to $(1/M)^2$ for the projectile, the use of protons instead of electrons results in a reduction in the continuum of about 3×10^6 for projectiles of the same velocity, Young et al (1973). This is offset to some extent by secondary electrons.

2.5.1 Bremsstrahlung From Secondary Electrons

In the generation of characteristic X-rays by protons, bound electrons are knocked out from target atoms. These ejected electrons lose most of their energy by Coulomb interaction with the target atoms and are finally caught by one of the ionic atoms when they do not possess sufficient energy. Folkmann et al (1974) give detailed calculations showing that the background radiation at low energies results from bremsstrahlung which is produced

by secondary electrons as a consequence of the radiative collision between the target nuclei and electrons which have been ejected from target atoms by the ion beam. This bremsstrahlung is very strong at low energies, but it decreases rapidly when the energy becomes larger than the energy:

$$T_m = (\frac{4m}{M}) E_p \qquad (2.14)$$

Where T_m is the maximum energy that can be transferred by a proton of mass M to a free electron of mass m. Since (4m/M) is approximately (1/460), it follows that proton energies of 1 to 3 MeV give approximately 2.17 to 6.52 keV for T_m. Thus T_m can be changed by varying the proton energy. Therefore the secondary electron contribution to the background could be greatly reduced to meet the requirement of a particular application.

Folkmann et al (1974) estimated the intensity of this bremsstrahlung radiation and found that the probability of the initial ion ejecting an electron of energy E_e decreases slightly with increasing E_e until $E_e \simeq T_m$. The probability for ejection of a secondary electron with $E_e > T_m$ decreases dramatically, approximately as E_e^{-10}.

Tawara et al (1976) have found that bremsstrahlung radiation is not isotropic and it is more intense at 90^o. This was confirmed by Ishii et al (1977) who have also shown that the angular distribution of bremsstrahlung is

not symmetric around 90^{o} and the intensity is minimized at angles greater than 90^{o}. More recently, Renan (1980) obtained results in agreement with the anisotropic emission of bremsstrahlung reported by Ishii et al (1977). Thus improved signal to background ratio may be obtained by viewing the emitted radiation at angles greater than 90^{o} with respect to the proton beam direction.

2.5.2 Bremsstrahlung From Projectile

The higher energy bremsstrahlung is produced when the projectile experiences a large acceleration in a close encounter with a nucleus.

For a projectile (Z_1, A_1, E_1) incident on a target (Z_2, A_2) the cross-section for the production of projectile bremsstrahlung of energy E_r is given by Alder et al (1956) as:

$$\frac{d\sigma}{dE_r} = C \frac{A_1 Z_1^{\,2} Z_2^{\,2}}{E_1 E_2} \left(\frac{Z_1}{A_1} - \frac{Z_2}{A_2}\right)^2 + \text{higher multipolarities} \qquad (2.15)$$

where C is approximately constant

The term $\left(\frac{Z_1}{A_1} - \frac{Z_2}{A_2}\right)^2$ arises from the interference between the radiation of the projectile and the recoiling nucleus. This implies that one can make the electric dipole bremsstrahlung vanish by employing projectiles of the same charge-to-mass ratio as that of the nuclei in the target. In that case, higher multipolarities will be important, but according to Folkmann et al (1974) are of much less intensity. Figure (2.5) from Folkmann et al

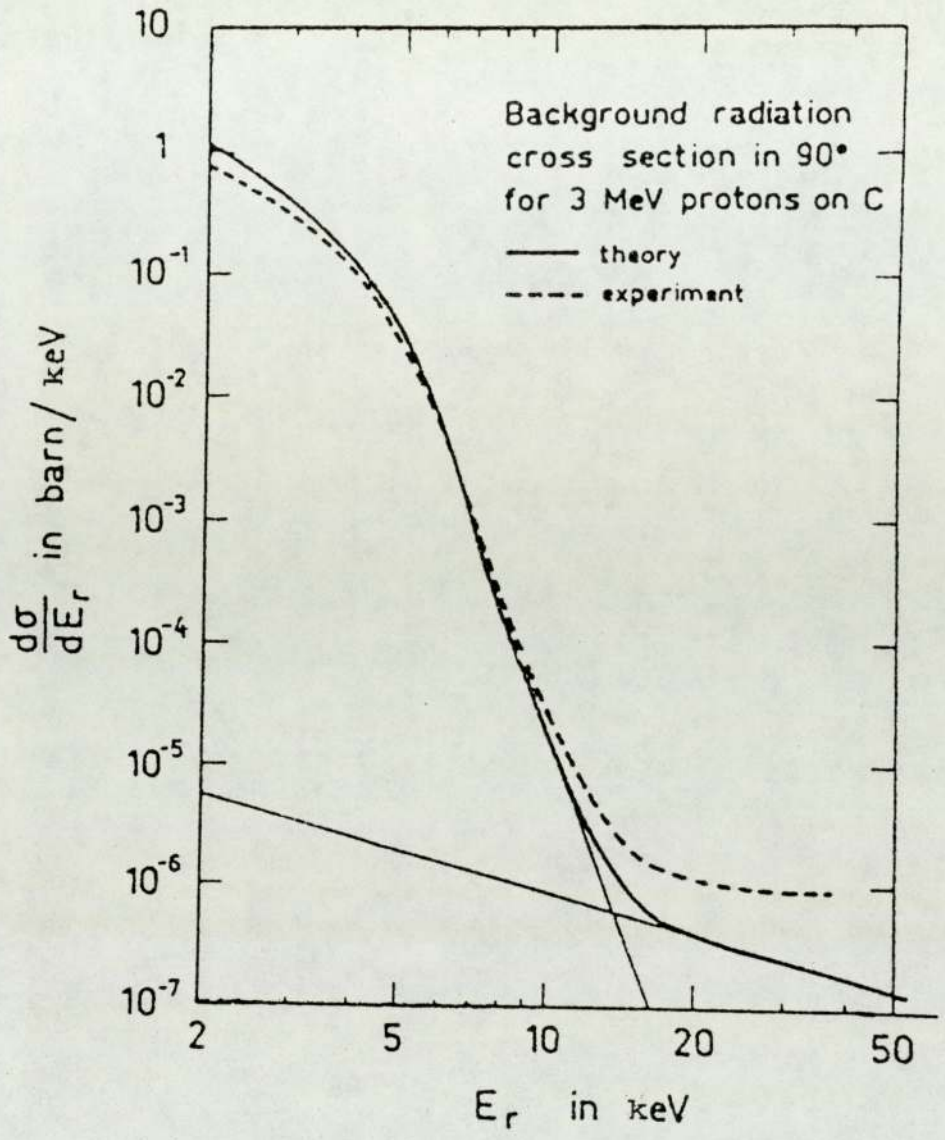

Figure (2.5) Experimental and theoretical background radiation cross-sections for a thin sample. (From Folkmann et al 1974).

(1974) illustrate the level of the bremsstrahlung background where the contribution at high energy is due to proton bremsstrahlung.

2.5.3 Compton Scattering of Gamma Rays From Nuclear Reactions

If energetic protons incident on a target can induce excited nuclear states then high energy gamma rays will be produced. Compton scattering of these gamma rays by the specimen and surrounding materials, and then in the detector produces a low energy continuous background in the X-ray energy region. Some elements like ^{19}F, ^{23}Na and ^{27}Al exhibit large resonance reaction cross sections for protons of energy less than 3 MeV. In these cases, Compton-scattered gamma rays may be a serious source of background. The production of gamma rays generally increases with increasing proton energy. Thus it is necessary to keep the proton energy as low as possible while still giving sufficient characteristic radiation in order to minimize the gamma ray background.

CHAPTER THREE

PROTON INDUCED X-RAY EMISSION IN RADIOGRAPHY

3.1 RADIOGRAPHY AND CHARACTERISTIC RADIATION

Radiography is the production of a picture in the form of shadows of various sizes, shapes and degree of blackness. Conventionally, radiography is performed using the broad spectrum of X-rays generated by bombarding target materials with energetic electrons. In medical or industrial radiography today, highly sophisticated modern X-ray apparatus is used and the radiographic picture is produced after a sequence of many processes.

The use of characteristic radiation in radiography as originally described by Clark and Shafer (1941) increases the contrast. If the radiation is chosen with regard to the position of the critical absorption edges of various constituents of the object to be radiographed it is possible to distinguish between elements of adjacent atomic numbers.

Mammography is considered valuable in the early diagnosis of breast cancer, but there is a wide variety of X-ray systems for mammographic examination. The first use of monoenergetic X-rays in mammography was by Ben and Delarue in 1966. They invented a new type of mammographic tube. Knowing that good contrast in soft tissue radiography is achieved with about 17.5 keV X-rays, they made an X-ray

tube with a Mo target. They also introduced a 0.03 mm Mo filter to remove most of the radiation with energy above and below the characteristic radiation range, thereby producing an approximate monoenergetic beam.

Fewell and Shuping (1978) discussed spectra produced by three types of anode materials used in mammographic X-ray tubes: tungsten, molybdenum and molybdenum-tungsten alloy with a Be window. They examined changes in the X-ray spectra emitted from the three anode materials after it penetrated various thicknesses of Lucite phantom. They also compared contrast of calcium sulfate in the phantom. They concluded that X-rays from Mo (with 0.03 Mo filter) and Mo-W (with 0.5mm Al filter) tubes produced radiographs with generally higher contrast than those from the tungsten tube. This is to be expected since the contrast varies directly with the mass attenuation coefficient, which is mainly photoelectric for the energy range used, and the latter varies approximately as E^{-3} where E is the incident photon energy. Therefore the contrast varies approximately as E^{-3}, provided that acceptable amounts of X-rays are transmitted through the radiographed object, and different thicknesses of Lucite phantom should give better contrast with lower energy. Also in the case of calcium sulfate in the phantom the contrast is expected to be improved with lower energy incident beam.

In an investigation to find an anode target material

better than Mo for mammography from the viewpoint of contrast, Johnson and O'Foghludha (1980) compared the radiographic contrast for a series of wedges of teflon, aluminium and polycarbonate (Lexan) by employing two X-ray tubes: a transmolybdenum and a transrhodium tube. Details of these tubes are available from Johnson and O'Foghludha (1978). They concluded that Rh anode, though fluorescing at an energy of about 3 keV higher than that of the Mo anode, produced images with radiographic contrast no worse than and possibly superior to that obtained with a Mo anode operated under similar conditions. The Mo anode producing lower energy K radiation should produce better contrast than the Rh anode. However they found that the reverse is true. If this is so, then more investigations and experimental evidence is required to explain the unexpected variation of contrast with energy. However, the implications of this phenomenon can only be determined through clinical trials.

The selection of X-ray wavelength or energy for contrast adjustment of a specific feature in a biological specimen has recently been discussed by Spiller (1980). He pointed out that elemental analysis becomes possible if two pictures taken on each side of an absorption edge are compared. This is because of the dependence of radiographic contrast on the ratio of the transmitted X-rays from the specific feature and the rest of the specimen. The large change in the absorption coefficient of the specific feature occurs with the application of two X-ray

energies. Therefore the specific feature transmits a high amount of radiation when radiographed with X-rays whose energy is below that of its absorption edge, and transmits a small amount of radiation when an X-ray energy higher than that of the absorption edge is used for radiography. For a wet biological specimen, water and carbon are the main constituents and transmit a higher percentage of the incident radiation. Thus other materials in the specimen produce good contrast.

Monoenergetic X-rays have an additional advantage of producing less scattered radiation and hence better contrast and less radiation damage to the radiographed specimen as compared to the broad energy spectrum of X-rays. This effect has been investigated theoretically by Smith (1980). He assumed a source of 50 keV monochromatic X-rays for his calculations and found that less scattered radiation is obtained as compared to the case of 50 keV broad energy spectrum. This is because in the latter case, most of the X-rays will have a lower energy and hence there will be more scattered radiation produced.

Gore and Hooker (1981) measured the relative opacities of catheters doped with barium and bismuth. The K absorption edge of bismuth (Z = 83) is at 90.5 keV whilst that of barium (Z = 56) is at 37.4keV. The mass attenuation coefficient of barium exceeds that of bismuth over most of the photon spectrum emitted by a tube operating at 70 kV. Their result indicated that the

relative opacities may well vary with beam quality. This expected variation implies that a complete description of catheter opacity requires measurements at different beam qualities.

Recent developments in radiography and fluoroscopy in the industrial field have been discussed by Stewart (1982). These include areas such as X-ray sources, fine micro-focus equipment and three-dimensional radiography. No reference was made however, to the use of monoenergetic X-rays, possibly because of the need for high intensities as well as high energies for thick heavy material radiography and these are not easily obtainable.

The use of secondary exciting sources in radiography is not widely known. In principle, a secondary fluorescer may be used for providing monoenergetic beams for radiography but limitations such as intensity or purity or beam size could restrict their usage.

3.2 PROTON-INDUCED X-RADIOGRAPHY

The use of characteristic X-rays induced by protons for radiography is not widely known. In this approach the protons are used only as a means of producing mono-energetic X-rays which are then used to take radiographs.

When radiographing an object in which two different regions are rich in different elements it is clear that maximum contrast between these regions will be achieved

by using radiation having a quantum energy between the absorption edges of two elements as shown in Figure (3.1). Indeed the contrast is reversed for photon energies outside this range and the net contrast obtained with a broad spectrum may be very small.

The characteristic X-rays in a spectrum obtained by using protons are superimposed on considerably less bremsstrahlung as compared to that obtained by electrons, Young et al (1973). A comparison is shown in Figure (3.2) between a spectrum obtained by 2.5 MeV protons on a Mo foil, Phull (1982), and a spectrum measured by Marshall et al (1975) for electron bombardment on tungsten target with 80 kV and 2 mm aluminium filter. The ratio of the number of bremsstrahlung photons is about 20:1 for 2.6 MeV protons incident on a Mo target. By comparison, for 40 keV electrons incident on a Mo target with 0.03 mm Mo as a filter this ratio is about 1:1. For 40 keV electrons incident on the usual tungsten target there are no K characteristic photons in the filtered radiation.

Cookson et al (1972) showed that monochromatic X-rays induced by protons can be used for radiography. They used molybdenum and copper K X-rays to radiograph a cross made of copper and iron foil. Because molybdenum X-rays are attenuated nearly equally by the two foils, the radiograph they obtained with these X-rays showed low contrast. With the application of copper X-rays, the radiograph obtained showed a high contrast because of the

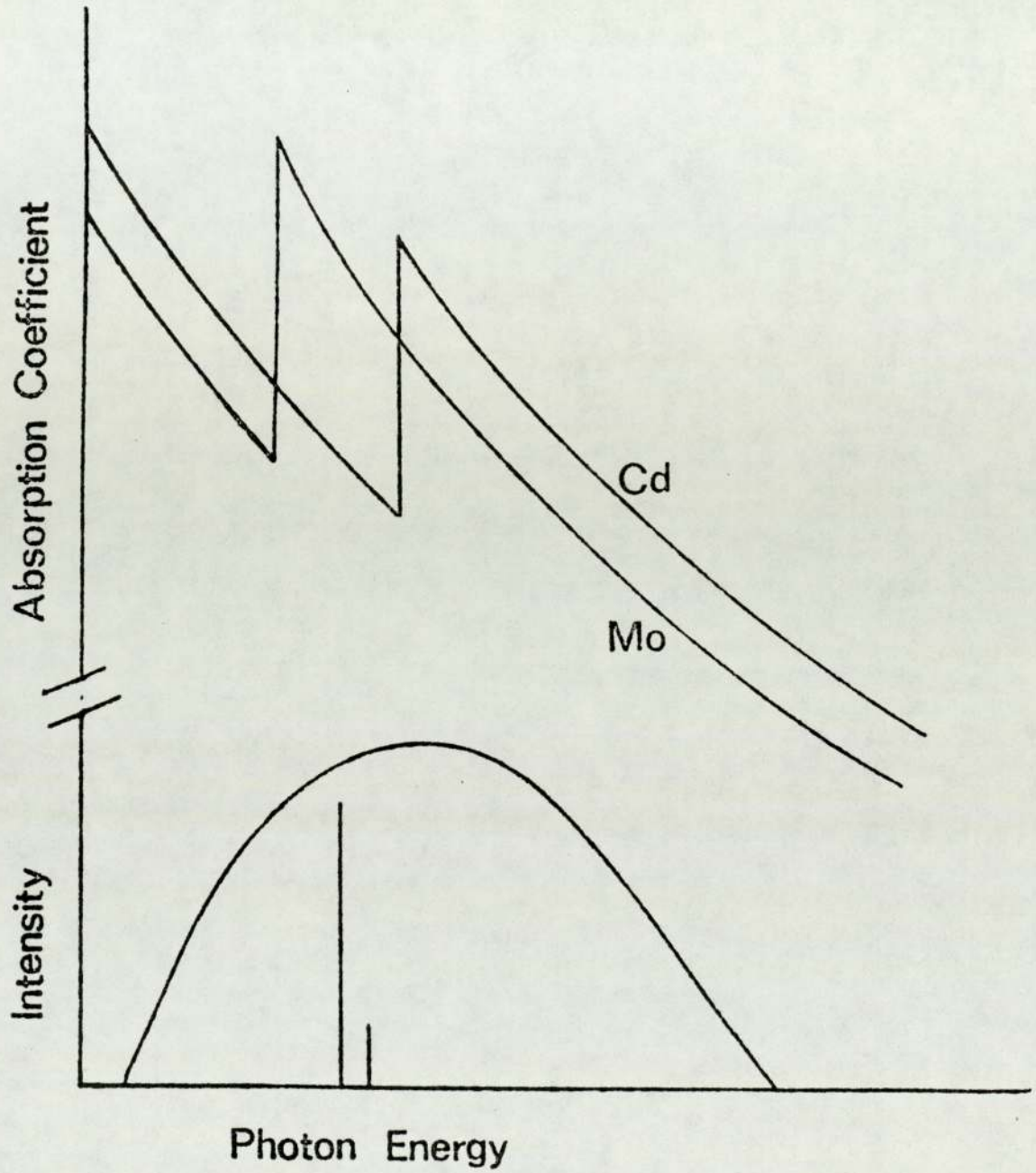

Figure (3.1) X-ray emission spectra and absorption coefficients as a function of photon energy.

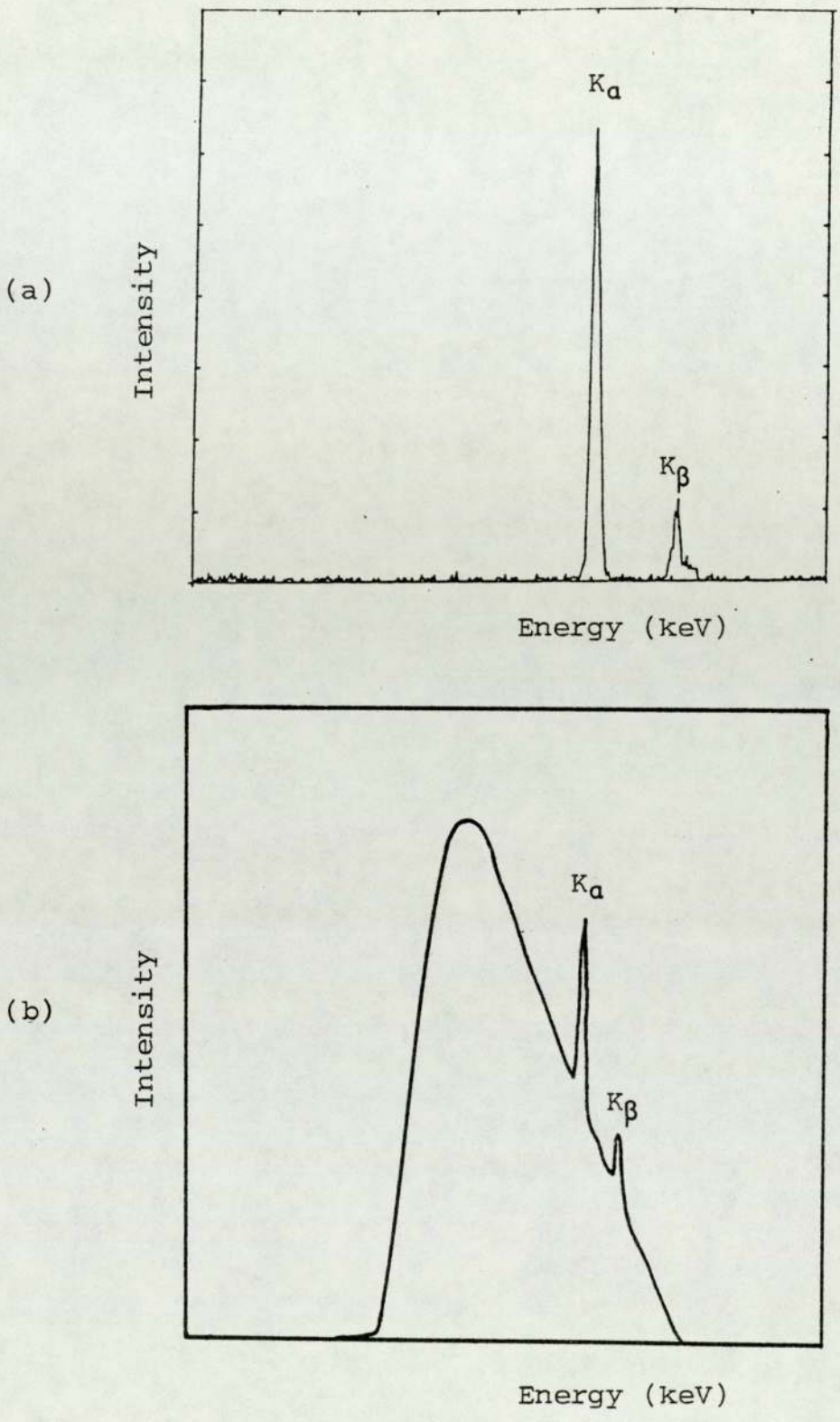

Figure (3.2) Comparison between two X-ray emission spectra obtained by (a) Proton bombardment on Mo foil (From Phull 1982) (b) Electron bombardment on tungsten target with 80 kV and 2 mm aluminium filter. (From Marshall et al 1975).

difference in the mass attenuation coefficient of these X-rays in copper and iron. The copper X-rays pass through copper foil with little attenuation because they are on the low energy side of the absorption edge of copper, but suffer high attenuation in passing through the iron foil because they are absorbed on the high energy side of the absorption edge of iron. The production of secondary fluorescence was not considered by Cookson et al (1972) because it is unimportant in their context. As it will be seen later, these radiations have a negative effect on contrast.

Photon Yield

The principal aim for radiography is the production of a measurable photographic density. This requires a certain number of photons to interact with the X-ray film. Therefore photon yields obtainable from a typical diagnostic X-ray set, which are mainly continuous, need to be known so that they can be compared with the photon yields practically obtainable from targets bombarded by energetic protons, which are mainly characteristic radiation. Consequently a number of photon emission spectra detailed in Table (3.1) were selected from three different sources namely; the tabular presentation of the experimental data of Brown et al (1975), the experimental spectra of Hettinger and Starfelt (1958), and the spectra calculated by Birch et al (1979) who created a theoretical model which allows the accurate prediction of spectral data from a semi-empirical fit

to a selected range of actual measurements. The photon yields per electron were then calculated for these spectra using numerical integration and found to be of the same order of magnitude which is clear from Table (3.1).

Photon yields comparable with those listed in Table (3.1) are available from targets bombarded by energetic protons. For example the photon yield per proton measured by Khan et al (1976) for K X-radiation from thick targets equals 5.4×10^{-3} for Cu and 2.58×10^{-4} for Mo at a proton energy of 2.6 MeV.

TABLE (3.1) PHOTON PER ELECTRON COMPARISON TABLE

kV	Target	Filtration	Photon/ Electron	Reference
40	W	1mm Be+1mm Al	1.02×10^{-3}	Birch et al (1979)
40	Mo	1mm Be+.03mm Mo	1.23×10^{-3}	Birch et al (1979)
45	W	1mm Be	5.8×10^{-3}	Brown et al (1975)
50	W	1mm Be+1mm Al	1.87×10^{-3}	Birch et al (1979)
100	W	4mm Al	2.76×10^{-3}	Hettinger and Starfelt (1958)

High currents are usually used with diagnostic X-ray tubes together with large target-film distance. The range of distances usually used for radiography is typically 90 to 150 cm, Jenkins (1980).

The photon flux at 100 cm from a Mo target for 1 mA and 40 kV electron is about 7.68×10^{8} photon.cm^{-2}.s^{-1}.

A comparable flux of about 6.88 X 10^8 photons.cm^{-2}.s^1 can be obtained at 20 cm from a Mo target for a current of 100 μA of protons at 3 MeV.

3.3 EXPERIMENTAL ARRANGEMENT FOR RADIOGRAPHY

A beam of energetic protons from the Universities 3MV Dynamitron accelerator was employed in the present study. The machine can accelerate electrons or positive ions. In the positive mode the specification for the machine is up to 2 mA of protons at energies from 600 keV to 3 MeV. The separation of the component ions, e.g. ^1_1H, ^2_1H and ^3_1H in the case of hydrogen, from the ion source is accomplished by using different extraction voltages prior to the beam entering the field of the permanent magnet.

The proton beam was accelerated vertically downwards and deflected through 45^o by a suitable bending magnet. Targets to be used as sources of monoenergetic X-rays were irradiated with a proton beam of 2.6 MeV.

The proton beam from the accelerator was transported in vacuum to the target. Stainless steel components were used for the vacuum system with ion pumping to provide a clean system. The pressure throughout the beam tube and target chamber was maintained near 10^{-5} torr or less.

A set of water-cooled apertures were used to collimate the proton beam to a diameter of not more than 11 mm

which was allowed to impinge on a water-cooled target inclined at 45° to the incoming beam. The target area seen by the proton beam must be large so that the proton beam power is spread over as large an area as possible. This reduces thermal stress on the target focal spot area. The power density due to the experimental conditions used of 30 μA proton current and 3 MeV proton energy was 90 Watt/cm^2, therefore it was necessary to cool the target and this was achieved by mounting the target onto a water-cooled copper anode.

Since geometric unsharpness is directly proportional to the size of the focal area of the target as seen by the film, the focal area should be as small as possible. Therefore a compromise on the size of the focal area should be reached. Consequently, a beam diameter of about 1 cm was used after considering the two effects mentioned above. X-rays were taken at 90° to the proton beam for radiography after being transmitted through a 50 μm thick Melinex window. The test object for radiography was fixed in front of an X-ray film which was positioned 20 cm from the target and wrapped in a light tight envelope. A shielding aperture of Pb-Al was arranged to shield the X-ray film except a circular area behind the specimen so that a number of exposures can be made on the same film. The purpose of using the Al was only to support the thin layer of Pb required as a shield. A beam interceptor was used instead of an X-ray shutter for starting and terminating the exposure. A beam

interceptor was preferred in order to minimize anode heating. The interceptor consisted of a piece of water-cooled copper thick enough to suppress the proton beam completely when introduced in the beam line and was operated by remote control. A photograph of the experimental arrangement for radiography is shown in Figure (3.3) and a schematic diagram is shown in Figure (3.4).

3.3.1 Ag and Mo Characteristic Radiation in Radiography

In order to exploit the advantage of high purity characteristic radiation obtained from the Dynamitron, an initial experiment was performed to test the feasibility of using characteristic radiation from targets bombarded by protons for radiography. A number of exposures were made on a piece of dural aluminium step wedge. Differential absorption of the X-ray beam as it passes through different steps results in the creation of a radiographic image. Figure (3.5) shows a radiograph of the dural aluminium step wedge obtained for 50 μA beam current and 4 minutes exposure time. The region of the radiograph where the photographic densities can be measured was found to correspond to a number of photons of the order of 10^8 per cm^2 incident on the film. The number of steps that could be recognised in the radiograph depends on the film latitude which refers to the ability of a film to respond to a range of exposures and record them as useful densities.

The uniformity of the X-ray field was measured by

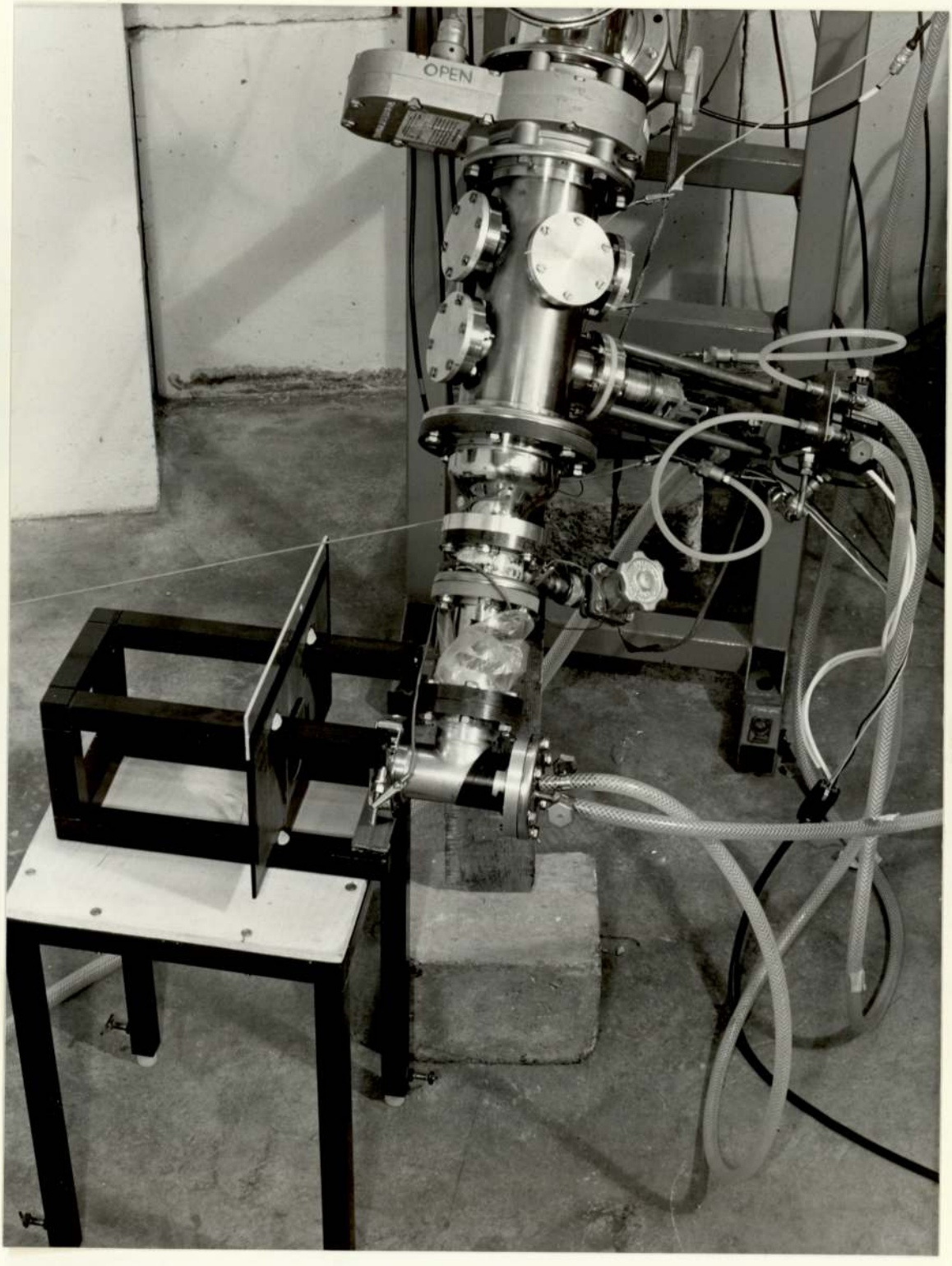

Figure (3.3) A photograph of the experimental arrangement for radiography.

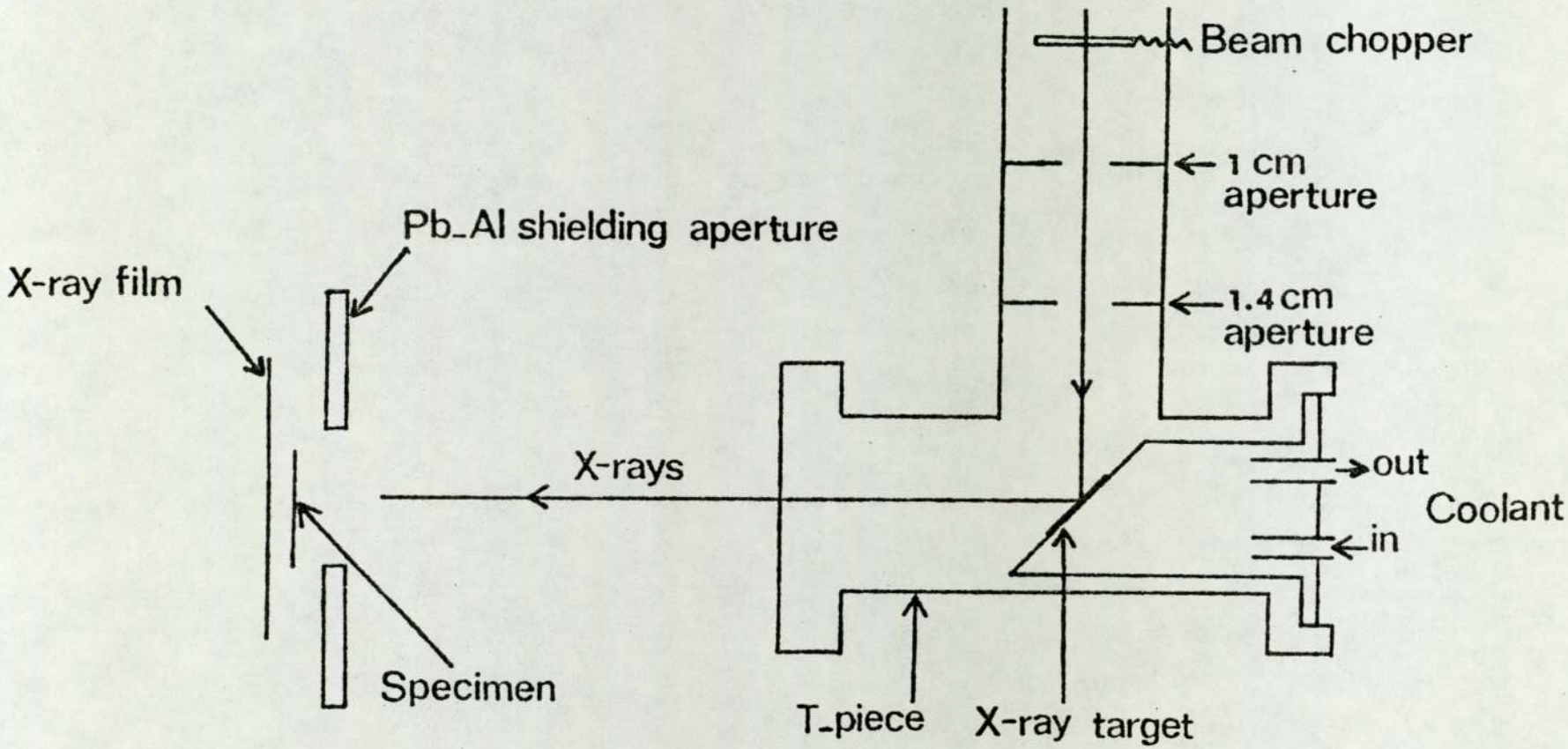

Figure (3.4) The mechanical arrangement used for radiography.

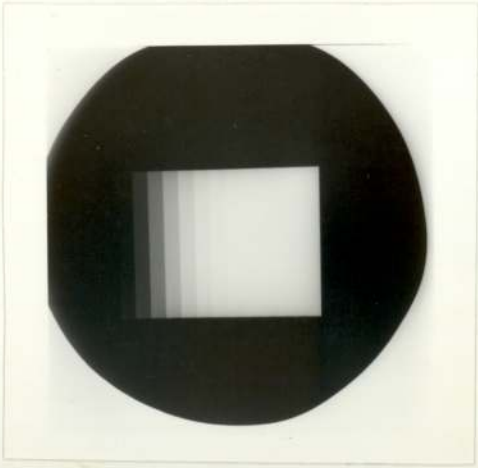

Figure (3.5) Radiograph of the dural aluminium step wedge obtained with K X-rays of Mo for 50 μA proton current and 4 minutes.

exposing an X-ray film to the Ag radiation for 2 seconds at 50 μA beam current. The X-ray field uniformity was then determined by measuring the photographic density of the resulted radiograph in steps of 2 mm along both X and Y directions. The X-ray field was found to be uniform over a circle of about 3 cm in diameter.

To demonstrate the high contrast that can be obtained with the proper use of monoenergetic radiation, K X-rays of Ag and Mo were used sequentially to radiograph a test object of Cd and Mo foils (Mahrok et al, 1981). This combination of X-rays and foils were selected such that high contrast is obtained when X-rays are absorbed in between the K edges of these foils while low and reversed contrast is obtained with X-rays obsorbed outside the

region between the edges. The foils were 0.005 cm thick and placed side by side on a cellotape backing. The K absorption edges of these foils are at 26.71 and 20.00 keV respectively. The test object was radiographed with K X-rays of Mo and Ag. The average energy of the K_α lines of Mo is 17.44 keV and that of Ag is 22.10 keV. The latter lies between the two absorption edges and so should give good contrast while the former lies below both edges and should give relatively poor contrast.

The radiograph taken of the test object with K X-rays of molybdenum was for 30 μA and the optimal exposure time does not differ significantly from the calculated one. These X-rays are attenuated nearly equally by both foils. Thus a contrast of 0.31 was obtained for the test object, Figure (3.6c). This contrast was calculated by measuring the photographic density of Cd and Mo sections and applying equation (3.1).

The radiograph with the silver K X-rays of the test object which was for 30 μA and 16 minutes, shows high contrast of 1.12 of the test object, Figure (3.6a). This is because of the large difference in the X-ray attenuation coefficients of the two foils.

The characteristic curve of the film used (Kodak Industrex C Film) was produced using Ag X-rays with a proton current of 30 μA. Different areas of the film were exposed to X-rays for different exposures ranged

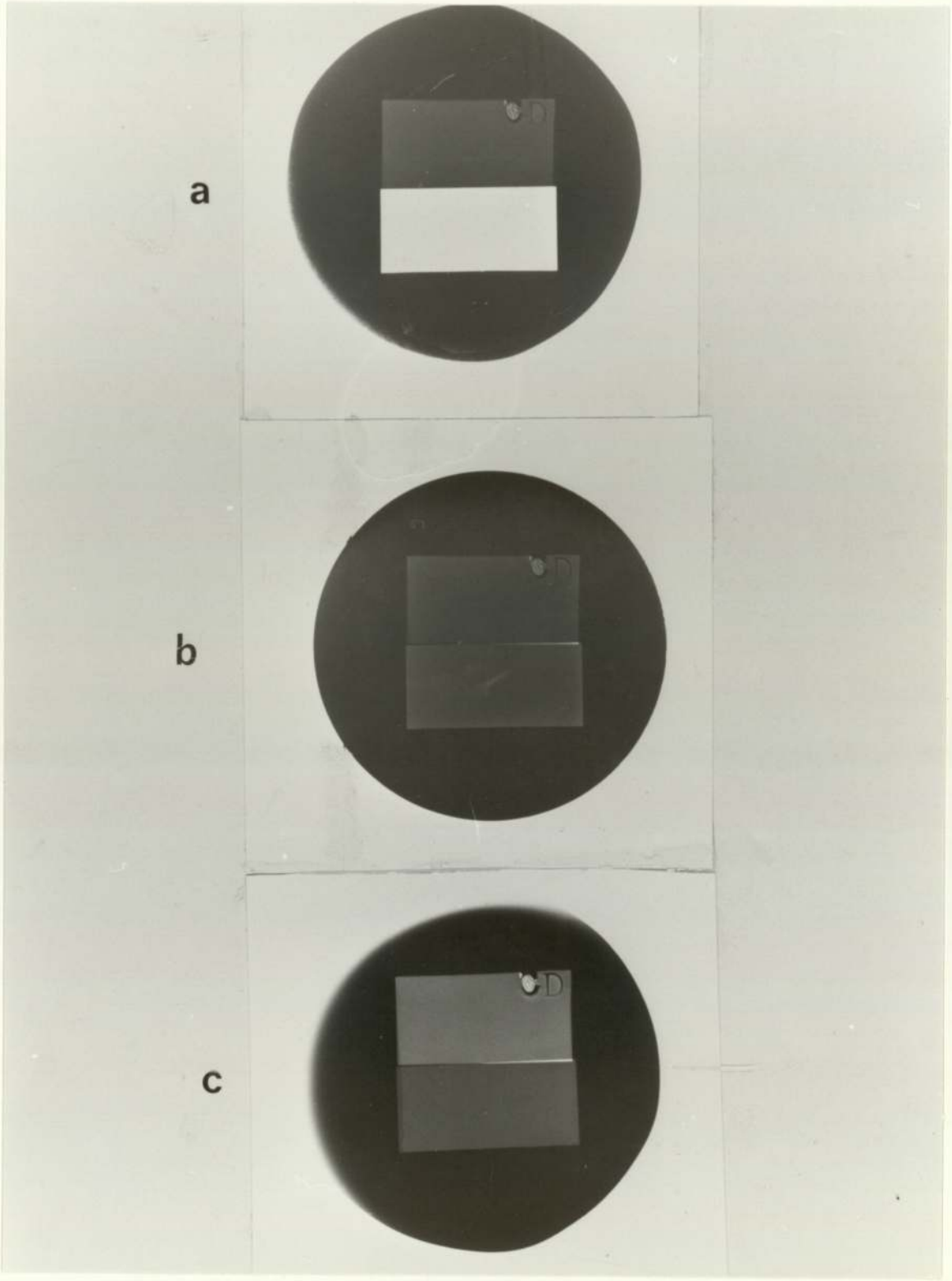

Figure (3.6) Radiographs of test object obtained using: (a) Ag characteristic radiation, (b) 45 kV electron excited radiation, (c) Mo characteristic radiation.

from 10-30 seconds and the characteristic curve obtained is shown in Figure (3.7). A photographic density of 2 which lies on the straight line portion of the curve corresponds to about 10^8 photons/cm^2. All exposures were then taken on the straight line portion of the curve in order to magnify the radiation contrast already present in the transmitted beam. The X-ray films were processed chemically with Kodak DX-80 developer for 4 minutes at 20^oC. The photographic densities of films were measured with a universal densitometer. In order to find the background density, also called base density, a film was processed without being subjected to any radiation. This background density is due to the blue dye present in the film base and the radiation the film has received during storage. For the film used this background density was measured and found to be 0.17.

The measured contrast of the test object with K X-rays of silver is 3.6 times as that obtained with K X-rays of molybdenum. This result shows that there is a marked improvement in contrast when radiographing the test object with radiation chosen to have an energy between the absorption edges of the two elements involved. Thus the use of the nearly monoenergetic X-radiation obtainable from the proton bombardment of targets has considerable potential for radiography particularly when a feature of interest in the object is known to be rich in a particular element. The target can then be chosen such that its characteristic radiation is just above or just

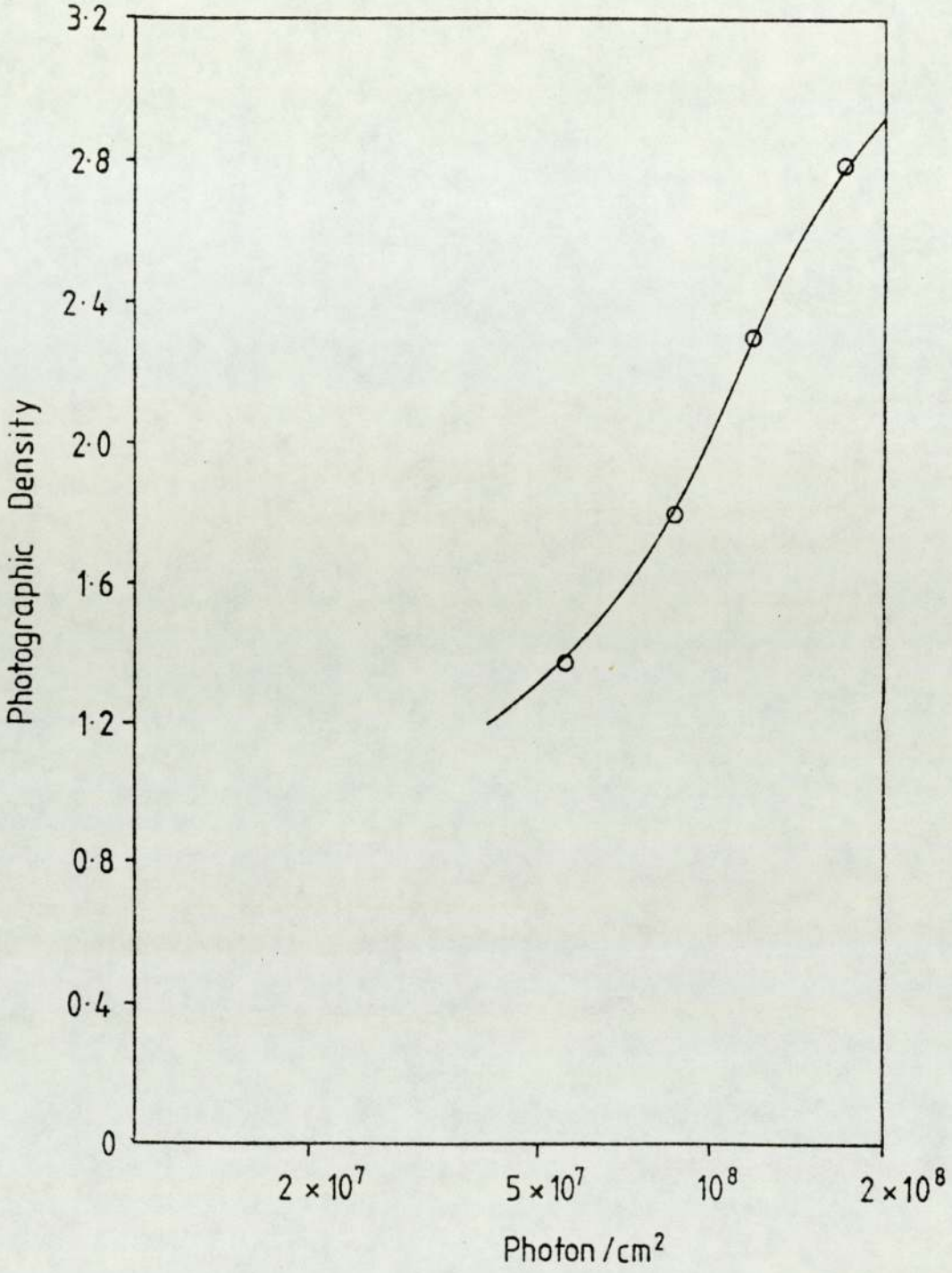

Figure (3.7) The characteristic curve of Kodak Industrex C film. Error bars were omitted since they were smaller than the symbol size.

below the absorption edge for that element depending on the relative absorption of the incident radiation between the element and its matrix. Because of the increase in flux of X-rays with low atomic number targets bombarded by protons, the method may be more appropriate for elements with intermediate atomic number targets.

3.3.2 Radiography Using Broad X-Ray Spectrum

In order to illustrate the advantage in the use of monoenergetic radiation over the use of a broad energy spectrum for radiography, a Pantak X-ray set at the Birmingham Radiation Centre was used to provide a broad X-ray spectrum to radiograph the test object described previously. The X-ray set was operated at 45 kV and 8 mA with a tungsten target and a 1 mm aluminium filter. Thus the emitted spectrum contained no K characteristic X-rays but only bremsstrahlung radiation. An exposure of 32 seconds was found sufficient to give a maximum and measurable contrast of the test object. The target-test object distance was 70 cm and the target-X-ray window distance was 18.4 cm. The radiograph obtained with this radiation shows a low contrast of 0.16 of the test object and is shown in Figure (3.6b). This is because photons with various energies in the incident broad spectrum are differently attenuated in a particular foil due to the variation of the mass attenuation coefficient with energy and a reduced contrast is obtained. Table (3.2) compares the measured radiation contrasts with the calculated ones for the test object which was radiographed

TABLE 3.2

COMPARISON OF THE MEASURED AND CALCULATED RADIATION CONTRASTS FOR THE TEST OBJECT

	measured radiation contrast C_R	calculated radiation contrast C_R
Ag K X-rays	0.35 ± 0.01	0.36
Mo K X-rays	-0.101 ± 0.003	-0.10
45 kV electron X-ray spectrum	0.035 ± 0.002	

by two monoenergetic X-rays and one broad X-ray spectrum. The measured radiation contrast is obviously greater for the Ag radiation than for either the Mo X-rays or the electron excited radiation. The negative sign value obtained with the Mo radiation indicates that in this case the Cd section of the test object is more highly absorbing than the Mo. Comments on the calculated radiation contrast are made in section (3.4).

3.3.3 Radiography of Perspex Phantom

The thickness of the test object described in section (3.3.1) is rather small, but the method may be employed for thicker objects. To investigate the possibility of radiographing a bulk of soft tissue, a cube of perspex 5 cm thick has been radiographed using K X-rays of molybdenum, the exposure time was 15 minutes and 50 μA proton current was employed.

The perspex phantom consists of soft tissues equivalent material, bone equivalent material and blood equivalent material. The solution used as blood equivalent material was $NaNO_3 + H_2O$, whose density equals 1.088 g/ml. The density of blood, which is about 1.059 g/ml, does not differ significantly from the prepared solution. The solution was put in the cylindrical hole which is inside the perspex phantom and sealed off by means of insulating tape which is made of polyvinyl chloride (PVC). The radiograph is shown in Figure (3.8). The following details can be recognised in the radiograph:

1) perspex material
2) bone equivalent material
3) blood equivalent material
4) insulating tape
5) air bubble under the insulating tape
5) dip over the insulating tape

This example demonstrates the feasibility of the technique for thick soft tissue object radiography. The long exposure time may be reduced by employing the maximum current of 2 mA that can be drawn from the accelerator and with the use of the intensifying screens.

3.4 CALCULATION OF RADIATION CONTRAST FOR THE TEST OBJECT

These calculations were intended to predict the values of the radiation contrast for the test object, expected for the radiations employed.

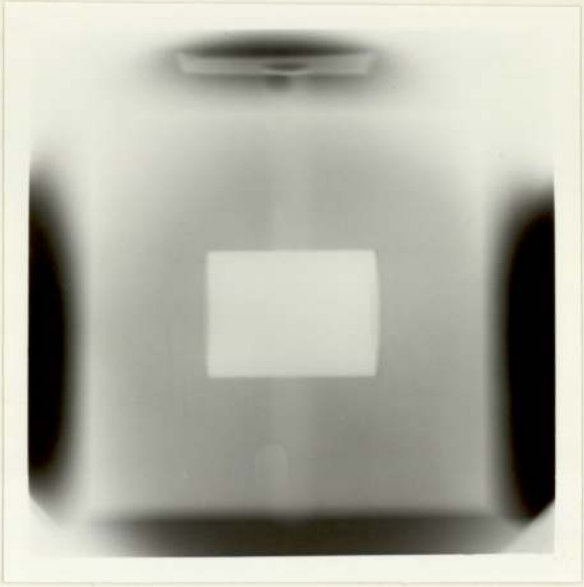

Figure (3.8) Radiograph of perspex phantom obtained with K X-rays of Mo for 50 μA proton current and 15 minutes.

The film contrast C_F may be defined as:

$$C_F = D_1 - D_2 \tag{3.1}$$

where D_1 and D_2 are the measured optical densities of Cd and Mo sections of the film respectively. The optical density of the film is defined as:

$$D = \text{Log}_{10} \left(\frac{I_o}{I_t}\right) \tag{3.2}$$

where I_o and I_t are the incident and transmitted light intensities respectively. The radiation contrast C_R is related to the film contrast by the expression:

$$C_F = \gamma \, C_R \tag{3.3}$$

where γ is the slope of the characteristic curve of the film. For a monoenergetic beam of X-rays, we have:

$$C_F = \gamma \, \text{Log}_{10} \left(\frac{E_2}{E_1}\right) \tag{3.4}$$

where $\left(\frac{E_2}{E_1}\right)$ is the ratio of two X-ray exposures transmitted through two regions of the test object.
$\text{Log}_{10} \left(\frac{E_2}{E_1}\right)$ is called the radiation contrast C_R.

$$C_R = \text{Log}_{10} \left(\frac{E_2}{E_1}\right) \tag{3.5}$$

Equation (3.5) shows that the radiation contrast does not depend upon the intensity of the incident beam. The effect of polyenergetic beam of X-rays on contrast can be obtained only by calculating the transmitted intensities for each energy contained in the incident beam and integrating these intensities over the whole range of energies, Betteridge (1957). The contrast is influenced

by the shape of the incident X-ray spectrum. The contrast obtained is determined by the ratio:

$$\frac{\sum I_{X2}}{\sum I_{X1}}$$

where I_{X1} and I_{X2} are the X-ray intensities transmitted from the two regions 1 and 2 respectively as it is shown in Figure (3.9).

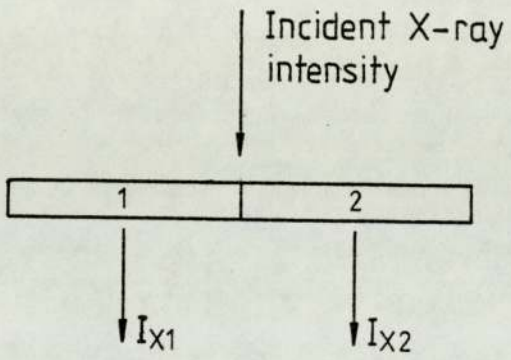

Figure (3.9) Transmitted X-ray intensities from two region sample.

The radiation contrast for a spectrum of energies is defined by, Meredith and Massey (1977):

$$\therefore \quad C_R = \text{Log}_{10}\frac{\sum I_{X2}}{\sum I_{X1}} \qquad (3.6)$$

For monoenergetic radiations the fractions of the incident radiations transmitted were calculated directly using the usual exponential law. Values of the mass absorption coefficient were obtained from the compilation of Storm and Israel (1970).

However, when considering incident radiation with energy

above the K absorption edge of the element to be radiographed, it is also necessary to estimate the effect of the fluorescent radiation as this was found to contribute significantly to the total transmitted flux and decrease the contrast. To do this the thickness of each foil was considered to be divided into 100 sections of equal thickness. The fraction of the incident radiation absorbed in each slab was calculated by applying the exponential law. The total flourescent production was obtained from a knowledge of the fluorescent yieldω,Bambynek et al (1972). It was then assumed that half of this was re-radiated in the forward direction and the fraction transmitted through the remainder of the foil was calculated by applying the appropriate absorption coefficient. This process was repeated for each of the slabs. This is expressed by the equation:

$$I_T = I_o \exp(-\mu_1 t) + I_o \sum_i \exp(-(\mu_1 X_i + \mu_2 Y_i)) (1 - \exp(-\mu_1 \Delta X)) \frac{\omega}{2} \qquad (3.7)$$

where I_T is the total transmitted flux. The significance of the other symbols is shown in Figure (3.10). In this calculation the K_{α_2}, K_{α_1}, K_{β_1} and K_{β_2} lines were treated separately. The continuous background radiation over which the characteristic X-rays induced by protons are superimposed was neglected in the contrast calculation because it was too small, Young et al (1973). Hence its small contribution to the contrast can be ignored.

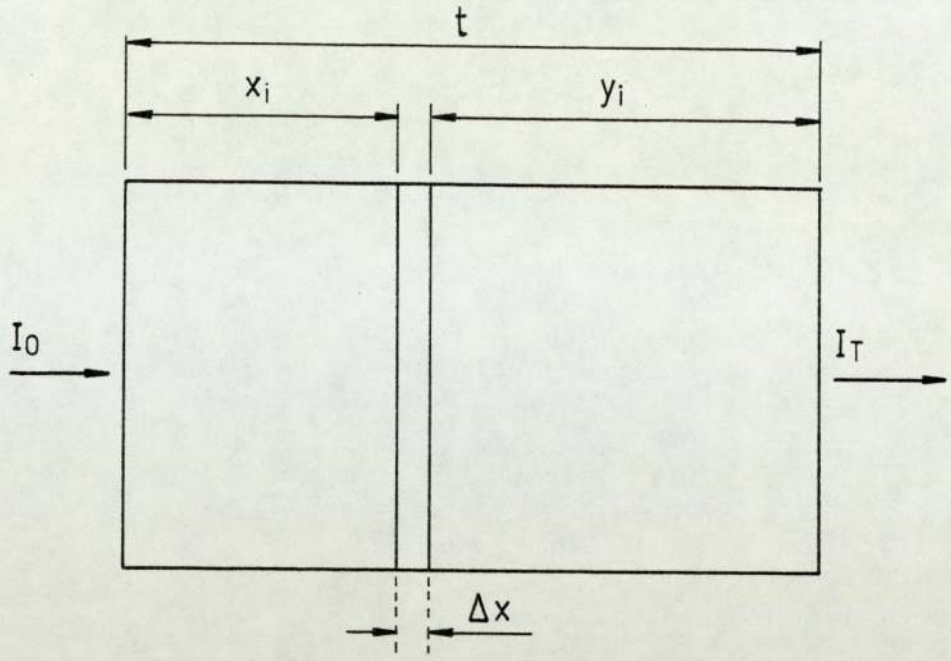

Figure (3.10) Fluorescent radiation calculation. μ_1 and μ_2 refer to the incident and fluorescent radiation respectivley.

The results of these calculations are shown in Table (3.2) together with the values of the measured contrast. The agreement is clear between these results. The small difference between the measured and the calculated radiation contrast could be attributed to the bremsstrahlung radiation produced by proton bombardment on Ag and Mo targets. This bremsstrahlung radiation was not accounted for in the theoretical calculations because it was too small.

Similar calculations for the electron generated X-rays are less easy because of uncertainties in the detailed spectral shape. However calculations based on typical spectra from 40 and 50 kV constant potential sets, Birch et al (1979), with a filtration of 1 mm Be and 1 mm Al have

been made. The radiation contrast has then been calculated using equation (3.6) by summing the contributions of the transmitted and the fluorescent X-rays at different energies for each foil of the test object. The results obtained are not dissimilar from the measured values.

3.5 RADIOGRAPHY DATA TABLE

In order to provide data for the range of soft tissue thicknesses that can be radiographed using different monoenergetic radiations obtained by this method a radiography data table has been produced.

Perspex was used as a soft tissue equivalent material for the calculations of photon density that is required to produce a measurable photographic density on the X-ray film.

The K X-ray yield per proton Y(E) was calculated using the expression given by Khan et al (1977):

$$\ln Y(E) = a_o(E) + a_1(E)Z \qquad (3.8)$$

where Z is the atomic number of the target and covers a range from 20 to 50. The constants a_o and a_1 are energy dependent coefficients and their values are 1.41 and -.21894 for 3 MeV proton energy respectively. The thickness of perspex (T) was calculated such that 10^8 photons per square cm interacted with the X-ray film which is located at a distance of 15 cm from the target. A charge of 30,000 μC on target was also assumed for

every exposure. This charge may be obtained by using a different combination of current and exposure time. For example, a current of 100 μA for 5 minutes or a current of 2 mA for 15 seconds.

The range of targets available are Ti, Fe, Cu, Zr, Mo and Ag with characteristic K_{α_1} of 4.51, 6.40, 8.04, 15.77, 17.47 and 22.16 keV respectively. The thickness required to reduce the number of photons, emitted from a particular target, to 10^8 per cm^2 at the film placed at 15 cm from the target was calculated using the expression:

$$\frac{Y(E)}{4\pi(15)^2} \times 30{,}000 \times 6.25 \times 10^{12} \quad \exp(-(\mu/\rho)\rho T) = 10^8 \qquad (3.9)$$

where 6.25×10^{12} is the number of protons in 1 μC, (μ/ρ) is the mass absorption coefficient for perspex and (ρ) is the density of perspex and was taken as one. The values of (μ/ρ) for the photon energies listed in Table (3.3) were obtained by the interpolation of the data for perspex given by Hubbell (1969) using a quadratic curve fit.

The result of the calculation are shown in a graphical form in Figure (3.11). From equation (3.9) we see that:

$$T \propto \ln Y(E)$$

$$T \propto \frac{1}{(\mu/\rho)}$$

This means that when Z increases, the thickness (T)

TABLE 3.3

RADIOGRAPHY DATA TABLE

Proton Target	Photons/ Proton	K_{α_1}(keV)	$(\mu/\rho)_{perspex}$	Perspex thickness T(cm)
$_{21}Sc$	$4.13X10^{-2}$	4.09	82.12	0.12
$_{22}Ti$	$3.32X10^{-2}$	4.51	58.77	0.17
$_{24}Cr$	$2.14X10^{-2}$	5.414	31.99	0.30
$_{25}Mn$	$1.72X10^{-2}$	5.898	24.24	0.38
$_{26}Fe$	$1.38X10^{-2}$	6.403	18.65	0.49
$_{27}Co$	$1.11X10^{-2}$	6.93	14.56	0.61
$_{28}Ni$	$8.91X10^{-3}$	7.477	11.52	0.75
$_{29}Cu$	$7.16X10^{-3}$	8.047	9.22	0.92
$_{30}Zn$	$5.75X10^{-3}$	8.638	7.46	1.11
$_{31}Ga$	$4.62X10^{-3}$	9.251	6.10	1.32
$_{39}Y$	$8.018X10^{-4}$	14.957	1.62	3.87
$_{40}Zr$	$6.441X10^{-4}$	15.774	1.41	4.28
$_{41}Nb$	$5.175X10^{-4}$	16.614	1.24	4.71
$_{42}Mo$	$4.157X10^{-4}$	17.478	1.09	5.16
$_{45}Rh$	$2.156X10^{-4}$	20.214	0.76	6.49
$_{47}Ag$	$1.391X10^{-4}$	22.162	0.61	7.37
$_{48}Cd$	$1.118X10^{-4}$	23.172	0.55	7.77
$_{49}In$	$8.979X10^{-5}$	24.207	0.50	8.16
$_{50}Sn$	$7.213X10^{-5}$	25.270	0.45	8.52

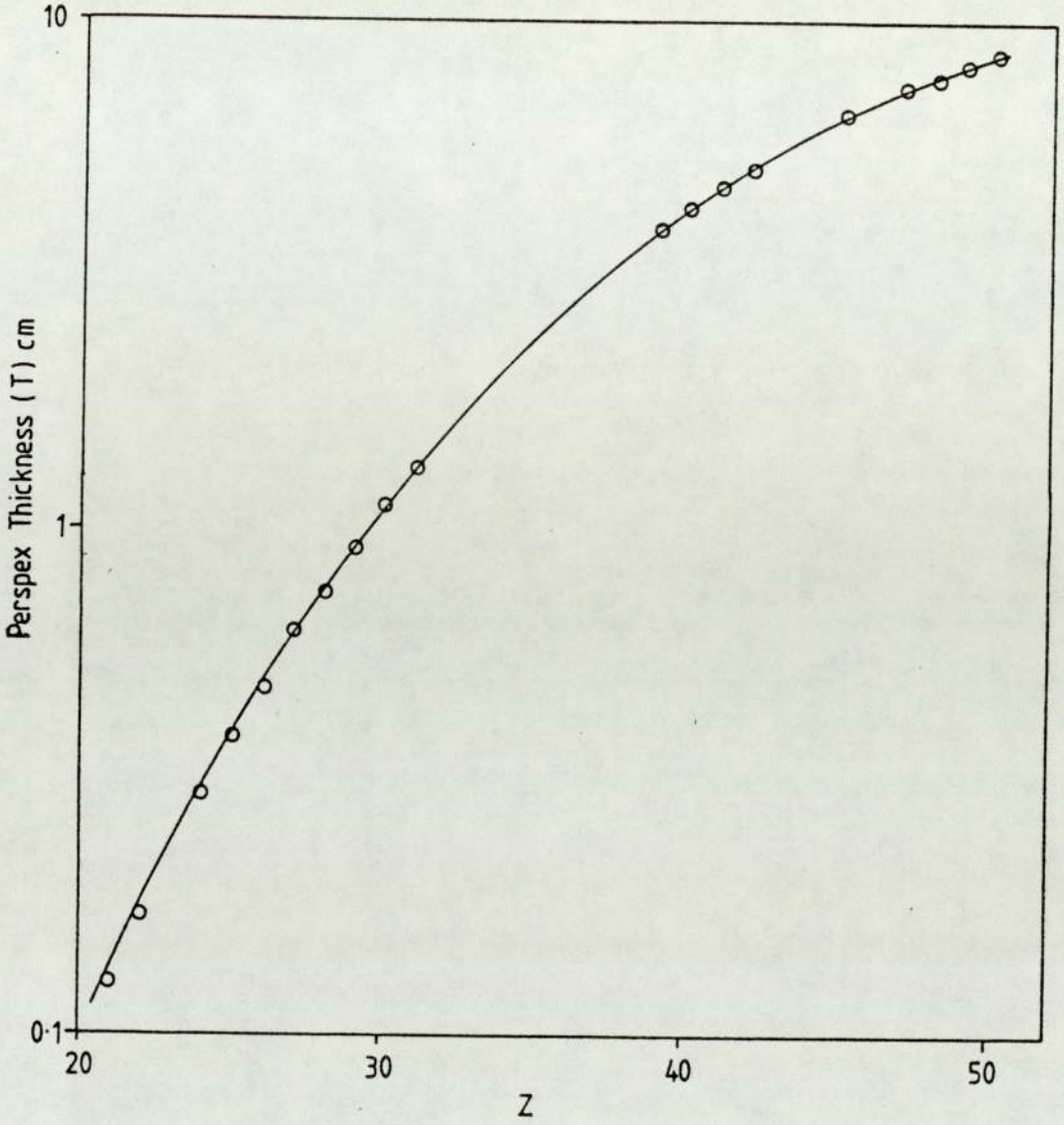

Figure (3.11) A plot of the perspex thickness that can be radiographed against the atomic number of the target.

increases. Higher values for Z means higher values for the energy (Moseley's Law) and lower values of (μ/ρ) for perspex.

The maximum thickness of perspex that can be radiographed is limited by the photon yields which fall rapidly with the increase in atomic number of the target. Also high absorption is obtained for low atomic number targets. The method may then be more suitable for elements with intermediate atomic number targets. The thickness (T) can be increased by increasing the charge on the target.

For the range of incident photon energies assumed in these calculations, perspex becomes very transparent and heavy elements can easily be observed.

This technique could possibly be applied for the radiography of hands and forearms, and for mammography.

Exploiting the maximum current that could be extracted from the accelerator, a thickness of about 9 cm tissue equivalent material (i.e. perspex) can be radiographed with Mo K X-rays for an exposure of 5 minutes. The duration of this exposure may be reduced by a factor of about 50 with the use of the intensifying screens. Thus biological or medical objects with up to 9 cm or more thickness may be radiographed by this method with moderate exposure times.

The potential of this technique is that it could be used to complement the conventional radiography using X-ray set especially when high contrast of a particular feature of the specimen is needed. Also the use of suitable contrast materials could even improve the contrast of the particular feature.

CHAPTER FOUR

XRF MODES OF EXCITATION AND APPARATUS DEVELOPMENT

4.1 MONOENERGETIC PHOTON EXCITATION AND APPLICATIONS

The X-ray fluorescence (XRF) analysis technique is based on the creation of vacancies in atomic shells of a sample to be analysed by primary radiation and the observation of the characteristic X-rays emitted from the sample when the vacancies fill by electrons from outer shells. Charged particles or photons may be employed as the primary radiation. In charged particle induced X-ray emission (PIXE) usually protons are employed and for this reason PIXE refers to proton induced X-ray emission. PIXE is a relatively new analytical technique and was first described by Johansson et al in 1970. Review articles concerning PIXE capabilities as a powerful analytical tool and its limitations have been written by Walter et al (1974), Folkmann (1975), Deconnink et al (1975), Johansson and Johansson (1976) and more recently Khan and Crumpton (1981). Here we are concerned with photon excitation.

Photons from X-ray tubes or radioactive sources are usually employed as the exciting source in XRF analysis. Certain samples are more efficiently excited if the primary photons are modified by suitable filters or secondary targets to obtain the most appropriate energy spectrum and considerable advantages can be obtained if

monoenergetic exciting sources are employed.

4.1.1 X-Ray Tube Excitation

The direct excitation method uses conventional X-ray tubes where the accelerated electrons are converted to X-rays at the target anode of an evacuated tube. The radiation produced passed out via a thin window usually made of beryllium. The efficiency of X-ray production, by which the fraction of the energy of the electrons that is converted into X-rays is rather low for the range of kV usually employed in XRF analysis. At 60 kV for example, only about 0.5% of the electron energy reappears as X-rays, the other 99.5% being converted into heat which has to be removed by cooling water.

The bremsstrahlung radiation generated by a conventional X-ray tube is not suitable for use as primary radiation in an XRF analyser, Goulding and Jaklevic (1973), since its scatter from the sample causes excessive background. Porter (1973) and Cooper (1973) found that bremsstrahlung generated by the deceleration of the electrons in the anode and scattered by the sample produces a high interference continuum which reduces the sensitivity for measuring the characteristic sample X-ray peaks.

The simplest method for reducing continuum background as described by Jaklevic et al (1972) is to use suitable X-ray filters to transmit as much of the characteristic radiation as possible while attenuating all other

energies. Since any given element is a good transmission filter for its own characteristic radiation, the anode of the X-ray tube can be made of an appropriate thickness to effectively filter the transmitted X-ray spectrum. Further filtering can be included to selectively reduce the K_β intensity and closely approach a monoenergetic X-ray beam.

Optimum filter thicknesses to transmit an adequate X-ray flux is determined empirically but 3 to 5 half-thicknesses of the target material are nearly optimum.

Kieser and Mulligan (1976) used a Mo transmission tube with 0.07 mm thick Mo filter to measure the elemental composition of fish tissues. In 1977 Gedcke et al found that monochromatic excitation can provide improved detection limits over 5-30 keV energy range. Owers and Shalgosky (1974) reviewed the use of X-ray fluorescence for chemical analysis.

The effective use of filters with the direct excitation method is described by Vane and Stewart (1980). They showed that the correct choice of filters and excitation potential moves the quasi-monochromatic radiation to almost any point in the spectrum to achieve the optimum excitation conditions for any given element. Also they pointed out that filters can create two excitation regions in a spectrum. An example is the analysis of AgBr with a Mo tube at 49 kV and a Mo filter. The Mo

characteristic lines excite Br and the high energy bremsstrahlung excites Ag with a low background under each peak.

An alternative approach uses secondary target excitation and this has the advantage of providing a better energy spectrum for excitation and lower detection limits. The method is widely used for XRF analysis and described by many authors. Goulding and Jaklevic (1977) used a system developed by Walter et al (1974) for a large scale analysis of air pollution filters. In their system a pulsed X-ray tube with a tungsten anode was used to produce a broad band X-ray spectrum which excites one of the three computer-selectable targets (Ti, Mo and Sm) whose characteristic radiation illuminates the sample. They pointed out that their detection limits were very similar to those obtained by the proton excitation method.

Standzenieks et al (1978) developed an XRF system with a rhodium target and Mo secondary fluorescer for trace element analysis. The system was used for the analysis of orchard leaves and blood samples. Because of the strong absorption of the characteristic X-rays from potassium and calcium in the 30 $mg.cm^{-2}$ sample and because the Mo exciting radiation differs by a great deal from the K absorption edges of these elements, they recommended the use of thinner samples for better evaluation of potassium and calcium. However, samples of less than 30 $mg.cm^{-2}$ are often too fragile to handle. The use of an

exciting radiation which does not differ greatly from the absorption edges of K and Ca (Ti for example) would give a better sensitivity for these elements

Christensen et al (1980) designed an irradiation chamber capable of carrying up to 6 secondary targets. Targets of Ti, Se, Mo, Ag, Te and Sm were employed. The direct beam from a tungsten anode X-ray tube is scattered twice; first by the secondary target and then by the sample. Despite attempts made to reduce the radiation scattered by the secondary target and the sample, by using elliptical collimator holes and shields, their minimum detection limit was above 10 ppm for all the elements. In comparison with other similar systems, the MDL is at least an order of magnitude below 10 ppm. This could be the result of the twice-scattered direct beam.

The application of energy dispersive XRF analysis using Si(Li) detector spectrometers to the problem of atmospheric aerosols has been discussed by Dzubay (1977). More recently, Jaklevic and Thompson (1982) employed pulsed X-ray tube excitation with Ti, Mo and Sm secondary targets in order to perform elemental aerosol analysis of a broad range of elements.

Maximum sensitivity is achieved by this method by employing a fluorescer whose K X-ray energy is slightly greater than the K absorption edge energy of the element to be analysed, but of sufficient energy that the

incoherently scattered radiation does not produce significant overlapping background. This method, however, has the drawback of requiring a high powered X-ray tube to make up for the low efficiency of the fluorescence process, Drummond and Stewart (1980). Also the twice-scattered bremsstrahlung in the secondary target and in the sample has the effect of increasing the detection limits.

The K X-ray beam intensity produced by the fluorescence method is at least an order of magnitude too low for such applications as X-ray crystal diffraction studies or the calibration of certain types of radiation detectors. This led Motz et al (1971) to produce high intensity K X-rays using constant-potential electron accelerators. They observed the K X-rays at large angles with respect to the incident electron direction in the energy region from 0.01 to 4.0 MeV. This is because for thin targets the K X-rays have an isotropic angular distribution while the bremsstrahlung becomes more peaked in the forward direction. There may be many applications in which it is advantageous to use this method but its wide usage depends on the availability of the electron accelerator. However, the ratio of the number of photons in the K_α and K_β lines to the total number of bremsstrahlung photons is about 2.6:1 for Cu and 1.3:1 for Ag for this method, while this ratio is at least 20:1 for 2.6 MeV protons incident on a Ag target.

4.1.2 Excitation by Radioactive Sources

Radioactive sources of suitable energies and half-lives are often used as monoenergetic excitation sources. There are two principal types (Birks, 1969); those that emit gamma rays such as ^{241}Am, ^{125}I, ^{109}Cd, ^{57}Co and those that emit beta particles which are converted to X-rays within the source such as ^{3}H + Ti or ^{3}H + Zr. Rhodes (1966) has tabulated the properties of many of the radioactive sources. Table (4.1) shows some of X-ray and γ-ray sources. The small size they have allows a compact and efficient geometry. Also they operate without external power so they require no associated equipment. The choice of suitable low energy monoenergetic photon emitters of convenient half life is however limited (see Table 4.1), and the photon flux available from reasonable activities is also small. The source emission spectrum often contains peaks in addition to the main exciting peak, and these can interfere with the peaks of interest from the sample. These peaks may emerge from the source itself owing to a complex emission spectrum (eg. ^{241}Am) or they may emerge as fluorescent peaks from the packaging, collimation materials or the sample chamber. Similar restrictions apply if radioactive sources are used to excite fluorescent radiation in secondary targets.

Different methods were used in the above examples to produce nearly monoenergetic photons for XRF analysis. However, the bremsstrahlung associated with the emission spectra using any one of the above methods is considerably

TABLE 4.1

COMMONLY USED LOW ENERGY X-RAY AND γ-RAY SOURCES

Source	Half-life	Useful radiations	Practical emission efficiency, photons per disintegration	Typical activity	Highest atomic number usefully excited, K X-rays
Iron-55	2.7 years	Manganese K X-rays, 5.9 keV	0.15	2 mCi	24 (chromium)
Cadmium-109	1.3 years	Silver K X-rays, 22keV γ-ray, 88 keV	0.8 0.04	1 mCi	43 (technetium)
Americium-241	470 years	γ ray, 59.6 keV γ ray, 26 keV	0.35 0.02	1 mCi	69 (thulium)
Cobalt-57	270 days	γ ray, 136 keV γ ray, 122 keV γ ray, 14 keV	0.10 0.88 0-0.06	0.5 mCi	98 (californium)

higher than that produced by the proton bombardment method. High intensity bremsstrahlung decreases the K X-ray beam purity, which is defined as the ratio of the number of K X-rays to the total photon number integrated over the energy spectrum of the beam. Unfortunately, the majority of authors do not report the purity of the beam used for excitation, so useful comparisons are not possible.

4.1.3 Excitation by Photons Induced by Protons

An alternative approach of producing monoenergetic photons for specimen excitation is to employ light ions, such as protons, to generate X-rays which can then be employed as an exciting source. The spectra obtained in this way contain less bremsstrahlung radiation compared with conventional X-ray generation, Figure (3.2). In addition the spectra contain no scattered radiation as is the case in secondary target excitation. So the useful region of the spectra provided by the photons induced by protons contains less background radiation. The method should, therefore, give better sensitivity as compared to the secondary target method.

This technique was first used by Lin et al (1978). They showed that this (pX,X) technique is a reliable analytical method that can be applied for elemental analysis. Their results were obtained with Cu as an X-ray producing target and liquid samples containing Co and Ni in various ratios. Ni filters of 2.54 μm, 5.08 μm and 7.62 μm thick

were used to suppress the Cu K_β X-rays. They found that a small amount of Co could be detected in the presence of a large amount of Ni. In principle, Ni K lines can be excited by Cu K_β but not by Cu K_α, Figure (4.1). However, the Ni filter they introduced absorbed Cu K_β, thus sensitivity improvement would be expected for Co relative to Ni. This improvement was obtained in comparison with the case where both Co and Ni are excited together. In such a case, the Co peak may be sitting on the tail of Ni peak. However, the fluorescence generated from Ni filter by Cu K_β is not considered by Lin et al (1978). It should be stated here that Ni K_β and not K_α can excite Co K lines (Figure 4.1) and hence affect the Co sensitivity.

This technique could also be used to solve a more complicated problem in analytical work. The secondary fluorescence of an element present in small amounts excited by the K lines of an element present in large amounts in a sample could be prevented if the exciting radiation is selected properly. This problem could be demonstrated by preparing a sample containing small amounts of Fe and large amounts of Ni. In this case, Fe is excited first by the primary radiation and second by the Ni K lines from the sample upon the application of broad X-ray exciting spectrum. This is because all K X-rays of Ni can excite Fe. So the application of Cu K X-rays as exciting radiation causes Fe to be excited by all the K lines of Cu and Ni by the K_β X-rays of Cu only.

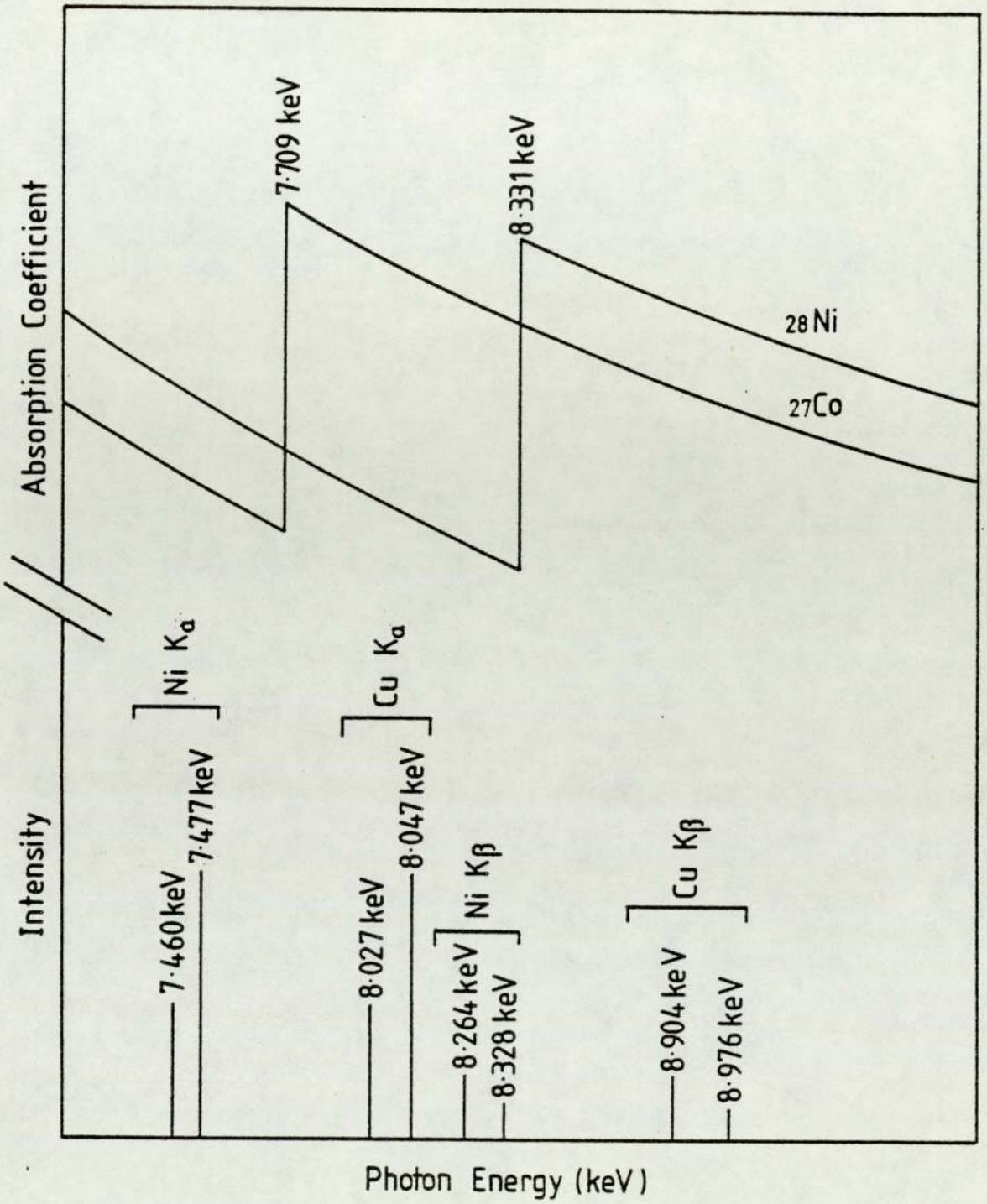

Figure (4.1) K lines of Cu and absorption coefficients of Co and Ni as a function of photon energy

This technique could provide a solution for a number of problems. For example, in the PIXE analysis of steel surfaces, the detection sensitivity for Mn is limited due to the presence of strong K X-rays from the iron, Ahlberg et al (1975). This problem could possibly be solved by the use of Co K X-rays as the exciting radiation.

A second problem, but in the biological field, is the analysis of human biological organs by PIXE where an uncertainty in the presence of Ti in blood, spleen and liver is reported by Guffey et al (1978). This is because an escape peak caused by the large concentration of Fe in these samples occurs at the energy of Ti making its presence uncertain. This interference can be avoided by the use of K X-rays of Cr, Mn or even Fe as the exciting source.

This technique is especially suitable for partial improvement of sensitivity because of the selective nature in excitation. Selection of exciting X-rays provides a possible solution for the detection of small amounts of trace elements when large quantities of neighbouring elements are present. If different exciting energies are available then many elements in the specimen can be detected with similar sensitivity.

4.2 EXPERIMENTAL ARRANGEMENT FOR XRF

The experimental arrangement first employed for proton induced XRF was based on the radiography system discussed

in section (3.3). A schematic diagram of the experimental beam line employed is shown in Figure (4.2). Three apertures A_1, A_2 and A_3 each of 1 cm diameter preceeding the target chamber served to collimate the beam. The aperture A_1, at 87 cm from the target was a water cooled copper aperture. The two tantalum aperture A_2 and A_3 were at 14.6 cm apart. Aperture A_3 was at 9.6 cm from the target. Another tantalum aperture A_4 of 1.4 cm diameter was connected electrically to the target and prevented the loss of secondary electrons and backscattered protons. The beam on the target after collimation was an elliptical spot of approximately 1.4 cm^2. The elliptical shape results from the target being mounted at 45^o.

The target chamber was electrically isolated from the main beam line and acted along with aperture A_4 as a Faraday cage, facilitating the measurement of the beam current. The number of protons incident on the target was measured by integrating the charge collected in the target chamber, using a Keithley electrometer.

The primary X-rays of the target passed through the 50 μm thick Melinex window to the sample position. An aluminium absorber was placed at the outer side of the Melinex window to reduce the high intensity of low energy X-rays. Samples were positioned at 45^o to the direction of the exciting radiation. The fluorescent X-rays from samples were detected with Si(Li) detector positioned at 90^o to the direction of the exciting

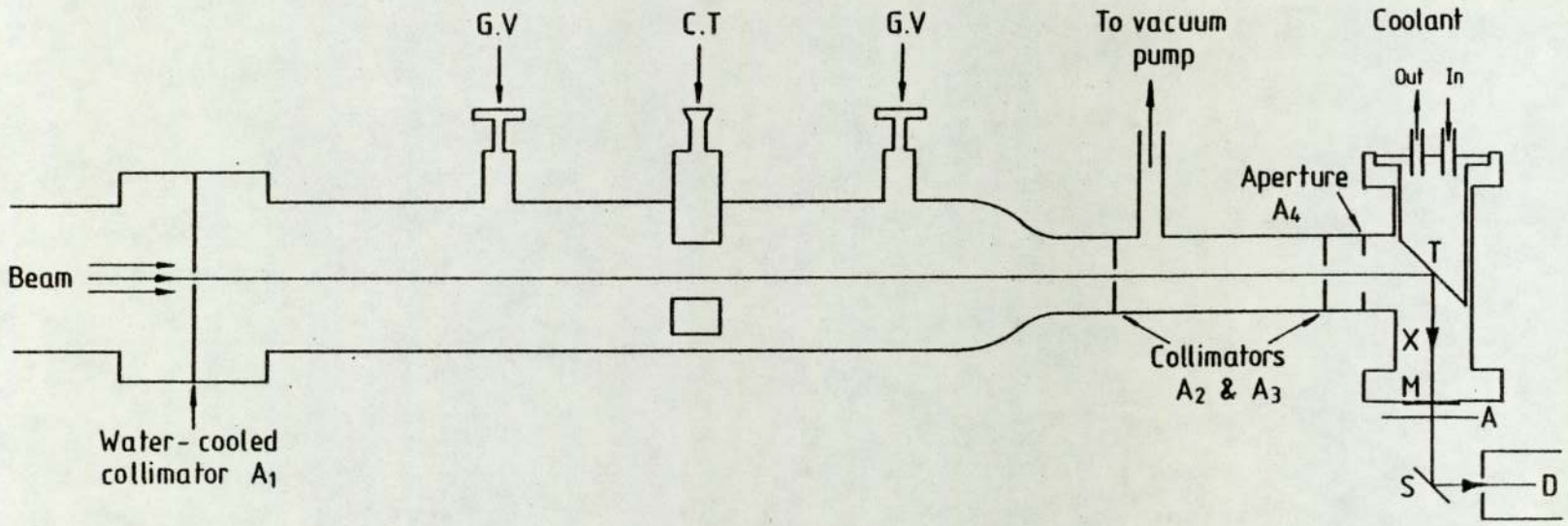

KEY

G.V	Gate valve
C.T	Cold trap
T	Target
X	X-ray
M	Melinex window
A	X-ray absorber
S	Sample
D	Si (Li) detector

Figure (4.2) Schematic diagram of the experimental set-up for XRF analysis

radiation as shown in Figure (4.2).

The time required to replace the target and to attain working vacuum was typically one hour. Refilling the target chamber with inert gas instead of exposing it to atmosphere before opening the chamber was found to be very useful to attain the vacuum in the shortest possible time.

4.3 DETECTION OF Mo USING X-RAYS INDUCED BY PROTONS

In order to obtain an indication about the potential of using proton induced characteristic X-rays for elemental analysis, preliminary experiments were carried out on the detection of Mo using the experimental beam line employed for the radiography work described previously.

A preliminary experiment was performed to detect various amounts of Mo in ammonium molybdate solution. Various amounts of Mo ranging from 20 to 1000ppm in ammonium molybdate solution were prepared.

Initially one litre stock solution of 1000ppm of Mo was prepared by dissolving the appropriate amount of $(NH_4)_2MoO_4$ in distilled water. Then a volume V_1 from the stock solution was taken and diluted with distilled water to obtain 50 cc volume of normality N_2. The volume V_1 was calculated from the expression:

$$N_1 V_1 = N_2 V_2$$

where N_1 = Normality of stock solution in ppm

V_1 = Volume taken from stock solution

N_2 = Normality of new solution

V_2 = Volume of new solution

Samples containing different concentrations of Mo were put into polystyrene cylindrical tubes with a polystyrene cover. Each sample tube contained an equal volume of 4.7 cc of solution.

The mass attenuation coefficients (μ/ρ) of polystyrene $(C_8H_8O_2)$ was evaluated from the coefficients (μ_i/ρ_i) for the constituent elements according to the weighted average:

$$(\mu/\rho) = \sum_i W_i(\mu_i/\rho_i) \qquad \text{(Bragg Additivity Rule)} \qquad (4.1)$$

where W_i is the proportion by weight of the i th constituent.

Assuming a parallel exciting X-ray beam, the transmission of Mo K X-rays through the wall of the polystyrene cylindrical tube was calculated to be 93%.

X-rays were produced at the Ag target by bombarding it with 10 μA of 3 MeV protons. The 1 mm thick Ag was mounted on a water-cooled copper anode, Figure (4.2). Samples in the cylindrical tubes were positioned at 90^o to the direction of the incident proton beam and placed on a perspex sheet 7 cm from the Melinex window. The fluorescent

X-rays from samples were detected with a Si(Li) detector placed at 7 cm from the sample and positioned at 90^{o} to the direction of the exciting radiation.

The time needed for each sample was determined by the number of Mo K_{α} photons emitted from each sample which gave a precision of 2-5% for 1000-40ppm solution respectively. The number of Mo K_{α} photons depends on the concentration of Mo present in each sample. For example the time required for 1000ppm sample was about 2 minutes while 40 minutes was required for 40ppm.

The number of photons in the K_{α} peak per μC of charge on target was plotted against the Mo concentration in ppm and the result is shown in Figure (4.3). The linear relationship between the number of K_{α} X-rays emitted (i.e. intensity) and the concentration of Mo in the sample is obvious.

The detection limit of Mo in the solution is greatly affected by the geometry of the specimen and its container in addition to the specimen supporting material and beam current employed. The minimum detection limit MDL is estimated for Mo to be 30ppm for 20 minutes and 10 μA. This MDL can be reduced by exploiting the maximum current of 2 mA that could be extracted from the accelerator. The concentration of many trace elements likely to occur in biological materials are less than 30ppm. For example, Cu, Zn and Br concentration in human whole blood are

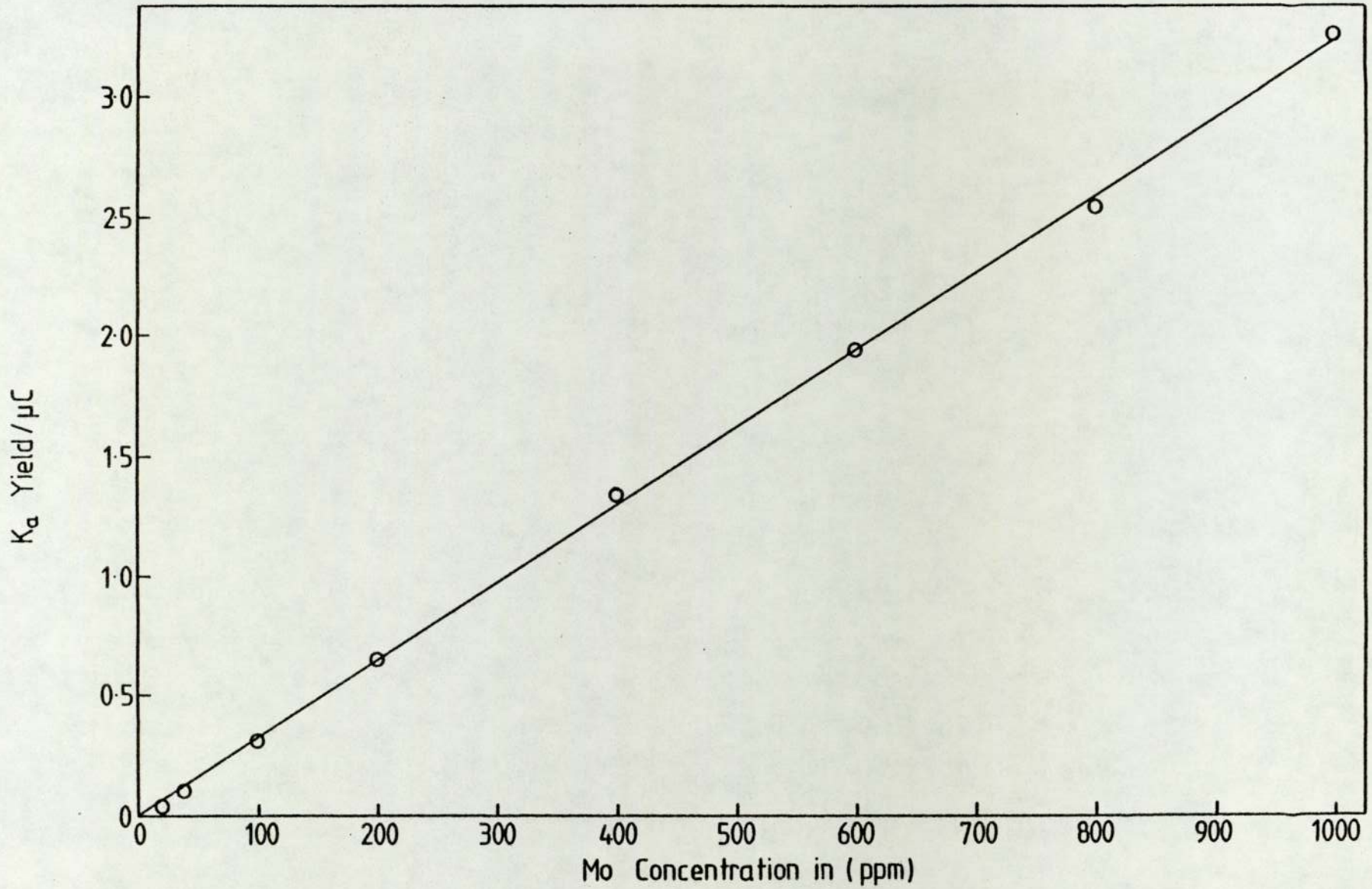

Figure (4.3) Variation of X-ray intensity with concentration
Error bars were omitted since they were smaller than the symbol size

(0.64-1.28), (4.8-9.3) and (1.3-8.1) ppm respectively, Iyengar et al (1978). The system as it stands, is incapable of measuring these elements. So efficient quantitative analysis of such elements requires improving the way of presenting the specimen to the primary X-ray beam as well as the availability of a number of exciting energies. This is described in section (4.4).

4.4 ROTARY TARGET CHAMBER AND SAMPLE-DETECTOR GEOMETRY

Specimens for elemental analysis are analysed with better sensitivity and efficiency by a sequence of mono-energetic photons. With this requirement, the target chamber used for radiography was inadequate for X-ray fluorescence analysis because it was designed to accommodate only one target at a time. Changing the target is a relatively lengthy process since the target is mounted in vacuum. Thus a necessity arose for making a target chamber capable of carrying a number of targets and bringing them one at a time in front of the beam.

A high power water-cooled anode chamber based on proton induced X-rays as the exciting source was constructed and is shown in Figure (4.4). The chamber walls were made of 2 mm thick stainless steel tubes. Targets of spectroscopically pure, Ag, Mo, Zr, Cu, Fe and Ti were mounted on the anode at an angle of 45^{o} with respect to the incident proton beam. The anode was made of copper. The cooling of the anode cannot be done via two adjacent tubes attached to the anode because of its rotation. Thus

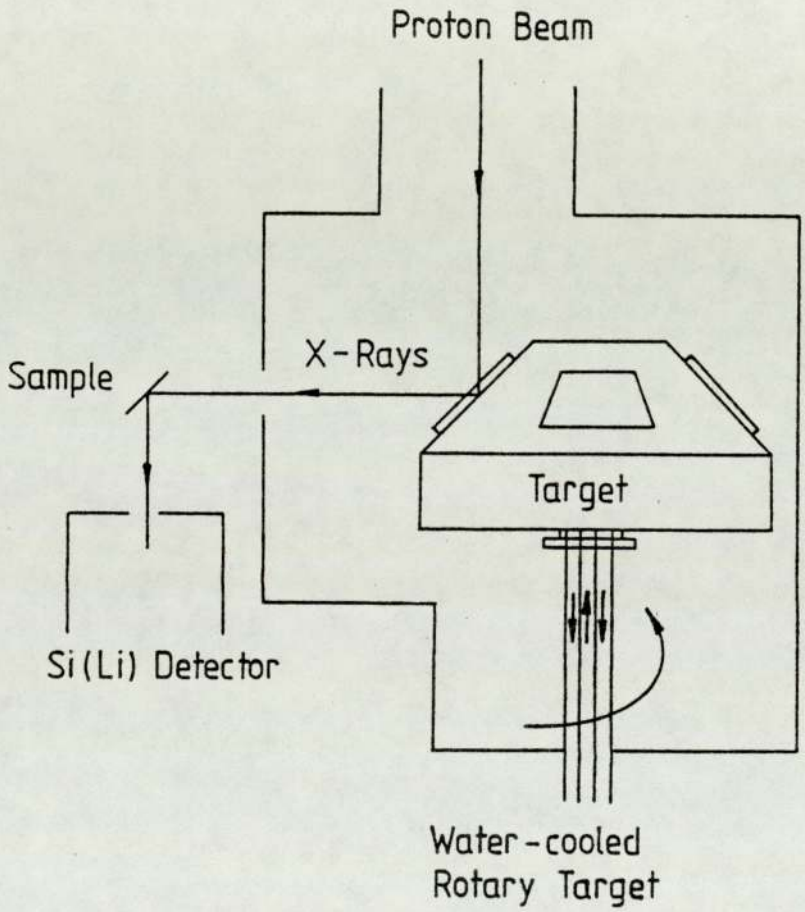

Figure (4.4) Schematic diagram of the experimental arrangement.

two concentric tubes were constructed and fitted to the anode. In order not to disturb the chamber vacuum and hence the beam line vacuum during the anode rotation, two rubber 'O' rings (A) shown in Figure (4.5) were fitted to the rotation shaft carrying the anode. The hollow cylinder surrounding the part of the rotating shaft inside the target chamber stops the anode from sliding down and from vibrating during rotation. The vacuum test of the target chamber proved no leakage from the anode rotation. A window of 50 μm thick Melinex was fitted to the chamber through which the X-rays passed to the sample position. An aluminium absorber was placed at the outer side of the Melinex window to reduce the high intensity of low energy X-rays.

The target chamber was connected to the accelerator beam line shown in Figure (4.2). The six targets can be positioned either manually or remotely from the computer room. The remote control was performed via two magnetic slips; one attached to the target mount and wired to the other which was located in the computer room. Targets could then be brought sequentially to a position of 45^{o} to the incident beam. An adjustable support was constructed to accommodate the target chamber and its accessories.

Samples to be analysed were usually in pellet form and were sandwiched between two pieces of Melinex and mounted in standard 35 mm slide mounts and positioned at 45^{o} to the direction of the exciting radiation. The slide was mounted

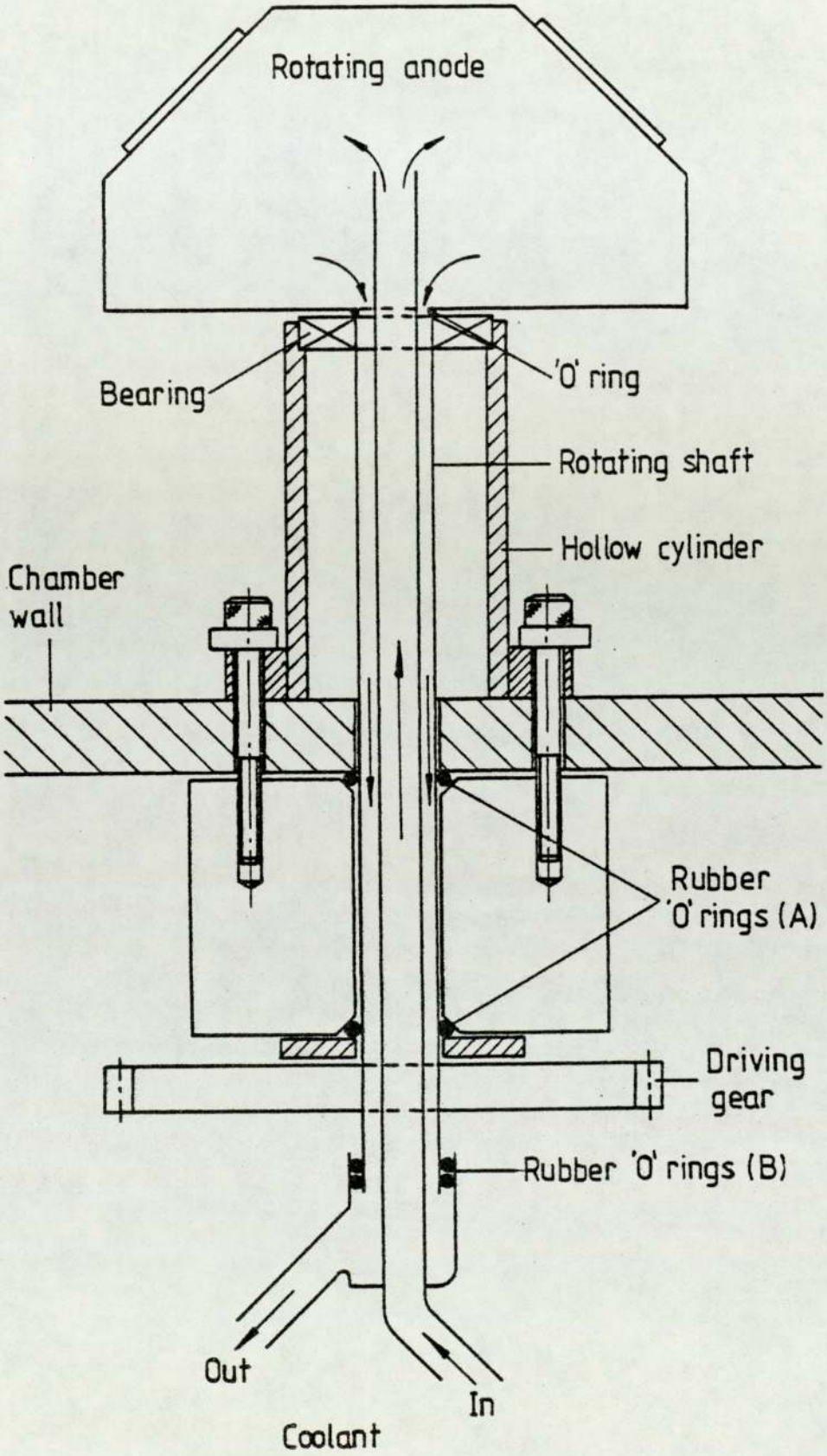

Figure (4.5) Cross-sectional view of the target rotating system

in a perspex compartment attached to the target chamber where it could be brought to a fixed point with the help of a perspex stop, such that its centre was opposite the direction of the exciting radiation. The fluorescent X-rays from samples were detected with a standard Si(Li) detector also positioned at 45^{o} to the sample.

Considerable care was required in selecting the material for the specimen support since it had to be free from impurities which could interfere with the signal from the specimen . The Melinex used initially to support the specimen was found to give a large Cl peak in the recorded spectra. This peak interferes with the Cl peak that might be present in the specimen. Thus a search for another supporting material was carried out and Kimfoil was found to contain neither Cl nor any other element above the Cl on Z scale at the level of MDL. The Melinex window used for the target chamber was proved to contain no Cl. This latter Melinex was obtained from different manufacturer. A photograph of the irradiation facility is shown in Figure (4.6).

The fluorescent X-rays from samples were detected with a Si(Li) detector positioned at 90^{o} to the direction of the exciting radiation. The reproducibility of the detector re-positioning is necessary for accurate XRF work. Therefore, the detector was kept rigidly in a fixed position at 45^{o} with respect to the sample position and subtended a solid angle of 0.0081 steradian at the

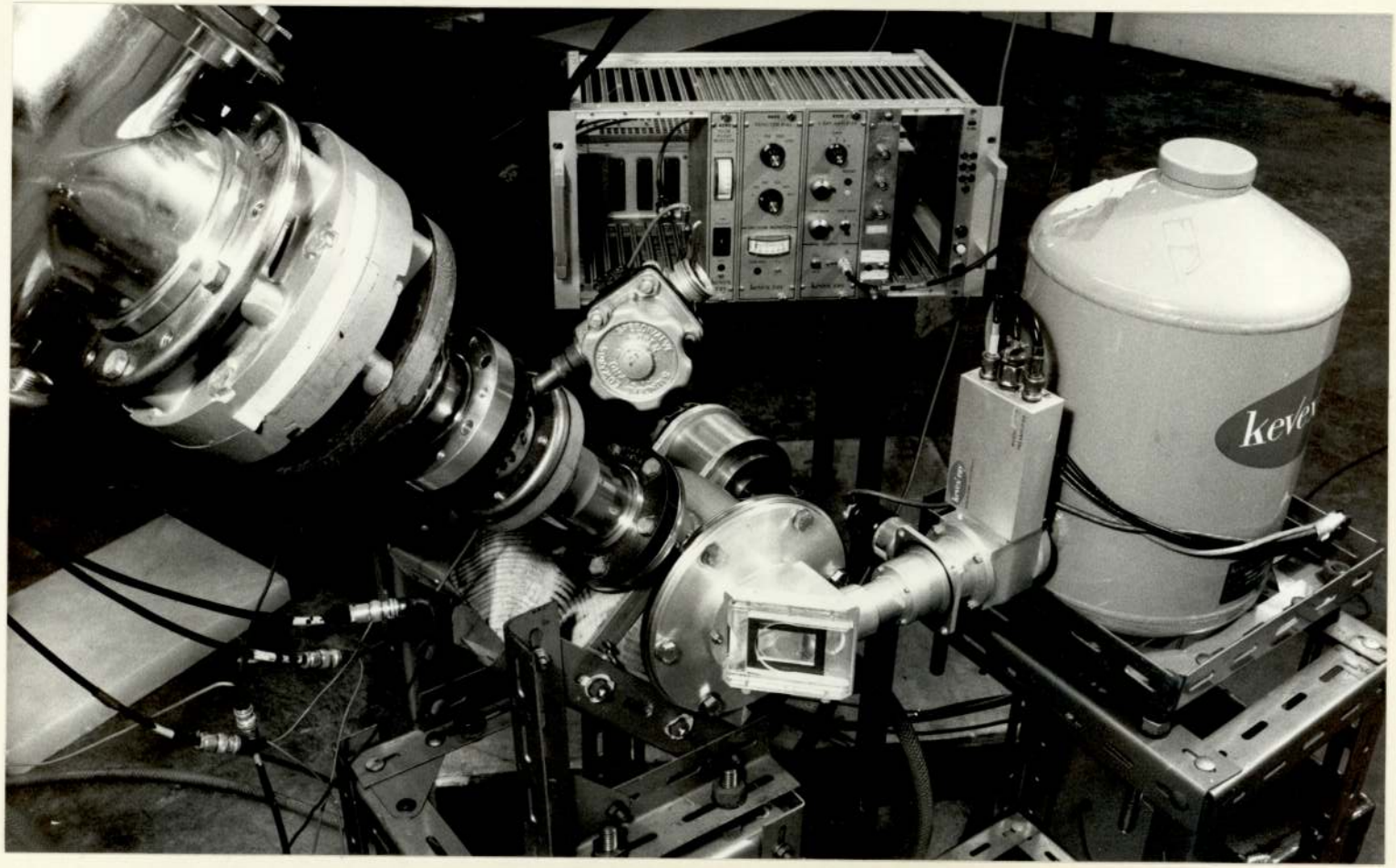

Figure (4.6) A photograph of the (pX,X) irradiation facility.

centre of the sample. The geometry was fixed by bringing the detector head inside a cup-like aluminium aperture which was designed and made especially for this geometry and positioned at 45^{o} with respect to the sample and fixed with part of the sample holder. A constant air gap of about 4 cm was maintained between the centre of the sample and beryllium window.

4.5 DATA ACQUISITION AND ANALYSIS

4.5.1 Data Acquisition

The data acquisition system used in the present work has been described by R.Khan (1975), O.R.Khan (1979) and Saied (1981) and only a brief description will be given here.

A schematic representation of the main components of the data processing system is shown in Figure (4.7). X-rays produced by proton bombardment of the target were used to excite fluorescent radiation from the sample. X-rays leave the target chamber and pass through approximately 4 cm of air before exciting the specimens. Specimens were at an angle of 45^{o} with respect to both incident radiation and the detector. X-rays leaving the specimen pass through approximately 4 cm of air before entering the 12.5 micron beryllium window of the detector. Each photon entering the Si(Li) detector gives rise to an electrical pulse which is proportional to the energy of the X-ray. These charge pulses were then collected by

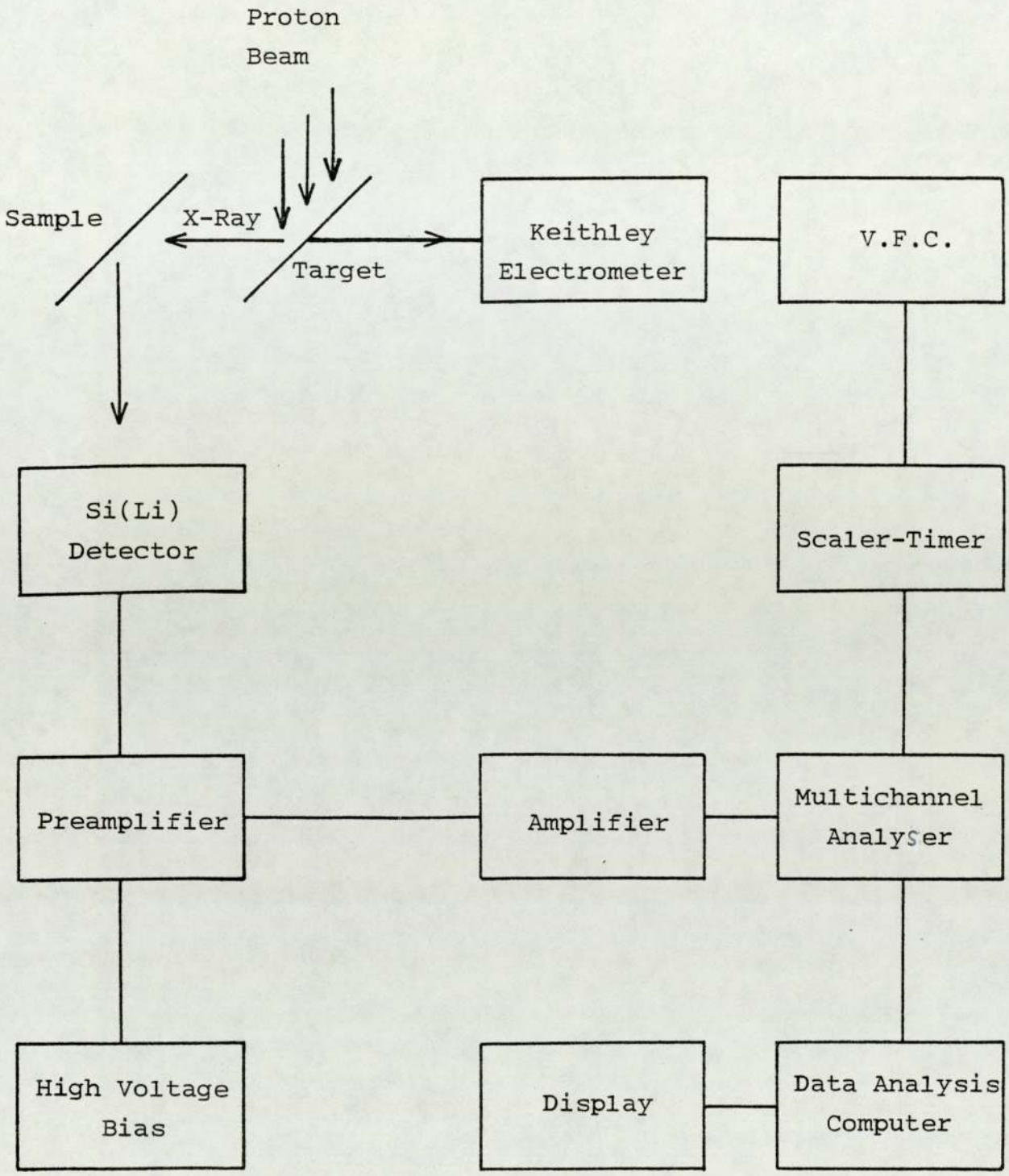

Figure (4.7) Electronic block diagram for X-ray detection and data processing.

the applied potential of 1000 V. The preamplifier which is an integral part of the detector assembly, converts the charge pulse into a voltage signal using a cooled field effect transistor (FET), while keeping the proportionality between the energy deposited and the pulse height. Pulsed optical feedback was provided to maintain the dc level. The output of the preamplifier was coupled to a spectroscopy amplifier where the pulses were shaped and amplified before being allowed to proceed to a multichannel pulse height analyser, where the ADC sorted the input signals according to pulse height into 2048 channels. This computer based data acquisition system was interfaced to Hewlett-Packard 2100 computer. A display unit working in conjunction with the ADC provided a visual display of the spectrum being accumulated. This helped greatly in deciding whether to continue an experimental run by observing the intensity of a desired peak in the spectrum.

The total charge collected on target was fed into a current integrator which outputs a voltage pulse for the charge collected. These voltage signals were fed to a Voltage to Frequency Convertor VFC, which produces a pulse chain of 10^5 Hz for 1 volt input. The output of VFC was again fed to a scaler through a thousand dividing unit to make it suitable for counting. The scaler and the divider were interfaced with an automatic stop device, to stop the accumulation of data once a preset count on the scaler had been reached, which was directly

proportional to proton charge. Spectra were accumulated for a preset charge since the beam intensity could vary with time.

The spectrum obtained at the end of an analysis was stored on a file manager (FMGR) which is a system for storing source information. Spectra stored on the (FMGR) were transferred to a magnetic tape for further analysis at a later time.

The on-line computer programme which controlled data acquisition provided the capability to analyse data from one of the spectra previously stored while the next X-ray spectrum was being accumulated.

4.5.2 X-ray Detection System

The semiconductor detector used was a Si(Li) detector directly coupled to a pulsed optical charge sensitive preamplifier. The Si(Li) detector (Kevex, 3201 cryogenic sub-system) comprised of a disc of 30 mm^2 area and 3 mm thick silicon crystal, drifted with lithium impurity atoms. The detector and first stage of the preamplifier are cooled to liquid nitrogen temperatures to reduce thermal noise and prevent diffusion of the lithium through the crystal. The lithium creates an intrinsic region within the silicon which can be regarded as a solid state ionization chamber. X-rays absorbed in this region lose their energy by excitation and ionization of the absorbing atoms, thus producing electron-hole

pairs. On average, the energy required to produce an electron-hole pair is 3.62 ev, (Khan and Crumpton 1981), in silicon at room temperature and is independent of the incident X-ray energy. The electron-hole pairs created are collected by the application of 1000 V across the intrinsic region. If a photon of energy E is absorbed in such a detector the number of electron-hole pairs produced, n, is given by:

$$n = \frac{E(\text{in ev})}{3.62} \qquad (4.2)$$

From which the total charge deposited in the crystal can be deduced. Hence, the charge collected is linearly proportional to the energy of the X-ray absorbed in the detector.

The detector has a 12.5 μm beryllium window to protect its vacuum. The parameters related to the performance of Si(Li) detector are as follows:

4.5.2.1 Detector Efficiency

The detector efficiency for the detection of X-rays should be known as a function of the photon energy for the calculation of any trace element present in a specimen. Assuming a narrow beam geometry, the detection efficiency can be approximately calculated using the expression:

$$\varepsilon = (1 - e^{-\mu_{Si} X_{Si}}) e^{-\mu_{Be} X_{Be}} \qquad (4.3)$$

where μ_{Si} and μ_{Be} are the absorption coefficients of the

silicon and beryllium respectively, and X_{Si} and X_{Be} are the thicknesses of the silicon crystal and beryllium window respectively.

The detector efficiency as a function of energy is shown in Figure (4.8). This was calculated using 12.5 μmBe window and silicon diode of 3 mm thickness only. The fall in efficiency at low and high energy is clear. Low energy photons are attenuated by the beryllium window before reaching the sensitive region, this causes a fall in the efficiency. For photons in the energy range of about 4-15 keV the crystal absorbs all the photons and the efficiency is 100%. For energies above 15 keV the increased transmission of the X-rays through the crystal causes a drop in the detector efficiency.

For the present analysis, the use of the calibration factor F'_{xz}, see section 5.1, eliminates the need to know the detection efficiency ε absolutely.

However, if the efficiency is required to be known absolutely then it should be measured experimentally. Many approaches have been used to measure the efficiency of Si(Li) detectors experimentally. The absolute emission rates of X-rays and gamma rays from calibrated radioactive sources have been employed by Hansen et al (1973) to determine the efficiency with a precision of 5% above 6 keV and 10% from 3 to 6 keV. Johnson et al (1978) measured the efficiency of a Si(Li) detector by using the fluores-

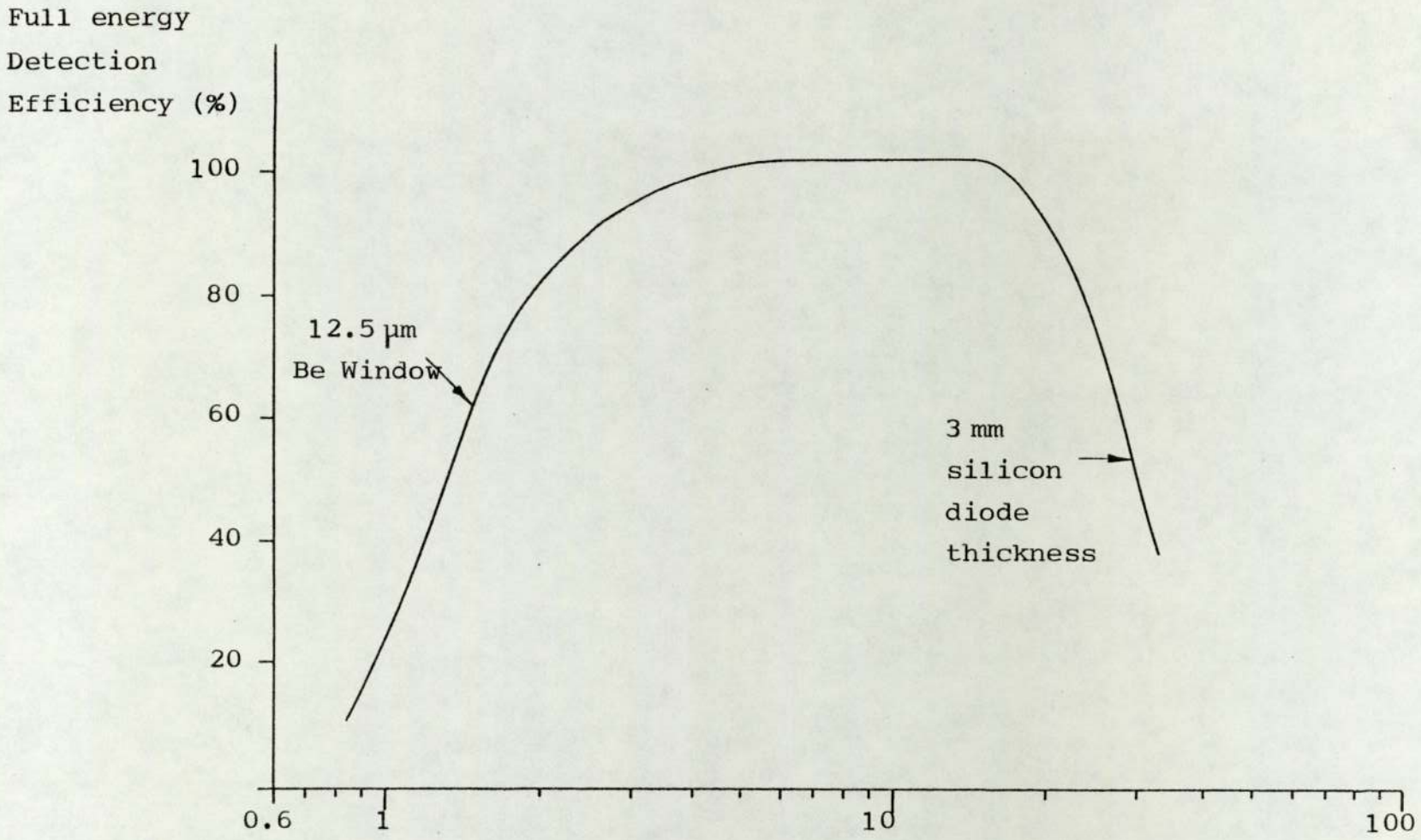

Figure (4.8) Detection efficiency of the Si(Li) detector with 12.5 μm Be window and 3 mm silicon diode

cent radiation from a series of targets exposed to the 59.5 keV photons from a 10 mCi ^{241}Am source. An overall uncertainty of $\pm$3% was estimated for the energy range 5 to 30 keV. This method is clearly convenient and does not deal with large numbers of radioactive sources. The absolute emission rate of the fluorescent radiation was obtained from a calibrated NaI(Tl) detector.

4.5.2.2 Detector Resolution

The high resolution of a Si(Li) detector makes it ideal for XRF analysis. The energy resolution of the detection system is a measure of its ability to distinguish between K_α X-rays of neighbouring elements in the periodic table. The resolution is defined as the full width of the energy peak at half maximum intensity (FWHM), and was measured as 162 eV at 5.898 keV at a counting rate of 1000 cps.

The effective resolution of the detector system is limited by the noise and count rate capability of the associated electronics. Therefore, the total resolution is the sum in quadrature of the intrinsic and electronic noise effects (Woldseth, 1973):

$$(FWHM)^2_{total} = (FWHM)^2_{detector} + (FWHM)^2_{noise}$$

$$(FWHM)_{total} = \left[(2.35)^2 F\varepsilon E + (FWHM)^2_{noise}\right]^{\frac{1}{2}} \quad (4.4)$$

where F = Fano factor (dimensionless)

ε = The average energy required to create an electron-hole pair in silicon at liquid nitrogen temperature and equals 3.62 eV.

E = The photon energy in eV.

The constant 2.35 relates one standard deviation of a Gaussian distribution σ to the FWHM.

The variation of the resolution with the energy of the detected photon is shown in equation (4.4). The resolution of the detection system is evaluated for different energy photons, since FWHM = 2.35σ , equation (4.4) becomes:

$$(\sigma^2)_{total} = (F\varepsilon)E + \left\{\frac{(FWHM)_{noise}}{2.355}\right\}^2 \qquad (4.5)$$

The resolution has been measured for 8 elemental standard foils. Figure (4.9) shows a plot of σ^2 versus energy. The value of F was calculated to be 0.103 ± 0.005, and it agrees reasonably with the experimental values of Musket (1974), Jaklevic and Goulding (1971) and Zulliger and Aitken (1970). The value of $(FWHM)_{noise}$ obtained from Figure (4.9) is 59 eV.

Energy separation for K_α lines of adjacent elements and K_α and K_β lines of intermediate and high Z elements is such as to be resolved with the present system. However, interference occurs for K and L lines of widely different Z or overlapping K_β line of an element Z with the K_α line of the element (Z+1) as discussed in section (4.6.3).

4.5.2.3 Detector Linearity and Energy Calibration

The detector linearity is tested by calibrating the detector system using different X-ray energies. The

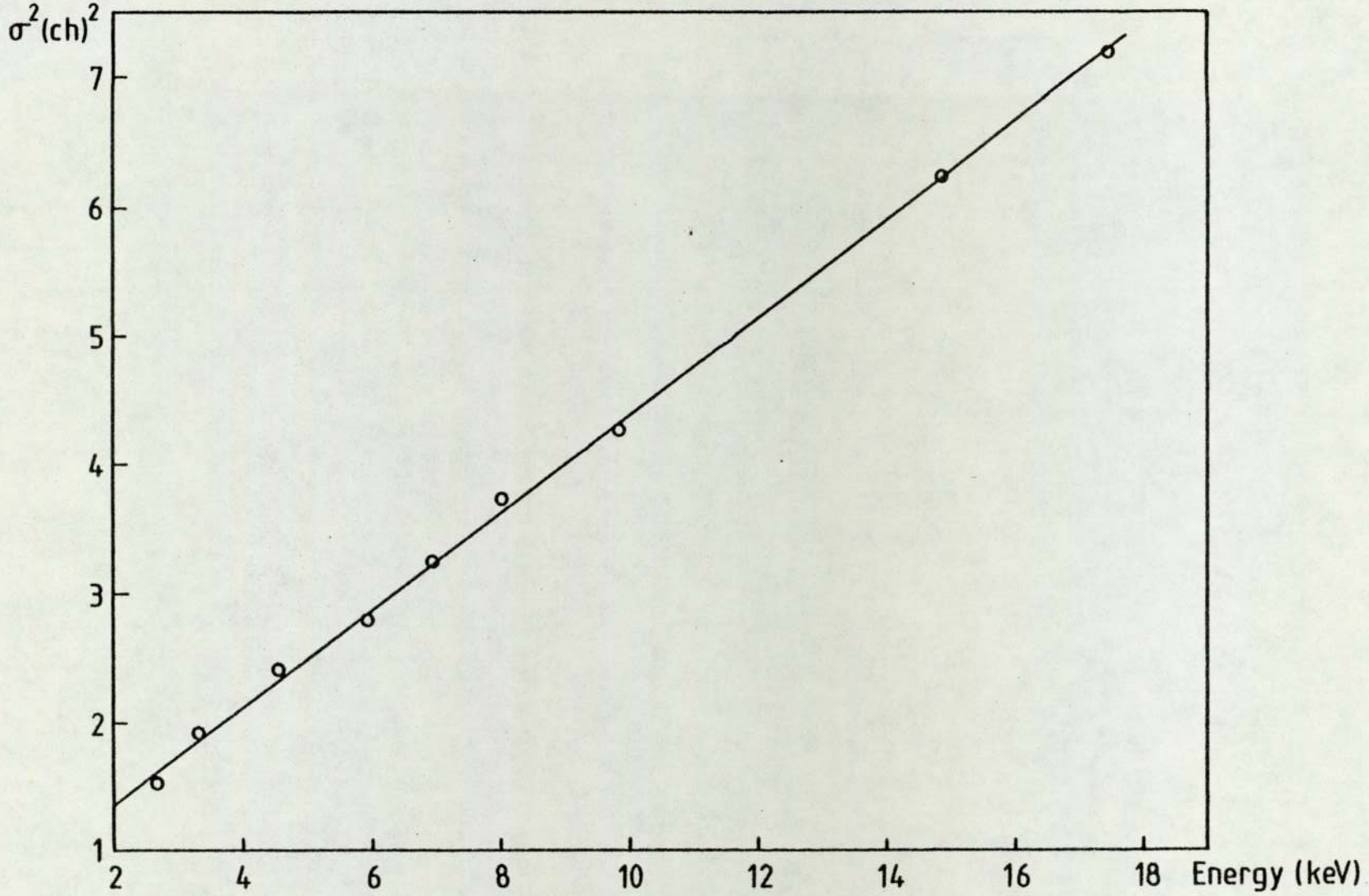

Figure (4.9) A plot of σ^2 vs X-ray energy presenting the measured FWHM resolution for the present system (where FWHM = 2·35 σ)
Error bars were omitted since they were smaller than the symbol size

output of the detector system should be linearly proportional to the incident radiation energy.

Variable energy X-rays obtained from a 10 mCi ^{241}Am ceramic sealed primary source of 59.5 keV gamma radiation with six different targets were used for establishing the relationship between the X-ray energies and their respective channel number (Figure 4.10).

The energy calibration was regularly checked from the characteristic X-rays emitted from the standard foils by photon excitation.

The least square method was used to calculate the slope and the intercept of the calibration line. Centres of different peaks in a spectrum were used to find their corresponding X-ray energy using this line. Elements in the sample are then found from the dependence of the characteristic X-ray energy on Z.

4.6 THE LIMITATION ON X-RAY DETECTION

The analysis of X-ray spectra using Si(Li) detectors is limited by a number of factors as detailed below.

4.6.1 Incomplete Charge Collection: The incomplete charge collection in the crystal periphery of the detector causes background in the X-ray spectra. This background results from the escape of photoelectrons produced in the detector and the emission and escape of bremsstrahlung

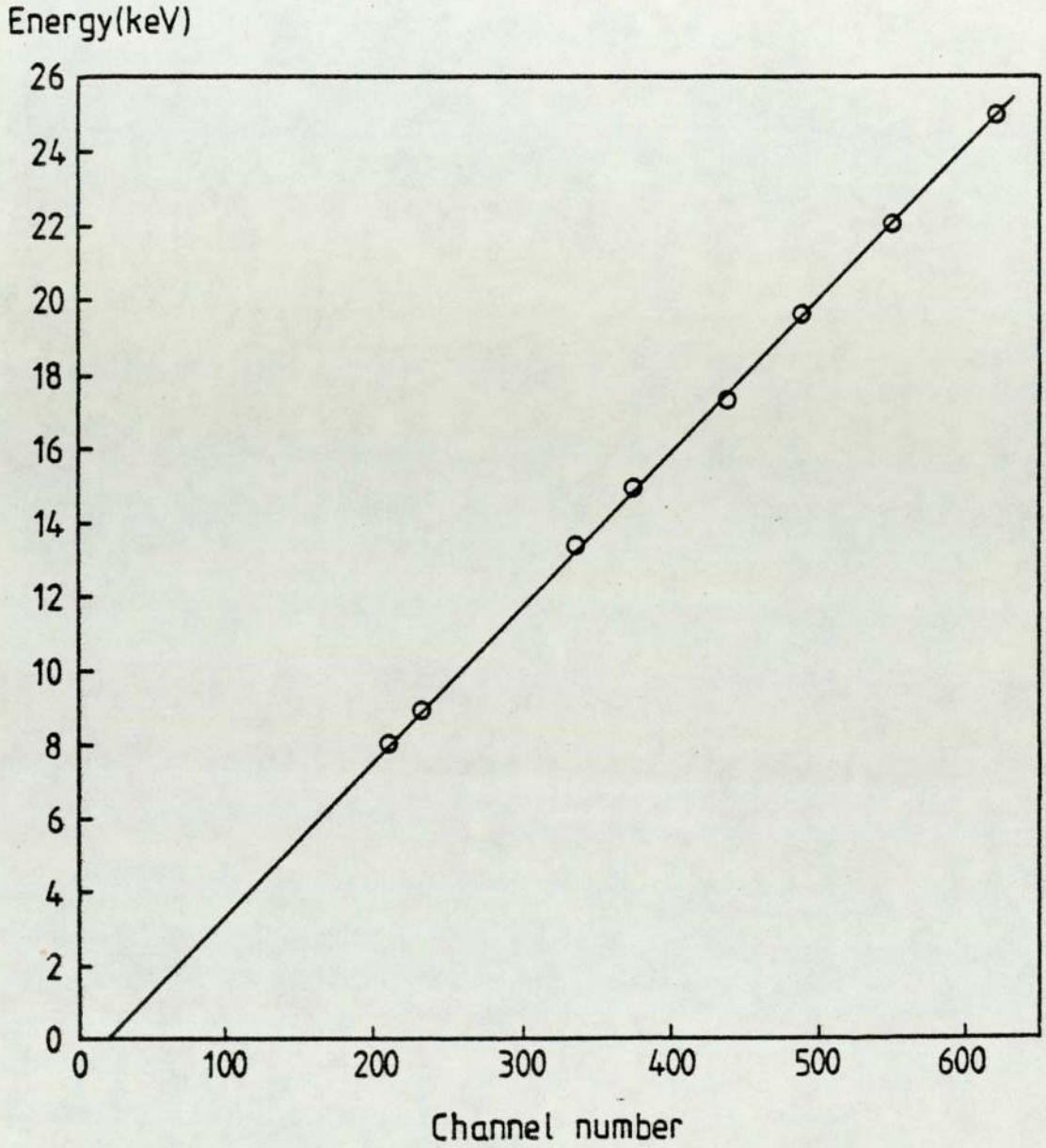

Figure (4.10) Energy calibration curve
Error bars were omitted since they were smaller than the symbol size.

photons produced by these electrons.

The generation of a Si escape peak can affect both the background and peak identification. If the incoming photon of energy E ionizes the K-shell of a Si atom, K X-rays of the Si are generated and usually interact in the intrinsic region, resulting in the complete transfer of energy. If the energy E is low (less than about 10 keV), there will be a significant number of these interactions occurring near the entrance surface of the detector where there is a high probability of Si K X-rays escaping the intrinsic region. Thus the enrgy (E-1.74) keV instead of E is deposited in the detector where 1.74 keV is the energy of the Si K_{α}.The escape peak intensity relative to the characteristic X-ray intensity decreases as a function of increasing X-ray energy, Cooper (1976). It should be noted that Si K X-ray escape would cause only weak peaks just below strong spectral features, but can not contribute a general background. The relative size of the Si escape peak compared with that of a photopeak is in the order of, or less than, 1%, Sioshansi and Lodhi (1979). Thus an escape peak can only be detected if the intensity of the incident X-ray is high.

Biological samples usually do not contain high elemental concentration required to generate detectable escape peaks. These peaks were not observed in the spectra of bovine liver, hair and blood samples.

4.6.2 Counting Rate: Another limiting factor in the use of solid state detectors is their counting rate capabilities. If two X-rays of energy E_1 and E_2 are interacting simultaneously in the intrinsic region of the detector, the voltage pulse V generated will be proportional to the sum of the two X-ray energies $(E_1 + E_2)$ and a peak will develop in this region of the spectrum which is called a sum peak. The detection of more than one X-ray photon at the same time is a random process, the probability of which depends primarily on the counting rate of the two X-rays summed. If E_1 and E_2 are of equal intensity, three sum peaks of equal intensity are possible, $E_1 + E_2$, $2E_1$, $2E_2$, Cooper (1976).

A sum peak, also known as pulse pile up, increases the problems in analysing a spectrum. One of its serious features is the pile up continuum which extends from just above the characteristic X-ray peaks to the pile up peaks which represent an energy equivalent to twice the original peak energy. This background continuum limits the detection for elements in this energy region.

Pulse pile up may be eliminated or minimized by reducing the counting rate either by lowering the current or by using filters to absorb preferentially the lower energy peaks being summed. The use of a pile up rejector reduces the pulse pile up phenomenon but does not eliminate it entirely, it also contributes to overall uncertainty of the system due to the associated dead

time correction. Further, pulse pile up problems can be improved by the application of on-demand beam pulsing, Cahill (1975).

4.6.3 Resolving Power: The resolution of the system was adequate to resolve K_α lines of adjacent elements and K_α and K_β lines of intermediate and high Z elements except those below potassium. However, in the biological samples analysed in the present work, interference between the K_β and K_α lines of the elements with Z and (Z+1) respectively was found to occur in two similar cases. A significant interference was found from the overlapping of Cu K_β with Zn K_α lines which occur at the same energy (within the system resolution). No interference occurs with Cu K_α X-rays. Using the K_β/K_α ratio (Table 5.3), the Cu K_β X-ray yield can be determined from the Cu K_α X-ray yield. Thus the Zn K_α X-ray yield may be calculated by subtracting the Cu K_β X-ray yield from it. The second similar case was the overlapping of Ar K_β with K K_α lines and was solved in a similar manner to the previous case.

The other possible kind of interference is the overlapping of L lines of a heavy element with the K lines of a light element. This can be solved by measuring the nonoverlapped line from either element and calculating the overlapped line of the same element using the appropriate K_β/K_α or L_β/L_α intensity ratio. Thus the intensity of the overlapped line from the other elements can be calculated.

CHAPTER FIVE

CALIBRATION, SENSITIVITY AND REPRODUCIBILITY

5.1 SYSTEM CALIBRATION

The ability to perform quantitative measurements with an X-ray fluorescence spectrometer is limited to the accuracy with which the output, in terms of counts/sec. can be converted into mass concentration, in terms of $\mu g/cm^2$. The task of calibration involves the determination of sensitivity factors for each element of interest.

In addition to the basic character of our system in performing quantitative analysis, qualitative information and the relative quantities of elements present in the specimens may be determined on line during the collection of data. The determination of absolute mass or mass concentration of an element in a specimen requires the system to be calibrated. X-ray intensities can then be related to the amounts of elements present in the specimen. The number of K X-rays N_x arriving at the detector per second from an element Z present in a thin foil is related to the number of K X-rays N_x' produced in the foil per second by:

$$N_x = N_x' \frac{d\Omega}{4\pi} \qquad (5.1)$$

where $d\Omega$ = detector solid angle.

In a thin foil the K fluorescent radiation generated in it suffers negligible attenuation in emerging.

Assume a parallel beam of monoenergetic X-rays incident normally on a thin foil, and assume that the incident beam is large enough to cover the foil. The number of K X-rays N_x' produced in the foil per second equals the number of incident X-rays (dI) absorbed in the foil per second times the fluorescent yield (ω_K):

$$N_x' = dI\,\omega_K \tag{5.2}$$

If I_o and I are the incident and emergent primary X-ray intensity per second, then:

$$dI = I_o - I = I_o(1 - e^{-\tau\rho t}) \tag{5.3}$$

where τ = total photoelectric mass attenuation coefficient in cm^2/g

ρt = areal density of the foil in g/cm^2

If $\tau\rho t$ is very small, equation (5.3) reduces to:

$$dI = I_o\tau\rho t \tag{5.4}$$

The fraction of the absorbed intensity which leads to K shell ionization is $\tau(\tau_{K,L} - \tau_L) / \tau_{K,L}$ where $\tau_{K,L}$ is the total photoelectric mass attenuation coefficient for the K shell plus all other lower energy shells, and τ_L is the mass attenuation coefficient for the L shell plus all other lower energy shells. This fraction can be written as $(1 - 1/J_{K,L})$ and is valid when the energy of the absorbed intensity does not differ greatly from

that of the absorption edge. $J_{K,L}$ is the ratio of the photoelectric mass attenuation coefficient on the high and low energy side of the K absorption edge. Thus equation (5.2) becomes:

$$N_x' = I_o \tau (1 - 1/J_{K,L})(\rho t)\, \omega_K \qquad (5.5)$$

Substituting this value of N_x' in equation (5.1) and allowing for the absorption of fluorescent X-rays in Melinex, air path and detector beryllium window, we get:

$$N_x = I_o \tau \left(1 - \frac{1}{J_{K,L}}\right)(\rho t)\, \omega_K\, T\, \varepsilon\, f\, \frac{d\Omega}{4\pi} \qquad (5.6)$$

where T = the fraction of fluorescent X-rays transmitted through the Melinex specimen cover, air path and beryllium window.

ε = detector efficiency

$f = \frac{K_\alpha}{K_{\alpha+\beta}}$ = the fraction of the K fluorescent radiation emitted as K_α.

Equation (5.6) may be written as:

$$F_{xz} = \frac{N_x}{I_o(\rho t)} \qquad (5.7)$$

where $$F_{xz} = \tau (1 - 1/J_{K,L})\, \omega_K\, T\, \varepsilon\, f\, \frac{d\Omega}{4\pi} \qquad (5.8)$$

F_{xz} has the units of number of K_α photons/(primary photon. $\mu g.cm^{-2}$). Alternatively, since I_o is related to the charge Q in (μC) deposited by the proton beam on the target by:

$$I_o = Q\, C_f \qquad (5.9)$$

where C_f is the conversion factor to allow for the variation of photon yield per proton with Z, and takes

into account the attenuation of the primary X-rays through different absorbers before interacting with the specimen. Equation (5.6) will be:

$$F'_{xz} = \frac{N_x}{Q(\rho t)} \qquad (5.10)$$

where $F'_{xz} = F_{xz}\, C_f$ (5.11)

The value of C_f is calculated for 1 μC from the expression:

$$C_f = \frac{I_\mu}{4\pi} \times 6.25 \times 10^{12} \times \frac{1}{R^2} \pi r^2 T_o \qquad (5.12)$$

where I_μ = photon yield per proton

$1\mu C = 6.25 \times 10^{12}$ protons

R = target-specimen distance in cm

r = specimen radius in cm

T_o = the fraction of primary X-rays transmitted through the Melinex chamber window, aluminium filter, air path and Melinex specimen cover.

The calibration factor F'_{xz} is constant for a given element Z, certain excitation energy and geometry. Inserting the appropriate value for F'_{xz} in equation (5.10) will lead to an absolute quantitative analysis of thin foils provided that N_x and Q are measured. Several methods are available to carry out the absolute calibration, these are:

1. Theoretical evaluation of F'_{xz} values.
2. Experimental evaluation of F'_{xz} values through
   a) using elemental thin film standards
   b) using standard reference materials.

An alternative approach is to calibrate the system on a relative basis using internal standards.

The absolute calibration approach using thin standards was adopted for the present system because these standards are readily available from a variety of sources with a quoted accuracy of $\pm$5%. Since all parameters in F'_{xz} expression vary smoothly with Z and exciting radiation, relatively few foils can calibrate the system as discussed below:

5.1.1 Theoretical Evaluation of F'_{xz} Values

The elemental calibration factors were calculated semi-empirically since most of the parameters in the F'_{xz} expression were obtained from published data. From equations (5.8) and (5.11) we write:

$$F'_{xz} = \tau (1 - 1/J_{K,L}) \omega_K T \varepsilon f \frac{d\Omega}{4\pi} C_f \qquad (5.13)$$

F'_{xz} was calculated for the 9 elements listed in Table(5.1) in the range $17 \leqslant Z \leqslant 42$, and for 6 energies of exciting radiation ranged from K lines of Ti to Ag. The total photoelectric mass attenuation coefficient τ differs from the total mass attenuation coefficient by less than 0.5 per cent near the K edge and by less than 2 per cent even at very high primary energies (Birks, 1961). Therefore the value of the total mass attenuation coefficient was substituted for τ in equation (5.13) and obtained from the tabulations of Montenegro et al (1978) for each calibrator, for different exciting radiations.

TABLE 5.1

CHARACTERISTICS OF THE FOIL CALIBRATORS EMPLOYED

Element	Mass/Unit area $g.cm^{-2}$	Form
Chlorine Potassium	48	KCl
Titanium	44	Element
Manganese	58	Element
Cobalt	64	Element
Copper	47	Element
Germanium	36	Element
Yttrium	45	YF_3
Molybdenum	50	MoO_3

These tabulations were obtained by fitting a third degree polynomial to the compilation of Storm and Israel (1970). Montenegro et al (1978) then calculated the mass attenuation coefficient for the elements $6 \leqslant Z \leqslant 33$ for characteristic K and L X-rays of elements with $17 \leqslant Z \leqslant 94$. A comparison between the mass absorption coefficients found by Montenegro et al (1978) and experimental data from Millar and Greening (1974) shows less than 4% difference in general. Values of the jump ratio were taken from Storm and Israel (1970). The K shell fluorescence yield ω_K and the fraction (f) of the K fluorescence radiation emitted as K_α were taken from Bambynek et al (1972) and used in equation (5.13).

The gold layer electrical contact on the front surface of the detector crystal and the silicon "dead layer" are usually thin. The thickness of the dead layer was found by Goulding (1977) to be about 0.3 μm. It is estimated that X-ray absorption for the elements of interest in such thickness is negligible.

The fraction of the fluorescent X-rays transmitted through the sample Melinex cover, air path and the detector beryllium window after emerging from different calibrators was calculated as:

$$T = \exp -\left[\mu_{mx}(\rho t)_{mx} \csc 45^{o} + \mu_{air}(\rho t)_{air} + \mu_{Be}(\rho t)_{Be}\right] \qquad (5.14)$$

where (ρt)'s are the mass thickness that the X-rays traverse; μ_{mx}; μ_{air} and μ_{Be} are the mass absorption coefficient of Melinex, air and beryllium respectively. The

μ_m of Melinex $(C_{10}H_8O_4)_n$ was calculated from the coefficient μ_i for the constituent elements according to the weighted average (equation 4.1). The same equation was applied to find the μ_{air}. The μ_{Be} was taken from Storm and Israel (1970).

The detector solid angle $d\Omega$ was determined by the geometry of the experimental arrangement, and the sample-aperture distance was fixed at (3 ± 0.1)cm. An aluminium collimator of 1 cm thick was fixed in front of the detector with (0.6 ± 0.05)cm aperture.

Values of the detector efficiency ε were calculated for each calibrator using equation (4.3).

Targets bombarded by protons were considered, for calculation purposes, to emit K_α and K_β photons at the energy of K_α. Excitation of calibrators by bremsstrahlung induced by protons was neglected because it was very small. The energy of fluorescent radiation emitted from a calibrator was considered as that of K_α of the calibrator.

The photon yields per proton were taken from the measured values of Khan et al (1976) for Ti, Cu, Mo and Ag target, and calculated from the expression given by Khan et al (1977) for Fe and Zr target, equation (3.8).

The calculated F'_{xz} values are listed in Table (5.2) and

TABLE 5.2

A COMPARISON OF CALCULATED FACTORS (F'_{xz}) OF THE PRESENT SYSTEM WITH EXPERIMENTAL VALUES

Element	Ag Excitation	
	F'_{xz} (theo.)	F'_{xz} (exp.)
Cl	$(3.3 \pm 0.8) \times 10^{-5}$	-
K	$(1.8 \pm 0.5) \times 10^{-4}$	-
Ti	$(6.8 \pm 2\ ) \times 10^{-4}$	-
Mn	$(1.8 \pm 0.5) \times 10^{-3}$	-
Co	$(2.9 \pm 0.4) \times 10^{-3}$	-
Cu	$(4.3 \pm 0.4) \times 10^{-3}$	-
Ge	$(6.7 \pm 0.7) \times 10^{-3}$	$(5.9 \pm 0.5) \times 10^{-3}$
Y	$(1.4 \pm 0.2) \times 10^{-2}$	$(1.3 \pm 0.1) \times 10^{-2}$
Mo	$(1.8 \pm 0.2) \times 10^{-2}$	$(1.7 \pm 0.1) \times 10^{-2}$

Element	Mo Excitation	
	F'_{xz}(theo.)	F'_{xz} (exp.)
Cl	$(1.9 \pm 0.5) \times 10^{-4}$	$(8.7 \pm 1.2) \times 10^{-4}$
K	$(1.0 \pm 0.3) \times 10^{-3}$	$(2.6 \pm 0.2) \times 10^{-3}$
Ti	$(3.9 \pm 1.0) \times 10^{-3}$	$(4.8 \pm 0.3) \times 10^{-3}$
Mn	$(1.0 \pm 0.3) \times 10^{-2}$	$(1.1 \pm 0.1) \times 10^{-2}$
Co	$(1.6 \pm 0.2) \times 10^{-2}$	$(1.7 \pm 0.1) \times 10^{-2}$
Cu	$(2.4 \pm 0.2) \times 10^{-2}$	$(2.4 \pm 0.1) \times 10^{-2}$
Ge	$(3.7 \pm 0.4) \times 10^{-2}$	$(3.7 \pm 0.2) \times 10^{-2}$
Y	$(7.4 \pm 0.8) \times 10^{-2}$	$(8.0 \pm 0.4) \times 10^{-2}$

(cont...)

TABLE 5.2 (continued)

Element	Zr Excitation	
	F'_{xz} (theo.)	F'_{xz} (exp)
Cl	$(3.7 \pm 0.9) \times 10^{-4}$	$(1.1 \pm 0.1) \times 10^{-3}$
K	$(2.0 \pm 0.5) \times 10^{-3}$	$(3.4 \pm 0.2) \times 10^{-3}$
Ti	$(7.7 \pm 1.9) \times 10^{-3}$	$(7.6 \pm 0.4) \times 10^{-3}$
Mn	$(2.0 \pm 0.5) \times 10^{-2}$	$(1.9 \pm 0.1) \times 10^{-2}$
Co	$(3.2 \pm 0.4) \times 10^{-2}$	$(3.2 \pm 0.2) \times 10^{-2}$
Cu	$(4.7 \pm 0.4) \times 10^{-2}$	$(4.7 \pm 0.3) \times 10^{-2}$
Ge	$(7.1 \pm 0.7) \times 10^{-2}$	$(7.8 \pm 0.4) \times 10^{-2}$

Element	Cu Excitation	
	F'_{xz} (theo.)	F'_{xz} (exp.)
Cl	$(2.9 \pm 0.7) \times 10^{-2}$	$(4.8 \pm 0.4) \times 10^{-2}$
K	$(1.5 \pm 0.4) \times 10^{-1}$	$(1.6 \pm 0.1) \times 10^{-1}$
Ti	$(5.6 \pm 2.0) \times 10^{-1}$	$(4.2 \pm 0.2) \times 10^{-1}$
Mn	1.4 ± 0.4	1.2 ± 0.1
Co	2.2 ± 0.3	2.1 ± 0.1

Element	Fe Excitation	
	F'_{xz} (theo.)	F'_{xz} (exp.)
Cl	$(7.6 \pm 1.9) \times 10^{-2}$	$(1.3 \pm 0.1) \times 10^{-1}$
K	$(4.0 \pm 1.0) \times 10^{-1}$	$(4.6 \pm 0.3) \times 10^{-1}$
Ti	1.4 ± 0.4	1.1 ± 0.1

Element	Ti Excitation	
	F'_{xz} (theo.)	F'_{xz} (exp.)
Cl	$(2.2 \pm 0.5) \times 10^{-1}$	$(2.4 \pm 0.2) \times 10^{-1}$
K	1.1 ± 0.3	0.9 ± 0.1

plotted as a function of Z of the foil in Figure (5.1). Absolute errors associated with the calculated F'_{xz} values are attributed to the uncertainties in the data used for calculation. The main source of uncertainty comes from the mass attenuation coefficient where 10% is quoted for photon energies up to 6 keV and $\pm$3% above 6 keV (Storm and Israel, 1970). The uncertainty in the photon yields per proton also contributes a significant amount where $\pm$5% was quoted for Cu and Mo, $\pm$6% for Ag, $\pm$10% for Ti (Khan et al, 1976) and less than $\pm$6% for Fe and Zr (Khan et al,1977).

The uncertainty in the jump ratio is derived from the uncertainty in τ and estimated to be less than $\pm$14% for photon energy up to 6 keV and about $\pm$3.4% above 6 keV. The uncertainty quoted on the fluorescent yields varies from $\pm$2% to $\pm$9.4% for the foil elements used. The total uncertainty in the absorption correction, T, varied from about 4% for Cu rising to about 7% for K. For elements higher than Cu these uncertainties are less than 1% and can be neglected. The errors due to uncertainty in the detector efficiency are zero for all X-rays between 5 and 15 keV, and above this increases to 1.6% for 40 keV X-rays. No error was assumed in connection with f values since these were calculated from the fitted K_β/K_α intensity ratios of Bambynek et al (1972). The error in the measured solid angle $d\Omega$ was estimated to be 1.7%. The overall uncertainty in the calculated F'_{xz} was obtained by combining the fractional error quadratically and estimated to be about 10% for photon energies above 6 keV

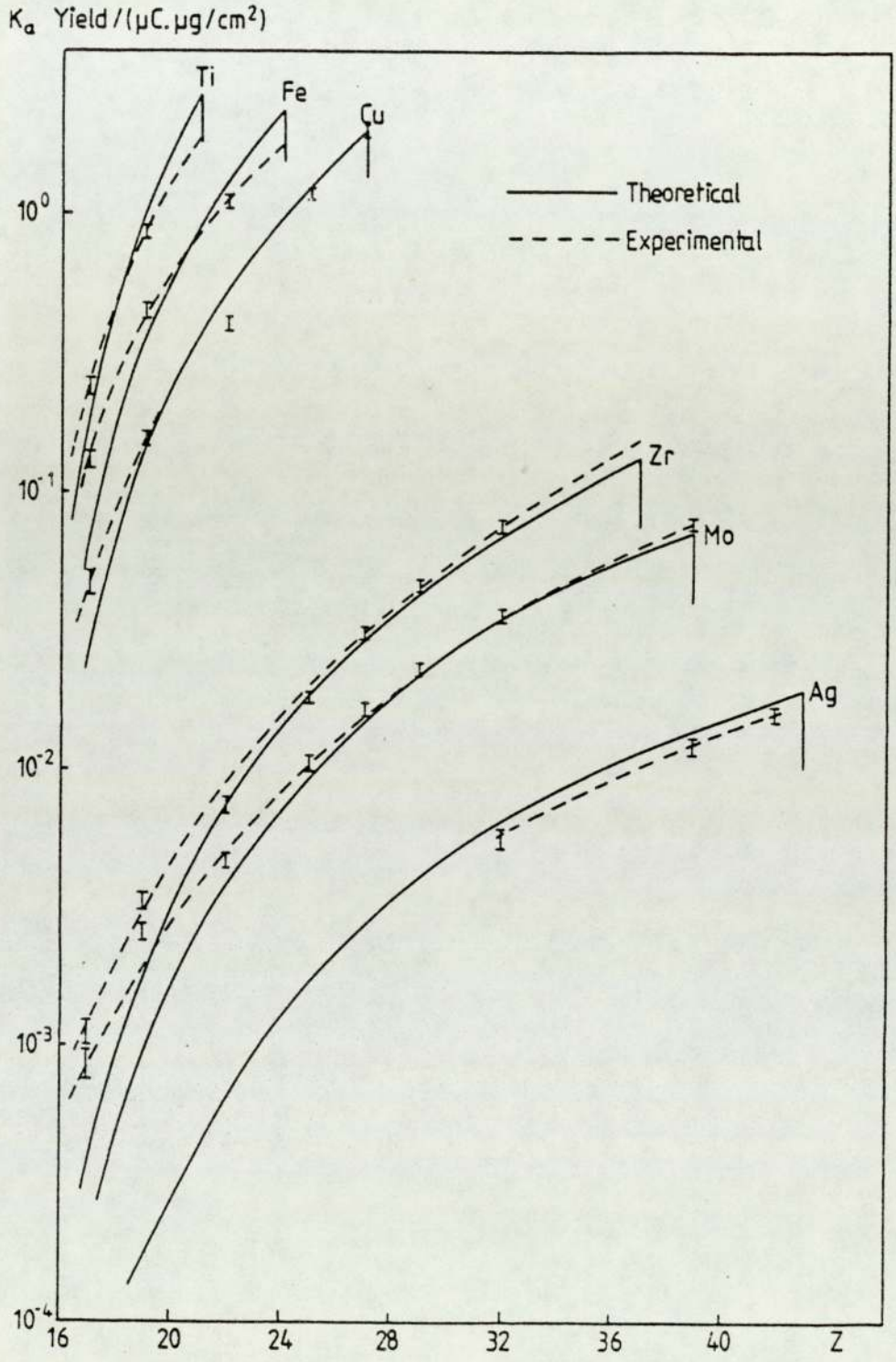

Figure (5.1) Calibration curves for (pX, X) analysis system
Error bars were omitted on the theoretical curves to avoid confusion

rising to about 27% for photon energies below 6 keV.

K_β/K_α Ratios

The K_β/K_α ratios were measured for the thin foil calibrators in order to find out how close the measured values are to the values of Bambynek et al (1972) employed in the theoretical calculation of F'_{xz} values. Also a knowledge of the K_β/K_α ratios is required in solving the interference from X-ray lines overlapping discussed in section (4.6.3). Consequently the spectra obtained for calibrating the system experimentally in section (5.1.2.1) were used to calculate ratios of K_β/K_α for thin foil calibrators. These ratios were then corrected for absorption in the Melinex foil, air path and beryllium window of the detector, and are listed in Table (5.3). The uncertainty quoted is a consequence of the uncertainties in K_α and K_β counts. Table (5.3) also compares these ratios with those reported in the literature. Present work results agree reasonably with the values of Bambynek et al (1972) as well as those of the PIXE work of Barfoot (1980). Values of Scofield (1974) are generally higher while those of Hansen et al (1970) are lower for most of the elements as compared to all the other values. The K_β/K_α ratio appears to increase slightly with Z as can be seen from Table (5.3).

5.1.2 Experimental Evaluation of F'_{xz} Values

5.1.2.1 Using Elemental Thin Standard

Nine thin elemental standard foils of low X-ray self

TABLE 5.3

COMPARISON OF MEASURED AND LITERATURE VALUES OF K_β/K_α RATIOS

Element	K_β/K_α ratio				
	Present work	Hansen et al (1970)	Bambynek et al (1972)	Scofield (1974)	Barfoot (1980)
K	0.0596±0.0060	0.0538	-	-	-
Ti	0.130 ±0.005	0.0945	0.133	0.1355	0.118-0.122
Mn	0.135 ±0.003	0.1219	-	0.1385	-
Co	0.135 ±0.006	0.1317	0.134	-	0.131-0.135
Cu	0.135 ±0.006	0.1339	0.135	0.1379	0.135-0.143
Ge	0.148 ±0.006	0.1395	0.148	0.1504	0.148-0.154
Y	0.178 ±0.027	0.1791	-	-	-
Mo	0.186 ±0.016	0.1930	0.193	0.1981	-

absorption were selected to cover the range of interest. These were supplied in the form of a single element or a stable compound with given areal density as listed in Table (5.1), ranging from 10-100 $\mu g/cm^2$ (Micromatter Co.). They were spectroscopically pure, vacuum evaporated on Nuclepore backings and the accuracy for the areal density is quoted to be $\pm$5%.

Exciting radiations obtained from six targets of Ag, Mo, Zr, Cu, Fe and Ti bombarded by protons were used to fluoresce these foils. Proton current of 10 μA was used with Ag, Mo and Zr targets and had to be reduced to 1 μA with Cu, Fe and Ti targets to avoid pulse pile-up due to high photon yields from low Z targets. Each foil was excited with the available radiation capable of fluorescing its K lines. Exposure time ranged from 2-8 minutes. Short exposures were used for foils whose absorption edge energies are near the energy of exciting radiation while long exposures were for foils far from the exciting energy. X-ray yields per unit charge Q in μC was determined for each foil. Experimental F'_{xz} values were then calculated from equation (5.10) and listed in Table (5.2). The X-ray yields in photon μC^{-1} μg^{-1} cm^2 as a function of Z of the foil are shown in Figure (5.1). Intermediate elements could be obtained quantitatively through these calibration curves by interpolation as calibrators do not cover all the elements in the region of interest.

The calibration curves show a smooth increase with Z of the foils. The low yield at low Z is mainly due to the fact that the fluorescence excitation efficiency decreases for elements with absorption edge energy away from the primary photon energy. The other factors decreasing the calibration curve at low Z are the fluorescence yield, the X-ray attenuation in passing from foil to the detector crystal and the fall in detector efficiency.

When the excitation energy is about 9 keV or higher than the absorption edge of the excited element, a departure of the experimental calibration from the theoretical one is seen. This is clear from Mo and Zr excitation where the experimental F'_{xz} for Cl, for example, is higher than the theoretical F'_{xz} by a factor of (4.6 ± 1.4) for Mo and (3 ± 0.8) for Zr excitation. The reason for this may be due to the assumption that the jump ratio was considered constant in the theoretical calculation. The jump ratio was commonly assumed to be independent of photon energy. An attempt to measure its constancy was made by Keith and Loomis (1978). They used different monoenergetic radiations of up to 7.259 keV above the absorption edge of Ni and found that its value is constant over the range of photon energies used. However, Jenkins et al (1981) pointed out that the assumption that the jump ratio is a constant at energies higher than the absorption edge is only an approximation. We believe that when the excitation energy is at a large distance in keV above the K edge of the excited element, the main contribution

to the photoelectric process is the K shell electrons. Thus the role of all other shell electrons in attenuating the incident beam photoelectrically is very small. This results in a higher value for the jump ratio and hence the factor $(1-1/J_{K,L})$. Therefore, higher values for F'_{xz} are obtained experimentally. This point needs to be further investigated on an experimental and theoretical basis.

A portion of the experimental F'_{xz} with Ag excitation is not displayed in Figure (5.1). This is because the Ag target was 99.99% pure where the impurities in the region of interest were mainly 5ppm Cu and 8ppm Fe (Goodfellow Metals). Therefore the exciting radiation contains, further to the Ag X-rays, characteristic X-rays of these impurities. The appearance of an accompanying Compton scattered peak in the observed spectra indicates the presence of a target impurity line scattered from the specimen. But this does not exclude the trace line emitted from the specimen. Therefore a problem is created in employing X-rays from the Ag target to excite, say, Cu foil. The Cu X-rays emitted from the Ag target are scattered from the Cu foil with Compton shift of 125 eV. The composite peak obtained for Cu foil, is thus partly emitted from Cu foil and partly produced by the Cu in Ag target and scattered by the Cu foil. This results in an elevation of Cu F'_{xz} point. Also the Cu X-rays originating from Ag target excite all other foils with lower absorption edge energies.

5.1.2.2 Using Standard Reference Material

These materials are secondary standards prepared from a mixture of different compositions. The National Bureau of Standards (NBS) has produced a number of Standard Reference Materials (SRMs) for testing the reliability of the analytical techniques. The trace element contents of these standards have been measured by independent methods and certified. The preparation procedure of two biological standards, SRM-1571 orchard leaves and SRM-1577 bovine liver have been discussed by La Fleur (1974). The homogeneous distribution of the trace elements with these standards make them appropriate for testing analytical methods.

Since these reference materials are in the form of a homogeneous powder, they can be easily prepared by pressing some 30 $mg.cm^{-2}$ into a self-supporting pellet, section (6.1). The X-ray yield from each element, which is present in a known amount, can then be determined. F'_{xz} values can then be evaluated for each trace element from equation (5.10) and interpolated for other elements, hence providing a calibration of the system.

In the present work, the SRM-1577 bovine liver was used for testing the system quantitatively, The samples were analysed using Cu, Zr and Mo excitation. The mass concentrations of the trace elements were obtained using the experimental calibration curves shown in Figure (5.1), making the appropriate corrections for the absorption of

both primary exciting and fluorescent X-rays in the sample as explained in section (6.2). The results obtained for the three excitation energies are shown in Table (5.4). The results are clearly in very good agreement. The absolute mass concentrations are compared with the certified values of NBS in Table (5.5) together with the results reported by other authors. The agreement obtained is a measure of the overall accuracy achievable and is again very satisfactory. The uncertainties quoted in the present work arise from the uncertainties associated with the measured X-ray yields, absorption correction factors, beam current integration and the mass standards. A spectrum of bovine liver obtained using Zr excitation is shown in Figure (5.2). As can be observed, the incoherently scattered peaks are more intense than the coherently scattered peaks. This is because the bound electrons responsible for the coherent peak are less tightly bound in light elements than in the heavier elements. The bovine liver, as any other biological sample, consists mainly of light elements.

5.2 STANDARD, SAMPLE AND BEAM SIZE COMBINATION

Throughout this section, only thin samples and standards are referred to. The appropriate expression for the areal density, mass and concentration of a particular element in the sample should be used when the system is employed for different size combinations of standard, sample and beam. Also the standard and sample size should be selected to meet the geometrical capability of the system.

TABLE 5.4

AVERAGE MASS CONCENTRATIONS IN NBS BOVINE LIVER OBTAINED FROM ANALYSING FOUR PELLETS. CONCENTRATIONS ARE IN (μg/g) - DRY WEIGHT.

Element	Exciting Radiation		
	Cu	Zr	Mo
K	(.94 ± .07)%	-	-
Mn	11 ± 2	-	-
Fe	287 ± 21	307 ± 23	306 ± 23
Cu	-	196 ± 15	202 ± 15
Zn	-	149 ± 11	139 ± 11
Rb	-	17 ± 2	19 ± 2

TABLE 5.5

A COMPARISON OF THE MASS CONCENTRATIONS IN NBS BOVINE LIVER OBTAINED IN THE PRESENT WORK WITH THE CERTIFIED VALUES OF NBS AND THOSE OF OTHER WORKERS. CONCENTRATIONS ARE IN (μg/g).

Element	Present work (average)	Cooper (1973)	Giauque (1979)	Van Dyck (1980)	Gladney (1980)	NBS Values
K	(.94 ± .07)%	.99%	-	(1.13 ± .04)%	(.943 ± .099)%	(.97 ± .06)%
Mn	11 ± 2	-	9.4 ± 1.1	10 ± 2	10.2 ± .9	10.3 ± 1
Fe	300 ± 14	250	267 ± 5	240 ± 7	263 ± 13	270 ± 20
Cu	199 ± 11	200	192 ± 4	174 ± 2	189 ± 21	193 ± 10
Zn	144 ± 8	130	134 ± 2	122 ± 3	132 ± 10	130 ± 10
Rb	18 ± 2	16	18.4 ± 4	17 ± 1	19.5 ± 3.6	18.3 ± 1

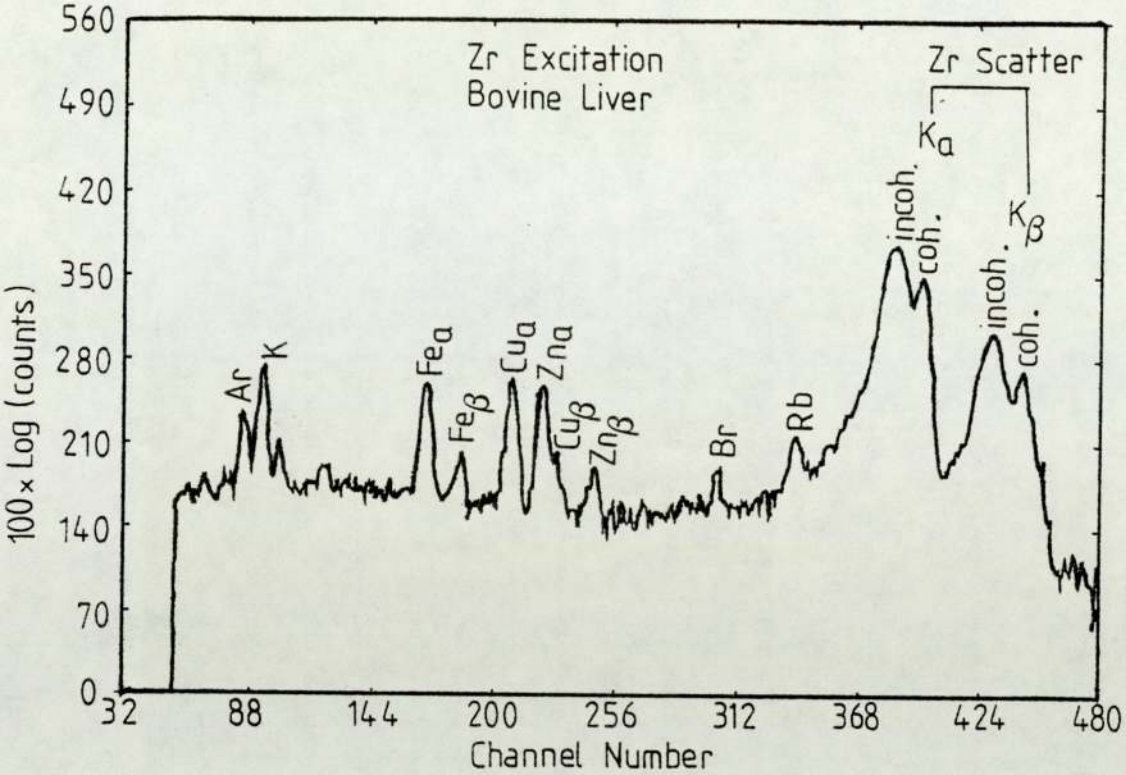

Figure (5.2) Photon excited spectrum of bovine liver for Ep = 2.6 MeV, proton current = 10μA and time = 15 minutes.
Note - The amount of Br detected is attributed to the impurity present in the sample supporting material.

Thus all possible size combinations for standard (st), sample (s) and beam (b) are evaluated for the present system because of their importance in selecting a suitable combination and for the validity of the calibration curves. These possibilities are eleven and can be grouped under four headings as follows:

1 - $st \leqslant b$, $s \leqslant b$ and $st = \text{or} \neq s$

When the standard and sample are equal or different and equal to or smaller than the beam, equation (5.7) can be written for the standard as:

$$\frac{(N_x)_{st}}{(I_o)_{st}\,(\rho t)_{st}} = F_{xz}$$

Also for the sample, equation (5.7) will be:

$$\frac{(N_x)_s}{(I_o)_s\,(\rho t)_s} = F_{xz}$$

If the element in the standard is the same element detected in the sample, then:

$$\frac{(N_x)_{st}}{(I_o)_{st}\,(\rho t)_{st}} = \frac{(N_x)_s}{(I_o)\,(\rho t)_s}$$

$$\text{or} \qquad (\rho t)_s = \frac{(N_x)_s\,(I_o)_{st}}{(N_x)_{st}\,(I_o)_s}\,(\rho t)_{st} \qquad (5.15)$$

For a homogeneous beam larger than the size of the standard, the number of photons incident on the standard is proportional to the area of the standard :

$$(I_o)_{st} \propto (A)_{st}$$

$$\text{or} \qquad (I_o)_{st} = K(A)_{st}$$

where K is a constant of proportionality and is expressed in number of photons per unit area. Assuming steady X-ray beam I_o we can write for the sample:

$$(I_o)_s = K\,(A)_s$$

then $$\frac{(I_o)_{st}}{(I_o)_s} = \frac{K\,(A)_{st}}{K\,(A)_s} = \frac{(A)_{st}}{(A)_s}$$

The expression for the areal density of the sample, equation (5.15) becomes:

$$(\rho t)_s = \frac{(N_x)_s\,(A)_{st}}{(N_x)_{st}\,(A)_s}\,(\rho t)_{st} \qquad (5.16)$$

Since the areal density (ρt) is defined as the mass, m, per unit area A, equation (5.16) becomes:

$$(m)_s = \frac{(N_x)_s}{(N_x)_{st}}\,(m)_{st} \qquad (5.17)$$

where $(m)_s$ is the mass of an element in the sample with the same Z as the standard. Trace element concentration in a sample is usually expressed in terms of the fractional mass in (g/g):

$$\text{conc.} = \frac{\text{mass of element in sample}}{\text{mass of sample}} = \frac{m}{M}$$

$$\text{then conc.} = \frac{(N_x)_s\,(m)_{st}}{(N_x)_{st}\,(M)_s} \qquad (5.18)$$

2 - $st > b$, $s > b$ and $st = \text{or} \neq s$

Here the standard size is either different or equal to the sample size. Equation (5.15) will be:

$$(\rho t)_s = \frac{(N_x)_s\,(I_o')_{st}}{(N_x)_{st}\,(I_o')_s}\,(\rho t)_{st} \qquad (5.19)$$

where $(I_o')_{st}$ and $(I_o')_s$ represent the intensity of the primary photons incident on that part of the standard and sample covered by the beam respectively. If the standard and sample are exposed to constant beam for the same time interval, then:

$$(I_o')_{st} = (I_o')_s$$

Equation (5.19) will be:

$$(\rho t)_s = \frac{(N_x)_s}{(N_x)_{st}} (\rho t)_{st}$$

In term of mass, the last equation will be:

$$(m)_s = \frac{(N_x)_s}{(N_x)_{st}} \cdot \frac{(A)_s}{(A)_{st}} \cdot (m)_{st}$$

The concentration of the element in the sample will be:

$$\text{conc.} = \frac{(N_x)_s}{(N_x)_{st}} \cdot \frac{(A)_s}{(A)_{st}} \cdot \frac{(m)_{st}}{(M)_s}$$

3 - $st > b$, $s < b$

In this case, equation (5.15) becomes:

$$(\rho t)_s = \frac{(N_x)_s}{(N_x)_{st}} \cdot \frac{(I_o')_{st}}{(I_o)_s} \cdot (\rho t)_{st} \qquad (5.20)$$

where $(I_o')_{st}$ is the intensity of the primary photons incident on that part of the standard covered by the beam. There are two approaches to substitute for $\frac{(I_o')_{st}}{(I_o)_s}$:

(i) For constant and homogeneous beam, the number of photons in the beam incident on part of the standard is proportional to the beam area, i.e. $(I_o')_{st} = K(A)_b$ where K is a constant equal to the number of photons per unit area of the beam. Also $(I_o)_s = K(A)_s$. Equation (5.20)

becomes:

$$(\rho t)_s = \frac{(N_x)_s}{(N_x)_{st}} \cdot \frac{(A)_b}{(A)_s} \cdot (\rho t)_{st} \qquad (5.21)$$

(ii) For constant and homogeneous beam, if the standard is exposed to the beam for the time (t), then the sample should be exposed to the beam for the time:

$$(t) \cdot \left(\frac{\text{area of standard exposed to the beam}}{\text{area of sample}}\right)$$

so that $(I_o')_{st} = (I_o)_s$

therefore equation (5.20) becomes:

$$(\rho t)_s = \frac{(N_x)_s}{(N_x)_{st}} \cdot (\rho t)_{st} \qquad (5.22)$$

Approach (i) is preferred because it is more practical.

In terms of mass, equation (5.20) becomes:

$$(m)_s = \frac{(N_x)_s}{(N_x)_{st}} \cdot \frac{(A)_b}{(A)_{st}} \cdot (m)_{st}$$

The concentration of the element in the sample is given by:

$$\text{conc.} = \frac{(N_x)_s}{(N_x)_{st}} \cdot \frac{(A)_b}{(A)_{st}} \cdot \frac{(m)_{st}}{(M)_s}$$

4 - $st < b$, $s > b$

Equation (5.15) is written as:

$$(\rho t)_s = \frac{(N_x)_s}{(N_x)_{st}} \cdot \frac{(I_o)_{st}}{(I_o')_s} \cdot (\rho t)_{st} \qquad (5.23)$$

For constant and homogeneous beam, the number of photons in the beam incident on part of the sample is proportional to the beam area, i.e. $(I_o')_s = K(A)_b$ where K is a

constant equal to the number of photons per unit area of the beam. Also $(I_o)_{st} = K(A)_{st}$. Equation (5.23) becomes:

$$(\rho t)_s = \frac{(N_x)_s}{(N_x)_{st}} \cdot \frac{(A)_{st}}{(A)_b} \cdot (\rho t)_{st}$$

In terms of mass, this becomes:

$$(m)_s = \frac{(N_x)_s}{(N_x)_{st}} \cdot \frac{(A)_s}{(A)_b} \cdot (m)_{st}$$

The concentration of the element in the sample will be:

$$\text{conc.} = \frac{(N_x)_s}{(N_x)_{st}} \cdot \frac{(A)_s}{(A)_b} \cdot \frac{(m)_{st}}{(M)_s}$$

The results of these evaluation are shown in Table (5.6). When the standard and the sample are equal in size, the calibration is valid whether they are smaller, equal or larger than the beam size.

The variation in the intensity of the primary photons due to the instability in the intensity of proton beam was avoided by counting for a preset charge. This ensures that both standard and sample are exposed to the same number of primary photons.

5.3 EXPERIMENTAL UNCERTAINTIES

The uncertainties which contribute to the final uncertainty in the areal density of an unknown element measured by this technique can be evaluated with reference to equation (5.10):

$$(\rho t)_z = \frac{N_x}{Q\ F'_{xz}}$$

The precision with which $(\rho t)_z$ can be determined is

TABLE 5.6

AREAL DENSITY, MASS AND SAMPLE CONCENTRATION FOR DIFFERENT SIZE COMBINATIONS OF STANDARD, SAMPLE AND BEAM

Size compared with beam size		Areal density $(\rho t)_s$	Mass $(m)_s$	Element concentration in the sample, conc. in (g/g)
Standard	Sample			
smaller smaller same	smaller same smaller	$\frac{(N_x)_s}{(N_x)_{st}} \cdot \frac{(A)_{st}}{(A)_s} \cdot (\rho t)_{st}$	$\frac{(N_x)_s}{(N_x)_{st}} \cdot (m)_{st}$	$\frac{(N_x)_s}{(N_x)_{st}} \cdot \frac{(m)_{st}}{(M)_s}$
same	same	$\frac{(N_x)_s}{(N_x)_{st}} \cdot (\rho t)_{st}$	$\frac{(N_x)_s}{(N_x)_{st}} \cdot (m)_{st}$	$\frac{(N_x)_s}{(N_x)_{st}} \cdot \frac{(m)_{st}}{(M)_s}$
larger larger same	larger same larger	$\frac{(N_x)_s}{(N_x)_{st}} \cdot (\rho t)_{st}$	$\frac{(N_x)_s}{(N_x)_{st}} \cdot \frac{(A)_s}{(A)_{st}} \cdot (m)_{st}$	$\frac{(N_x)_s}{(N_x)_{st}} \cdot \frac{(A)_s}{(A)_{st}} \cdot \frac{(m)_{st}}{(M)_s}$
larger	smaller	$\frac{(N_x)_s}{(N_x)_{st}} \cdot \frac{(A)_b}{(A)_s} \cdot (\rho t)_{st}$	$\frac{(N_x)_s}{(N_x)_{st}} \cdot \frac{(A)_b}{(A)_{st}} \cdot (m)_{st}$	$\frac{(N_x)_s}{(N_x)_{st}} \cdot \frac{(A)_b}{(A)_{st}} \cdot \frac{(m)_{st}}{(M)_s}$
smaller	larger	$\frac{(N_x)_s}{(N_x)_{st}} \cdot \frac{(A)_{st}}{(A)_b} \cdot (\rho t)_{st}$	$\frac{(N_x)_s}{(N_x)_{st}} \cdot \frac{(A)_s}{(A)_b} \cdot (m)_{st}$	$\frac{(N_x)_s}{(N_x)_{st}} \cdot \frac{(A)_s}{(A)_b} \cdot \frac{(m)_{st}}{(M)_s}$

dependent upon the uncertainties in the variables as follows:

1 - Uncertainties in N_x which are due to:

a) Counting Statistics

X-ray emission obeys the rules for statistics of random processes. Therefore the standard deviation, σ, in a measurement of N total counts is $\sigma = \sqrt{N}$. If N_T is the total count in a peak region and N_B is the background count in the same region, the number of counts in the peak N_P is:

$$N_P = N_T - N_B \tag{5.24}$$

The statistical uncertainty associated with the number of counts, N_P in the peak is given by:

$$\sigma_P = \pm\sqrt{N_T + N_B} \tag{5.25}$$

A large peak area gives small fractional counting error. In the present work, this error varied from about 1% for the elements with absorption edges just below the excitation energy to about 12% for the elements with edges away from it.

b) Peak Fitting

The PEAK integrating programme used for the analysis of spectra, outputs the area of the peak representing the intensity of a characteristic X-ray together with its standard deviation and location of its centroid. The peak area was found by selecting two background regions, one on each side of the peak. Then the programme computes

the average of the background per channel from the two background regions and draws a straight line between these averaged values. The number of counts in the peak was then computed.

An error of up to 10% in the peak area could result if appropriate channels for the background were not estimated properly. The plot of σ^2 versus X-ray energy where σ is the standard deviation of a Gaussian distribution, Figure (4.9), provides better estimation of the standard deviation for each energy of K_α peak of an element of interest. These values of standard deviation were employed in addition to the PEAK routine to define the peak width and to minimize the uncertainty in the peak area.

If the peak of interest is interfered with by another peak, the above method cannot be applied. This is discussed in section (4.6.3).

c) Sampling Error

The error encountered in sample weight was less than $\pm$2% since pellets were usually weighed after being prepared and those which differed by more than $\pm$2% from the precalculated weight were rejected.

Any change in target angular position will change the exciting X-ray yield and hence the fluorescence X-rays emerging from the sample. The target rotation was

reproducible to better than 1^{o}, thus its effect on the exciting X-ray yield was calculated to be approximately 1%. The variation in sample position relative to both the target and the detector affects the total number of primary X-rays exciting the sample as well as the fluorescent X-rays reaching the detector. Samples in pellet form were sandwiched between two layers of Kimfoil and mounted in standard 35 mm slide mounts. The error in the sample lateral placement as well as forward and backward position was estimated to be $\pm$1 mm. Since the primary X-ray beam has a diameter of 19 mm at the centre of the 15 mm diameter sample, the small variation in sample position was found to be insignificant.

Sample inhomogeneity discussed in section (5.4.1) affects both the accuracy and the precision of the sample analysis results, so great care was excercised in the preparation of the pellets in order to obtain a homogeneous sample. In addition, the preparation and analysis of 4-5 different samples of the same specimen was found to be useful to examine the uniformity of the sample.

d) Beam Energy

The uncertainty in the proton beam energy contributes in an indirect way to the uncertainty in the concentration of trace elements in samples. The uncertainty in the beam energy is usually less than 10 keV at 2.6 MeV, which is less than 0.4% of the beam energy. This uncertainty produces 2.4% uncertainty in the photon yield per proton

from thick targets as it varies as E_p^6.

2 - Uncertainty in the Beam Charge Integration

The number of X-rays incident on the sample is directly proportional to the charge accumulated on the target. The uncertainty in the total accumulated charge arises from instrumental error and leakage current problems. Target current was checked for leakage by using different scales on Keithley electrometer and found to be negligible. The uncertainty in the Keithley electrometer measurements introduced an error of 1% at full scale deflection.

3 - Uncertainty in F'_{xz}

The experimental uncertainty in the calibration factor F'_{xz} can be evaluated with reference to equation (5.10):

$$F'_{xz} = \frac{N_x}{Q(\rho t)_z}$$

The uncertainty in the N_x and in the beam integration has been discussed previously. The uncertainty in the areal density of the standard foil is quoted by the manufacturer to be $\pm$5%.

5.4 SYSTEM SENSITIVITY AND MDL

The sensitivity of the system depends mainly on the screening of scattered radiation and the choice of optimal excitation conditions. High intensity of exciting radiation is necessary for low detection limits.

The energy of the exciting radiation from a target bombarded by protons should be as near as possible to the absorption edge of the element of interest in the sample, provided that the energy of Compton scattered photons falls above the energy of fluorescent X-rays of the trace element of interest. However, it should be noted that this is only true when both scattered and fluorescent radiation are detected at angles different from zero. The reason for this is that at zero angle there are no Compton scattered photons. The criterion usually used to evaluate the capability of different analytical systems is the detection limit. The optimization of the present system regarding experimental parameters was carried out on the basis of the minimum detection limit MDL.

The methods available for calculating the MDL are critically reviewed by Currie (1968) and discussed by Saied (1981).

According to Currie (1978), two concepts that are particularly valuable for expressing the measurement capabilities of an analytical method are the detection limit C_D and the quantitation limit C_Q. The detection limit C_D is the smallest concentration that a particular process can reliably detect. The quantitation limit C_Q, on the other hand, is defined as the concentration for which the relative standard deviation of the measured concentration is 10%.

The detection is considered "reliable" when the probability for detection concentration C_D is 95%.

A number of definitions of MDL are still in use. Three criteria of statistical detectability are considered to illustrate the importance of selecting a statistically meaningfull definition.

1) The integrated number of peak counts has to be larger than a value needed to give a well defined peak with a good statistical uncertainty, e.g. 100 counts for 10% statistics. This criterion has been used by Johansson et al (1970, 1972) and Gordon et al (1972). To specify the peaks in the spectra, 1000 counts was used by Katson (1978). The criterion is satisfactory for the elements present in high concentration in the specimen, giving rise to a large number of X-ray signals compared with the background.

2) The peak-to-background ratio must not be less than a certain value. This emphasises the importance of the background radiation at the peak position. Folkmann et al (1974), Raith et al (1977) and Moriya et al (1978) have employed a peak-to background ratio of one. Since peak and background have the same dependence on the experimental parameters, this criterion does not depend on geometry or photon flux. Furthermore, X-ray attenuation and detector efficiency are cancelled since peak and background are in the same energy region. The disadvantage of this criterion is that peaks with high or low counts

may give the same peak-to-background ratio, although a statistically strong peak has a better precision and is easier to distinguish as compared to a statistically ill defined peak. This criterion has no theoretical basis and the MDL never improves with increased beam current, which is contrary to experience.

3) The peak counts must be greater than the statistical uncertainty of the associated background, i.e.

$$N_x \geqslant K\sqrt{N_B} \qquad (5.26)$$

where the coefficient K varies from 1 to 10, Currie (1968). The International Union of Pure and Applied Physics (IUPAP) recommends a value of 3 for K. The (IUPAP) defines N_B as the background taken over the same interval as the peak. The commonly used criterion is equation (5.26) with K = 3. However, different definitions for N_B are used by different workers. N_B was taken as 2FWHM of the peak.

This criterion is dependent on experimental parameters such as photon flux where the MDL was found to improve with increased photon flux. This criterion has been used to evaluate the MDL of the present system.

5.4.1 Thick and Thin Sample Criteria

The term thick and thin sample are relative terms associated with photon exciting energy, fluorescent X-ray energy and sample composition.

Fluorescent X-rays, being less energetic than the exciting radiation, are absorbed more in the sample than the exciting radiation. Hence the sensitivity decreases as the sample thickness approaches the critical thickness which is the thickness that any increase in it does not increase a fluorescent X-ray intensity. Thus high sensitivity is obtained using thin samples.

For thick samples, both absorption and interelement fluorescent enhancement effects are involved, while enhancement effects can be minimized, if not ignored, for thin samples by selective excitation especially for samples of biomedical nature where elements of interest are present only as traces.

Thick samples are usually easier to handle and faster to prepare and the preparation procedure involves less risk of contamination.

Sample inhomogeneity becomes more severe for thin samples. Sample inhomogeneity arises from one or both of the following possibilities:

1- Variation in sample density throughout the sample.

2- Variation in thickness along the sample.

Sample thickness giving the best peak to background or signal/noise ratio (S/N) should be found in order to prepare samples with thickness yielding high sensitivity. Thus an experiment was performed to measure the variation

of (S/N) ratio with sample thickness. Five pellets of bovine liver with thicknesses of 30, 60, 90, 120 and 180 $mg.cm^{-2}$ were prepared and the signal from Fe was measured with the associated background for each pellet using Zr excitation. Each pellet was exposed to the same number of photons by depositing a proton charge of 8000 μC on Zr target. This charge corresponds to about 10 μA proton current for 14 minutes. The variation of (S/N) with sample thickness for the trace element Fe in bovine liver is plotted in Figure (5.3) where 30 $mg.cm^{-2}$ gave the highest (S/N) ratio. The shape of the curve can be explained as follows. As background radiation is caused primarily by photons scattered from the sample (section 5.4.2), thick samples produce more intense background than thin ones because there are more electrons playing role in the scattering process. Also thick samples attenuate fluorescent radiation more than thin samples. Therefore a decrease in (S/N) ratio is expected as sample thickness increases. Thus improved (S/N) ratio is obtained for thin samples.

5.4.2 Factors Affecting the MDL

The effect of various experimental parameters on the MDL has been assessed. The three sigma criterion has been used to evaluate the sensitivity of the present system, i.e.

$$N_x \geqslant 3\sqrt{N_B} \qquad (5.27)$$

Here, N_B is the number of background counts taken within an interval of 2FWHM of the X-ray signal of interest.

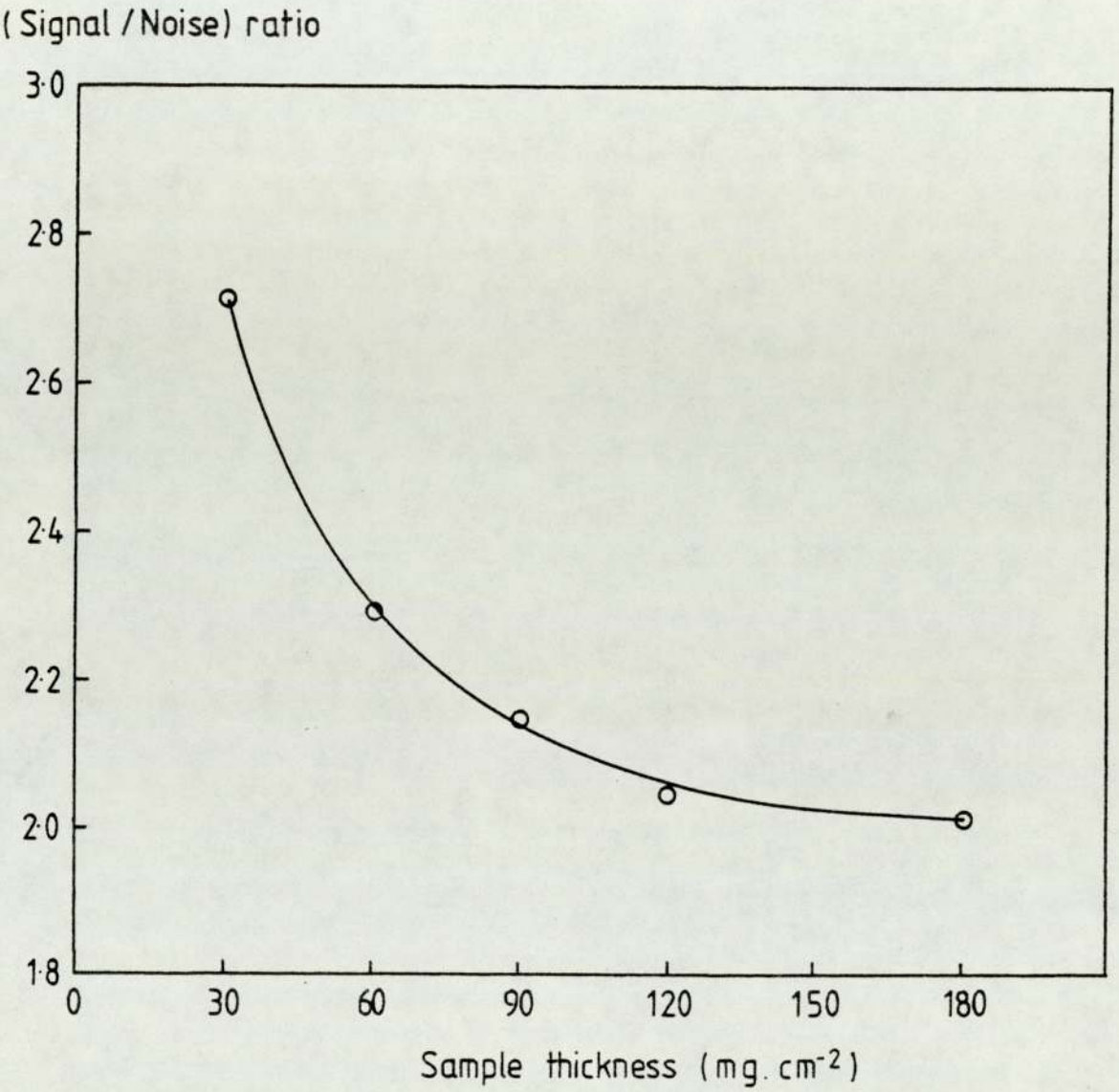

Figure (5.3) Variation of S/N ratio for Fe in bovine liver with sample thickness. Zr excitation was used.
Error bars were omitted since they were smaller than the symbol size

The contribution to the background are (Goulding and Jaklevic, 1977):

1- Bremsstrahlung produced by photoelectrons in the sample. These photons arise mainly from the interaction of the incident X-rays with atoms of the main constituent of biological samples (i.e. carbon). Interaction of incident photons in a carbon matrix are predominantly photoelectric when the photons are of low energies. Therefore significant bremsstrahlung background in the energy range where interference with trace element lines might occur arises from photoelectrons whose initial energy can be taken as that of the incident photons.

2- Escape mechanisms in the detector. These involve:

a) The escape of photoelectrons from the front surface of the detector. Since the photoelectrons result mostly from photons scattered by the sample because the radiation entering the detector is mainly scattered by the sample, the escape electron rate is directly proportional to the scatter rate from the sample. Since the electrons produce some ionization in the detector before leaving its surface, they cause signals through the whole range of interest.

b) Escape of bremsstrahlung photons produced by photoelectrons. The amount of the bremsstrahlung escape background is directly proportional to the number of scattered photons reaching the detector for the same reason stated in (a).

c) Escape of fluorescent silicon X-rays from the

detector. This is discussed in section (4.6.1).

3- Any detector process causing loss of ionization signal will produce background. As the photons entering the detector are mainly scattered by the sample, these will be the main source of degraded signal.
Processes 2 and 3 are directly attributed to scattered photons from the sample.

The integrated counts in the scatter peaks are much larger than those in the rest of the spectrum. This was measured and found that 87-92% of the total counts were contained in these peaks.

The beam coming out of the sample is composed of three main components: scattered, fluorescent and bremsstrahlung radiation from the sample and supporting material. If the detector is not contributing to the background in the spectrum, then:

$$N_T = N_x + N_s + N_{sp} \qquad (5.28)$$

where N_T = the total number of counts in the K_α peak.

N_x = number of characteristic X-rays in K_α peak.

N_s = number of background X-rays generated by the sample.

N_{sp} = number of background X-rays generated by the supporting material.

In terms of equation (5.7) and following Cahill's (1975)

approach, the number of K X-rays N_x can be written as:

$$\left.\begin{aligned} N_x &= (\rho t)_x\, I_o\, F_x \\ N_s &= (\rho t)_s\, I_o\, F_s \\ N_{sp} &= (\rho t)_{sp}\, I_o\, F_{sp} \end{aligned}\right\} \qquad (5.29)$$

The criterion for the detectable limit of an element whose characteristic radiation occurs at E_x can be written as:

$$N_x \geqslant 3\sqrt{N_s + N_{sp}} \qquad (5.30)$$

Substituting (5.29) in (5.30) we get:

$$(\rho t)_{x,min} \geqslant \frac{3}{\sqrt{I_o\, F_x}} \sqrt{(\rho t)_s\, F_s + (\rho t)_{sp}\, F_{sp}} \qquad (5.31)$$

Since the composition of the supporting material is approximately similar to that of biological material, therefore $F_s = F_{sp}$ and equation (5.31) becomes:

$$(\rho t)_{x,min} \geqslant \frac{3\sqrt{F_s}}{\sqrt{I_o\, F_x}} \sqrt{(\rho t)_s + (\rho t)_{sp}} \qquad (5.32)$$

The detection limit $D_{x,min}$ is defined by:

$$D_{x,min} = \frac{(\rho t)_{x,min}}{(\rho t)_s} \geqslant \frac{3}{\sqrt{I_o}} \frac{\sqrt{F_s}}{F_x} \frac{\sqrt{(\rho t)_s + (\rho t)_{sp}}}{(\rho t)_s} \qquad (5.33)$$

The maximum improvement in $D_{x,min}$ is when $(\rho t)_{sp} = 0$. Also $D_{x,min}$ can be reduced by decreasing $(\rho t)_s$ but not to zero because $D_{x,min}$ approaches infinity as $(\rho t)_s$ decreases to zero.

Using equation (5.10), we can write for the standard:

$$F'_{xz} = \frac{(N_x)_{st}}{Q\,(\rho t)_{st}} \qquad (5.34)$$

$(N_x)_{st}$ and Q are measurable quantities. $(\rho t)_{st}$ is known, hence F'_{xz}. Using the criterion $(N_x)_{st} \geqslant 3\sqrt{N_B}$ for the detection limit, equation (5.34) becomes:

$$(\rho t)_{min,z} = \frac{3\sqrt{N_B}}{Q\,F'_{xz}} \qquad (5.35)$$

Dividing both sides of equation (5.35) by $(\rho t)_s$ we get:

$$C_{min,z} = \frac{(\rho t)_{min,z}}{(\rho t)_s} \geqslant \frac{3\sqrt{N_B}}{Q\,F'_{xz}}\,\frac{1}{(\rho t)_s} \qquad (5.36)$$

$$\text{or,}\quad C_{min,z} \geqslant \frac{3\sqrt{N_B}}{Q\,\dfrac{(N_x)_{st}}{Q(\rho t)_{st}}}\,\frac{1}{(\rho t)_s}$$

$$\text{or,}\quad C_{min,z} \geqslant \frac{3\sqrt{N_B}}{(N_x)_{st}}\,\frac{(\rho t)_{st}}{(\rho t)_s} \qquad (5.37)$$

where $C_{min,z}$ is the minimum concentration in ppm of the element Z that can be detected in the sample. Expression (5.33) represents the response of the detection limit to change in the various parameters as follows:

Variation of minimum detection limit $D_{x,min}$

Parameter	Variation
solid angle (dΩ)	$(d\Omega)^{-\frac{1}{2}}$
count rate (R)	$(R)^{-\frac{1}{2}}$
$(\rho t)_s$	$\left[(\rho t)_s + (\rho t)_{sp}\right]^{\frac{1}{2}} / (\rho t)_s$
τ	$\tau^{-\frac{1}{2}}$
$J_{K,L}$	$(1 - 1 / J_{K,L})^{-\frac{1}{2}}$
ω_K	$(\omega_K)^{-\frac{1}{2}}$
Intensity I_o	$(I_o)^{-\frac{1}{2}}$

Parameter	Variation
Energy (E) of exciting radiation	(E), provided that E > the energy of absorption edge of the excited element.
Time (T)	$(T)^{-\frac{1}{2}}$
Target atomic number (Z)	$(Z)^{6}$
Proton energy	$(E_p)^{-3}$
Proton integrated current	$(Q)^{-\frac{1}{2}}$

The minimum detection levels obtainable for the system with three different exciting radiation were determined for a range of elements. In evaluating the MDL's, the background radiation for a bovine liver matrix of 30 mg. cm^{-2} thick was taken for the calculation. The analysis was performed and normalized to a 20 minutes irradiation time. The MDL curves are shown in Figure (5.4) and they decrease generally with atomic number Z. Maximum sensitivity is obtained for elements with absorption edge energy just below the exciting energy. The slight increase in the MDL curves at high Z is due to the signal being superimposed on the high background of Compton tail. The MDL curves show better detectability (i.e. maximum sensitivity) with lower exciting energy provided that this energy is higher than the absorption edge of the excited element. This is attributed to the increase in excitation efficiency as well as increased photon per proton ratio for low Z targets. The actual values of the MDL are given in Table (5.7). It should be stressed, that these figures do not represent the optimum MDL's that can be achieved with the system since in any analysis the counting rate in the detector was limited to less than

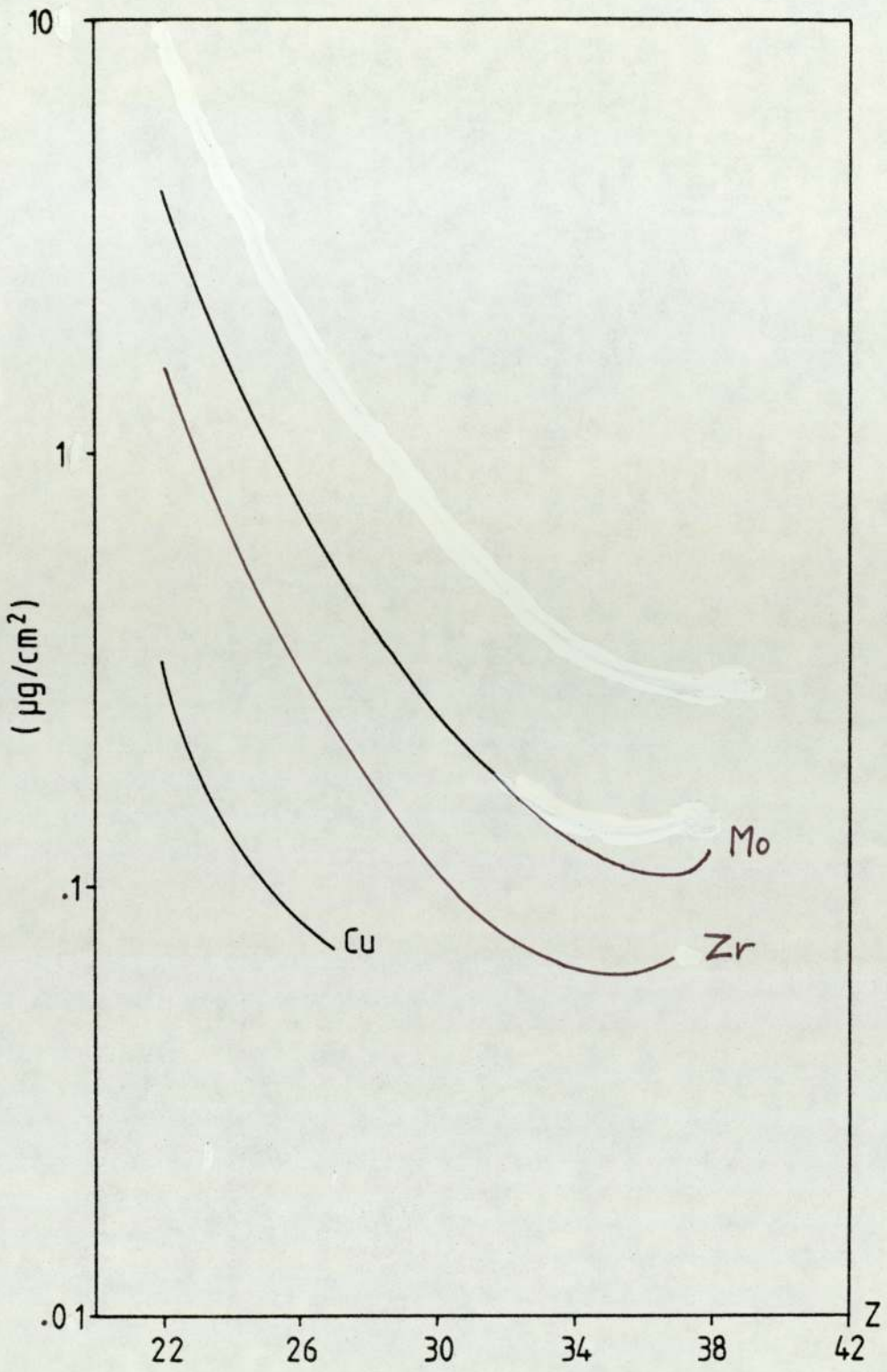

Figure (5.4) Calculated MDL curves in ($\mu g/cm^2$), using experimental F'_{xz} values, for elements detected in 30 mg/cm^2 bovine liver, utilizing the criterion $N_x = 3\sqrt{N_B}$ for 20 minutes. The curves are calculated for Mo, Zr and Cu excitation.

TABLE 5.7

CALCULATED MINIMUM DETECTION LIMIT IN (g/cm^2), USING EXPERIMENTAL F'_{xz} VALUES, FOR ELEMENTS DETECTED IN 30 mg/cm^2 BOVINE LIVER, UTILIZING THE CRITERION $N_x = 3\sqrt{N_B}$ FOR 20 MINUTES.

Element in (g/cm^2)	Excitation		
	Cu	Zr	Mo
Ti	3.47×10^{-7}	1.87×10^{-6}	3.49×10^{-6}
V	2.07×10^{-7}	1.16×10^{-6}	2.11×10^{-6}
Cr	1.36×10^{-7}	7.54×10^{-7}	1.39×10^{-6}
Mn	1.14×10^{-7}	5.60×10^{-7}	1.02×10^{-6}
Fe	9.30×10^{-8}	4.14×10^{-7}	7.17×10^{-7}
Co	7.60×10^{-8}	2.87×10^{-7}	5.10×10^{-7}
Cu	-	1.78×10^{-7}	3.29×10^{-7}
Ge	-	8.90×10^{-8}	1.73×10^{-7}
Br	-	6.30×10^{-8}	1.18×10^{-7}
Rb	-	6.70×10^{-8}	9.90×10^{-8}
Sr	-	-	9.80×10^{-8}
Y	-	-	1.20×10^{-7}

1 kHz. These figures could clearly be improved by the addition of a suitable pulse pile up rejector or for preference an on-demand beam pulsing system, Cahill (1975)

5.5 REPRODUCIBILITY STUDIES

In X-ray fluorescence analysis, the precision of the analytical results is determined by the statistical counting error when the operating conditions and system geometry are constant. As non-reproducible results make any analytical measurement unreliable, it is important that the analytical measurements of the technique are reproducible. Initial measurements of X-ray fluorescence yield obtained with the present system from exciting the standard foils by the primary X-rays induced by protons were not reproducible, and variations of up to 20% were found in performing successive measurements. Thus a systematic study was initiated to identify and eliminate the major sources contributing to the non-reproducibility.

Several aspects concerning system reproducibility may be identified. The short term reproducibility relates to repeated measurements made on a particular foil for a fixed target-sample-detector geometry. The factors that may affect the long term reproducibility are; switching the machine off, rotating the primary targets, removal and reinsertion of the standard foil and moving the detector from its stable position. When the reproducibility is measured over a long period of time, then specimen integrity will be an additional factor. In short term

reproducibility the factors contributing to the uncertainty of the measurement are:

1) Proton beam energy
2) Pulse pile up
3) Peak integrating programme
4) Sample position
5) Charge collecting system

The uncertainty in the proton beam energy produces about 2.4% random uncertainty in the photon yield per proton, section (5.3). The uncertainty in the X-ray detection was insignificant as pulse pile up was reduced by keeping the count rate below 1000 c/s. The peak integrating programme may introduce up to 10% uncertainty if the peak region is not properly selected. However, for the reproducibility studies for each foil this region was kept nearly constant and hence the only uncertainty is due to counting statistics. The uncertainty due to sample position is insignificant as the standard foil does not move during the measurement. The total uncerainty due to the charge collecting system is difficult to quantify. Although the uncertainty due to Keithley electrometer is 1% at full scale deflection the instrument has a high input impedance, typically $10^6\Omega$ on the μA range. Hence leakage currents are important and may change as the experiment is being performed.

In order to investigate the origin of these variations, an X-ray beam monitor was introduced into the system. This eliminated the need for accurate charge measurements.

Andermann and Kemp (1958) proposed the use of scattered X-rays as internal standards to correct for instrumentation variables. However, they can only serve the purpose when samples made from the same specimen are of strictly the same weight and composition because the scattered intensity is proportional to the primary beam intensity times the number of scattering atoms in the sample, Van Espen and Adams (1976). To correct for the variation of the flux of exciting radiation, Van Espen and Adams (1976) and Ahlberg and Adams (1978) normalized the signals to the yield of a wire of pure Zr placed in front of the sample while Burke et al (1964) and Gunn (1965) suspended disks of an appropriate reference element with the sample. The technique is used in the last two cases as an internal reference for the sample and serves the purpose of correcting for absorption effects. Giauque et al (1977) used a 227 $\mu g/cm^2$ thin-film copper standard to correct for the slight deviation in the X-ray tube output or the excitation radiation-specimen-detector geometry. The limitations of the latter approach are:

1) Corrections due to the attenuation of primary and fluorescent X-rays passing through the thin film monitor must be made.

2) The fluorescent X-rays from the specimen may cause additional fluorescence of the monitor, the intensity of which depends on the atomic number of the specimen and thus makes the monitor yield inconsistent.

3) The fluorescent X-rays from the thin film monitor may fluoresce some of the elements present in the specimen.

For the present work, an external thin wire X-ray beam monitor was employed as an alternative approach. The element selected to serve as a monitor was a Ti wire of 0.025 cm in diameter and was positioned in front of the sample in the path of the primary radiation as shown in Figure (5.5). The wire thickness must be small enough to cover an insignificant area of the sample but still provide statistically adequate counts in the spectrum for the normalization purposes. The Ti wire covered an area of about 4.6% of the total sample area with respect to both exciting and fluorescent radiation. It was positioned reproducibly by fixing its ends into two opposite holes in the specimen perspex compartment, such that it can be, together with the sample, affected by the same exciting conditions. Changing samples does not affect the Ti wire position. Its K X-rays do not interfere with those from the standard foils above Ti on Z scale and should give constant X-ray yields per primary photons for each of Ag, Mo, Zr, Cu and Fe excitation. Finally it can be safely assumed to be present at a non detectable concentration in the biological samples analyzed.

Following the introduction of the flux monitor, measurements were again made on the standard foils. The short term reproducibility measurements obtained without removing the standard foil from the specimen compartment were comparable to those of Table (5.8). The long term reproducibility of the analysis for two standard foils

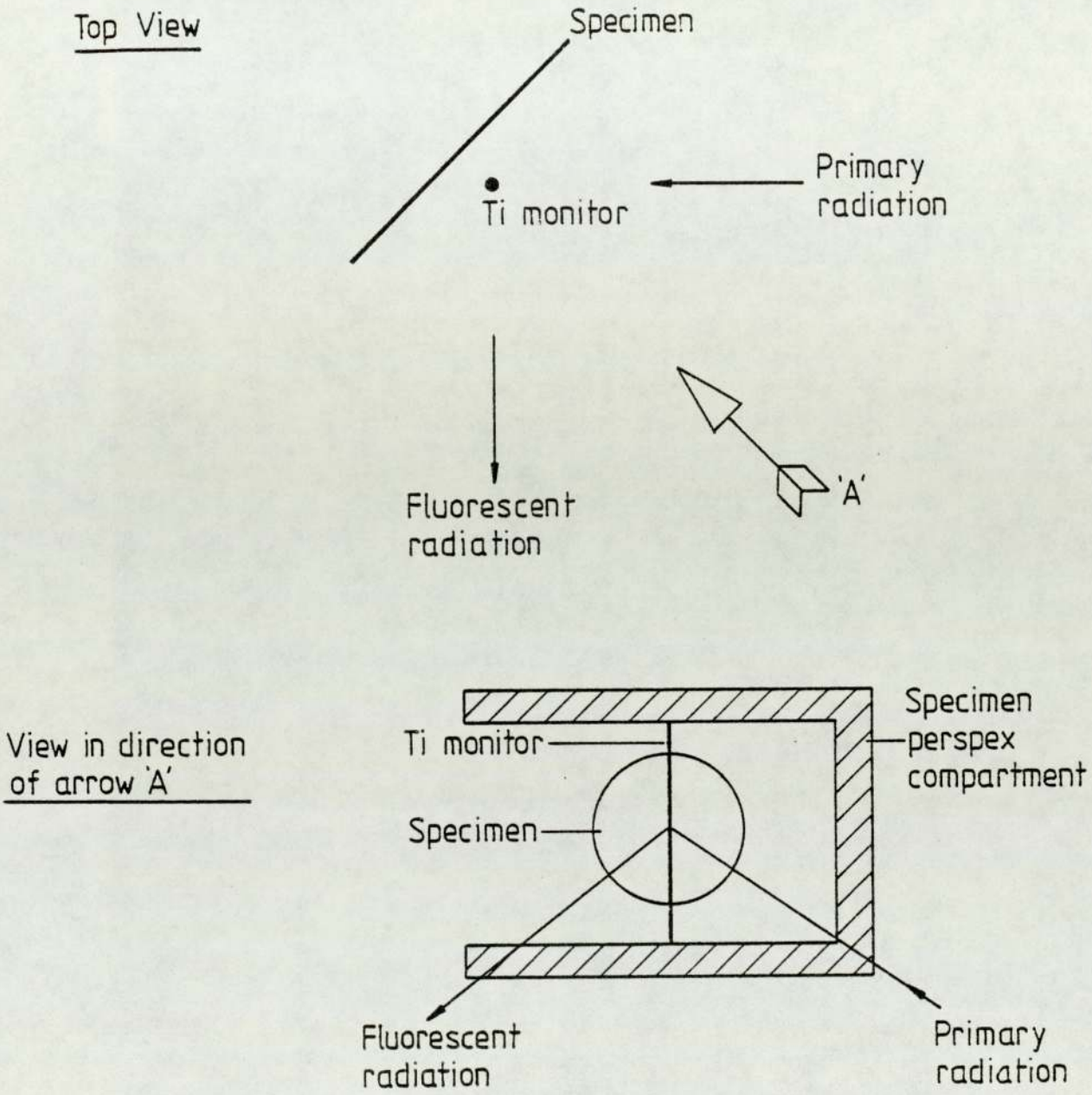

Figure (5.5) Schematic showing location and support of Ti monitor

TABLE 5.8

REPRODUCIBILITY OF ANALYSIS OF STANDARD FOILS. THESE DATA WERE NORMALIZED TO THE YIELD OF Ti MONITOR AND OBTAINED FROM MORE THAN ONE RUN.

Reading Number	Excitation		
	Cu	Zr	Mo
	Co K_α counts	Mn K_α counts	Mn K_α counts
1	$5775^{+}_{-}79$	$1882^{+}_{-}47$	$942^{+}_{-}36$
2	$5710^{+}_{-}79$	$1862^{+}_{-}47$	$932^{+}_{-}36$
3	$5753^{+}_{-}79$	$1802^{+}45$	$1005^{+}39$
4	$5681^{+}_{-}80$	$1794^{+}_{-}47$	$952^{+}_{-}37$
5	$5589^{+}_{-}79$	$1770^{+}_{-}47$	$978^{+}_{-}37$
6	$5522^{+}_{-}78$	$1832^{+}_{-}47$	$1008^{+}_{-}38$
7	$5712^{+}_{-}79$	$1878^{+}_{-}48$	$1009^{+}_{-}38$
8	$5640^{+}_{-}78$	$1856^{+}_{-}47$	$1041^{+}_{-}38$
9	$5700^{+}_{-}79$	$1883^{+}_{-}48$	$1003^{+}_{-}38$
10	$5511^{+}_{-}77$	$1839^{+}_{-}47$	$1045^{+}_{-}38$
11	$5699^{+}_{-}79$	$1852^{+}_{-}47$	$960^{+}_{-}37$
Mean	5663	1841	989
SD	88	38	39
C.V.	1.6%	2.1%	3.9%

C.V. = coefficient of variance = $\frac{SD}{Mean} \times 100$

and three excitation energies is shown in Table (5.8). These data were normalized to the yield of Ti monitor and obtained from 3-4 runs separated by periods of time. The proton current used was 1 μA for the Cu target and 10 μA for Zr and Mo targets. The time of analysis was selected to give a statistical uncertainty of 2-4%. The uncertainty of the measurements for a particular foil and certain excitation energy is represented by the standard deviation (SD) of the 11 measurements. These SD are comparable with figures expected from the counting statistics. The higher coefficient of variance of the Mn K_α measurements excited by Mo results from the smaller number of counts on each measurement.

The reproducibility of biological samples was studied to test the sample preparation technique and the reproducibility of the primary X-ray beam uniformity striking the sample. It should be noted that if the uniformity of the primary X-ray beam was not reproducible, different values for a particular intensity ratio (e.g. Fe/K) would result due to the fact that the fluorescent photons from Fe and K in the sample will be differentially absorbed in the air path between the sample and the detector. This differential absorption is more severe for lighter elements. Two sets of four NBS-1577 bovine liver samples were prepared as described in section (6.1) and analysed, separated by a period of time, during which time the accelerator was running on other beam lines. Two types of reproducibility may be identified here. First, the reproducibility of a particular sample pellet

when it is analysed a number of times in more than one run. Second, the reproducibility of a number of pellets analysed as described above. This second type of reproducibility presented a much more severe test of reproducibility than simply analysing samples prepared from the same specimen one after the other. Table (5.9) compares X-ray count ratio of Cu/Fe, Cu/Zn and Zn/Fe obtained for the eight pellets mentioned above. Also included in Table (5.9) are the mean ratios and their relative standard deviations. The X-ray count ratio is a measure of the reproducibility of the sample preparation method and the uniformity of primary X-ray beam further to the sample integrity and system geometry which were tested by the standard foils. In addition, systematic errors are eliminated.

The reproducibility of the biological samples was further investigated by measuring the X-ray count ratios of K/Cl, Fe/K, Fe/Br and K/Br for five freeze dried human whole blood pellets of 30 $mg.cm^{-2}$ using Ti, Cu and Zr excitation energy. The results of these measurements together with their respective means and standard deviations are shown in Table (5.10). The X-ray count ratio of Fe/K obtained with Cu excitation energy is different to that obtained with Zr excitation energy. The actual concentration of any one of Fe and K is the same regardless of the excitation energy as shown from Table (6.1) where similar concentrations are obtained for Fe and for K using Cu and Zr excitation energy.

TABLE 5.9

X-RAY COUNT RATIOS FOR EIGHT PELLETS OF 30 $mg.cm^{-2}$ EACH OF BOVINE LIVER OBTAINED USING Zr EXCITATION

Pellet Number	Cu/Fe	Cu/Zn	Zn/Fe
1	1.38	1.10	1.26
2	1.33	1.05	1.26
3	1.35	1.02	1.32
4	1.36	0.95	1.29
5	1.40	1.16	1.22
6	1.51	1.16	1.31
7	1.46	1.03	1.42
8	1.33	1.01	1.30
Mean	1.39	1.06	1.30
SD	0.065	0.074	0.059
C.V.	4.6%	7.0%	4.6%

TABLE 5.10

X-RAY COUNT RATIOS FOR 5 PELLETS OF 30 $mg.cm^{-2}$ EACH OF FREEZE DRIED WHOLE BLOOD OBTAINED USING Ti, Cu AND Zr EXCITATION.

Pellet Number	Ti excitation	Cu excitation	Zr excitation		
	K/Cl	Fe/K	Fe/K	Fe/Br	K/Br
1	4.52	10.43	8.24	13.00	1.58
2	4.40	10.58	8.79	13.65	1.55
3	4.24	10.36	8.77	12.39	1.41
4	4.46	10.03	8.32	12.00	1.44
5	4.31	10.75	8.32	12.27	1.48
Mean	4.39	10.43	8.49	12.66	1.49
SD	0.113	0.269	0.269	0.663	0.072
C.V	2.6%	2.6%	3.2%	5.2%	4.8%

In conclusion, the uncertainty due to proton beam energy, X-ray detection and charge collecting system appears to be accurately corrected by the use of a thin Ti wire as an external beam monitor which gives rise to a photo peak in the spectra. The reproducibility of the system and the sample preparation technique is reliable.

CHAPTER SIX

SPECIMEN PREPARATION AND ANALYSIS OF BLOOD AND HAIR SAMPLES

6.1. SPECIMEN PREPARATION FOR XRF

The term preparation indicates any treatment to which the sample is subjected prior to its presentation to the primary X-ray beam. The present system can accommodate relatively large objects which need not be damaged by cutting into smaller samples for analysis. Since specimen composition does not change during analysis, XRF analysis can be considered as a nondestructive technique in that sense. Specimen presentation indicates the physical form in which the specimen is placed in its compartment to the primary X-ray beam.

Powdered samples may be analysed in loose forms but more often as a pressed pellet. The biological samples analysed in the present study, were either supplied in powder form or reduced to powder by some physical means. The prepared powder was finely ground and pressed into a 1.5 cm diameter pellet with a high pressure press. The areal density of the samples was 30 $mg.cm^{-2}$. The prepared pellets did not break or fracture while being handled and mounted in the slide compartment. Thus the use of a binder was not considered necessary, which might have been a source of contamination and also increased background radiation. Freeze-drying and homogenizing biological samples has been discussed by Iyengar (1976). Great care was exercised

to distribute the powder homogeneously in the die before pressing it into a pellet. Since no chemistry is involved, contamination by and losses of trace elements are unlikely to occur. These pellets were then sandwiched between two layers of Kimfoil, each 5 μm thick, and mounted in standard 35 mm slide mounts and positioned, one after the other, in the slide compartment which was fixed at 45^{o} to the direction of the exciting radiation.

6.2 CORRECTION FOR X-RAY ATTENUATION

Because of the attenuation of primary and fluorescent radiation inside the sample, the sensitivity and accuracy of the system changes with increasing sample thickness, section (5.4).

For thin samples, matrix attenuation effects are insignificant and can be neglected, but specimens prepared for analysis are not infinitely thin, thus correction must be applied for matrix attenuation effects. Two processes of attenuation occur, one for the primary radiation and the other for the fluorescent radiation. The total attenuation at a particular depth by the specimen equals the product of these two absorption effects:-

$$\exp(-((\mu/\rho)_1 \csc\theta_1 + (\mu/\rho)_2 \csc\theta_2)\ \rho t) \qquad (6.1)$$

where $(\mu/\rho)_1$ and $(\mu/\rho)_2$ are the total mass attenuation coefficients of the specimen for the primary and the fluorescent radiation respectively. θ_1 and θ_2 are the

angles formed by the primary and fluorescent radiation with the specimen surface. ρt is the areal density of the specimen. Integrating these two effects over the thickness of the specimen, and assuming $\theta_1 = \theta_2 = \theta$ we get:

$$\int_0^{\rho t} \exp(-((\mu/\rho)_1 + (\mu/\rho)_2)\ \csc\theta . \rho t)\, d\rho t$$

$$= \frac{1-\exp(-((\mu/\rho)_1 + (\mu/\rho)_2)\ \csc\theta . \rho t)}{((\mu/\rho)_1 + (\mu/\rho)_2)\ \csc\theta} \qquad (6.2)$$

The reciprocal of the R.H.S. of equation (6.2) times (ρt) represents the correction factor that is required to obtain the number of fluorescent photons generated in the specimen from the observed fluorescence.

In order to assess the magnitude of this factor it was evaluated for different thicknesses and for different elements assumed to be present in a bovine liver matrix. This was repeated for different exciting energies. The value of θ was taken as 45^o which was used in the present geometry. The (μ/ρ) values required for evaluation of equation (6.2) were determined experimentally using a 10 mCi ^{241}Am source. Transmitted X-ray intensities with and without the bovine liver specimen of 30 mg.cm^{-2} were measured. The X-ray beam was collimated to 3 mm diameter before it penetrated the bovine liver specimen. This was done to ensure a reasonable parallel and a narrow beam and thus minimizing the contribution due to scattering processes. The measurements were taken at eight X-ray energies. The first five X-ray energies, namely Ag, Mo, Rb and Cu K_α and Tb L_α X-rays were obtained from a variable energy X-ray source which is a 10 mCi ^{241}Am

ceramic sealed primary source of 59.5 keV gamma radiation with six different targets. The sixth was Mn K X-rays obtained from 0.1 mCi ^{55}Fe source. The latter source was used to excite the seventh X-ray energy which was the K X-rays of Ti from a Ti metallic plate. The eighth energy was obtained by preparing a pellet of $CaCO_3$ (chalk) and exciting Ca K X-rays by ^{55}Fe source. The mass attenuation coefficient of bovine liver at the above energies was then calculated using the equation:

$$\ln \frac{I_1}{I_2} = (\mu/\rho)_B \, (\rho t)_B \qquad (6.3)$$

where I_1 and I_2 are the X-ray intensity without and with the bovine liver specimen and were measured for the same intervals of time. $(\rho t)_B$ is the areal density of the bovine liver pellet which equals 30 $mg.cm^{-2}$. $(\mu/\rho)_B$ is the mass attenuation coefficient of bovine liver. The results of these measurements are shown in Figure (6.1). The uncertainties plotted are the uncertainties associated with the statistical uncertainties. The values of the mass attenuation coefficient for the K_α X-rays of different Z elements used in equation (6.2) were obtained by interpolation of the values measured and plotted in Figure (6.1). The fitting of the measured values was attempted and a quadratic equation of the following form was found most appropriate:

$$Y = A_o + A_1 X + A_2 X^2 \qquad (6.4)$$

where $Y = \ln(\mu/\rho)_B$

$X = \ln E$

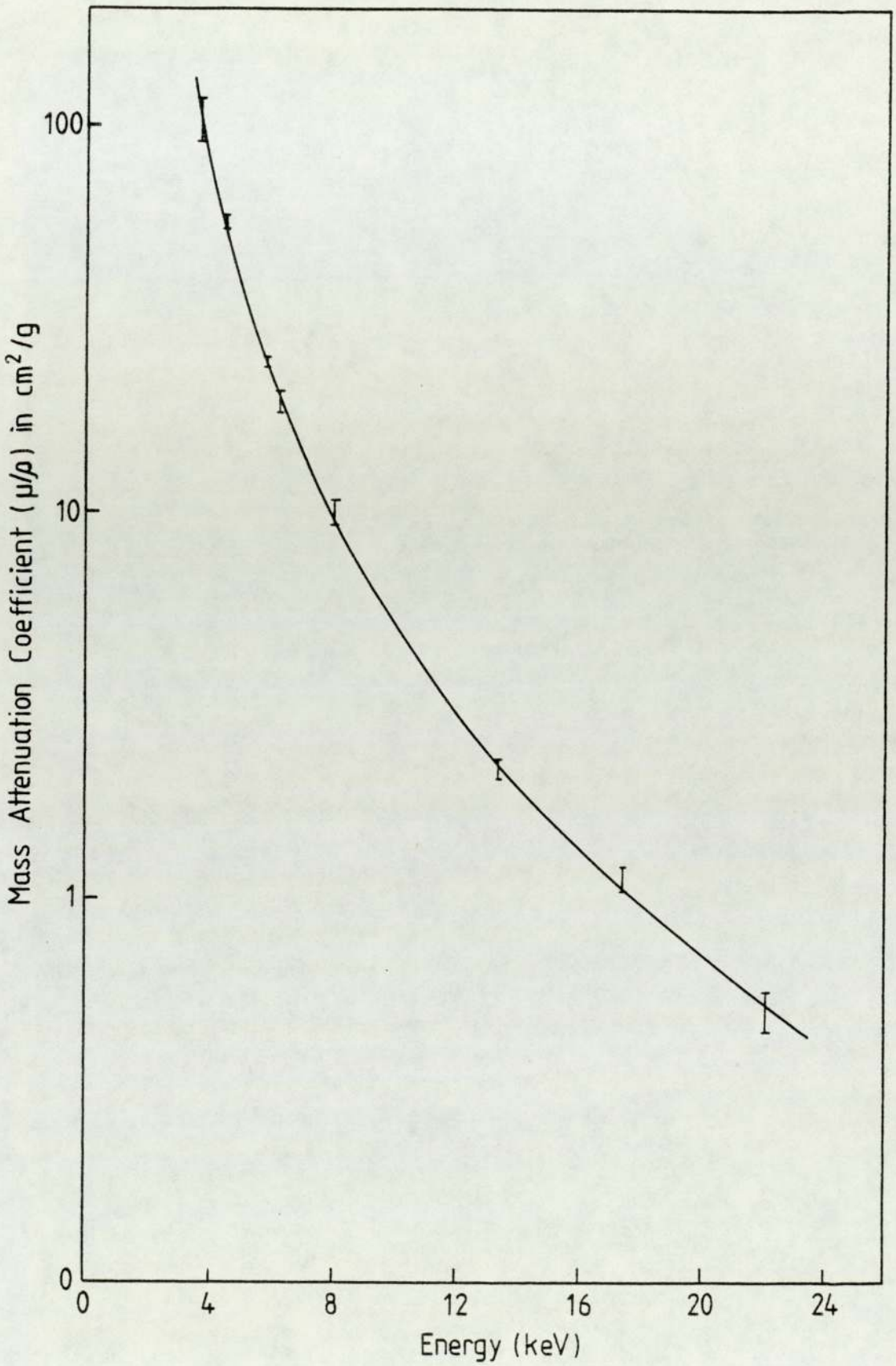

Figure (6.1) Mass attenuation coefficient of bovine liver vs X-ray energy

E is the K_α X-ray energy in keV. The energies of K_α lines were taken as the average weighted by the intensities of the energies of the $K_{\alpha 1}$ and $K_{\alpha 2}$ given by Storm and Israel (1970). This interpolation was done for most of the elements assumed for calculation except those below Ca where their values were extrapolated. The attenuation correction factor was calculated for Mo, Zr and Cu excitation. Its value for Mo excitation ranges from 64% for Mn down 6% for Sr. Using Mo transmission tube, Campbell (1977) found that attenuation corrections for 30 $mg.cm^2$ NBS orchard leaves range from 50% for Mn down to 8% for Sr. Irons et al (1976) found that the absorption correction varied between 1.7 and 1.86 for Cr in 30 $mg.cm^{-2}$ for two human livers using Mo transmission tube. The attenuation correction obtained in this work for Cr in NBS bovine liver is 1.85 using Mo excitation which is very similar to that obtained by Irons et al (1976). Figure (6.2) shows the results of the calculation for some elements using Zr excitation. The attenuation correction is clearly higher for both thick samples and low atomic number elements. Also the use of thin samples requires small correction, especially for low Z, and hence leads to small uncertainty. For high Z elements, the difference in the correction factors for different Z is not so marked especially for thin samples. This is because the difference in matrix absorption is small for high Z elements. This implies that thinner samples are better for both low and high Z elements. However, samples of less than 30 $mg.cm^{-2}$ are too fragile to handle. As a consequence of this all samples used in the present study

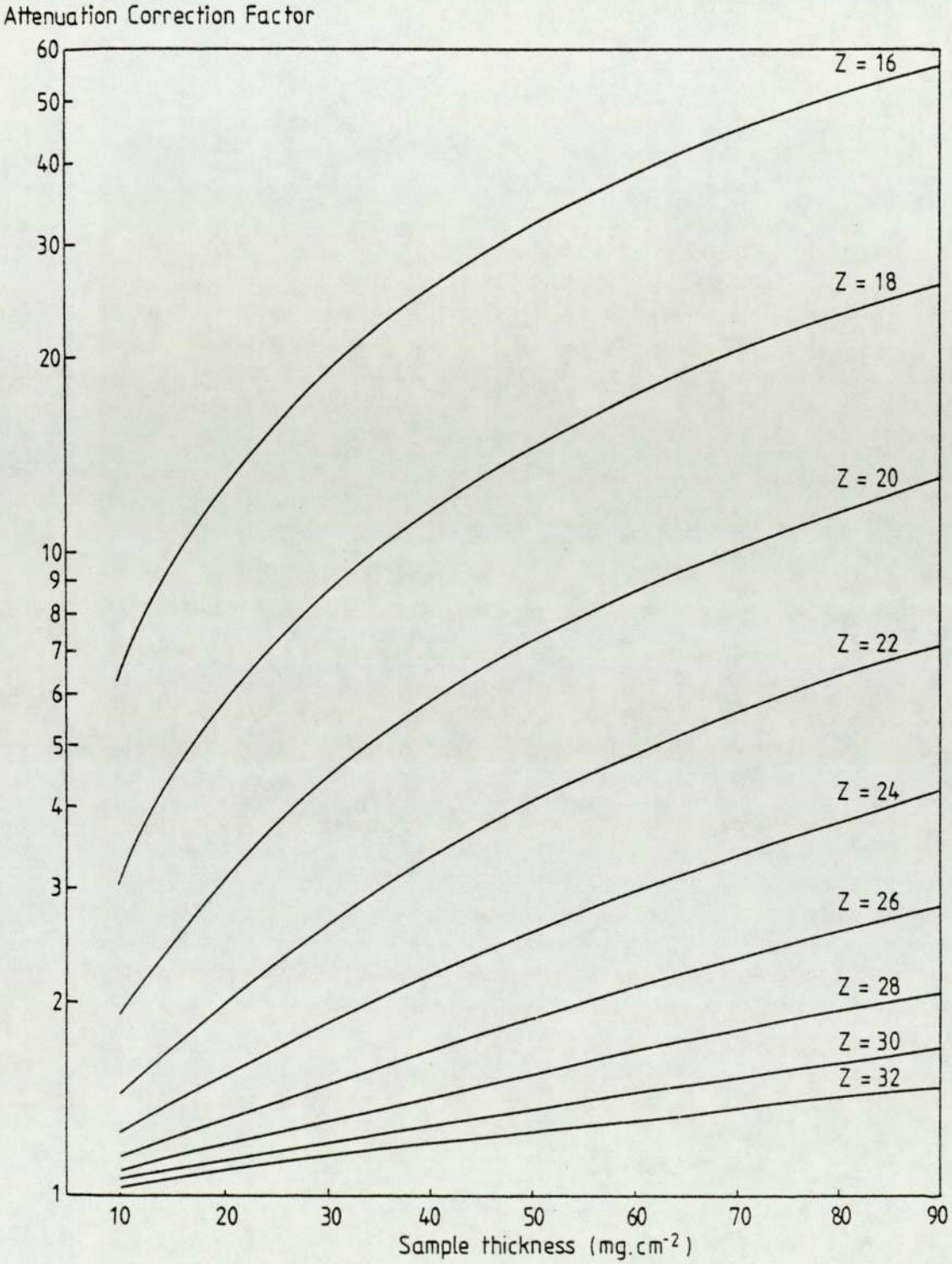

Figure (6.2) Attenuation versus sample thickness for the elements indicated and Zr excitation

were of the order of 30 mg.cm^{-2} thick.

6.3 ANALYSIS OF LYOPHILIZED HUMAN BLOOD

Many trace elements in man are important from the medical point of view, both as essential nutrients and as hazardous substances, Underwood (1971) and Prasad (1976). As a result of the growing interest to correlate human diseases with the presence or absence of trace elements and/or the changes in their concentration in healthy and diseased tissues, Morrison (1965) and Valkovic (1975, 1977), information is required on mineral contents of human tissues.

The trace element content of human blood carries a great deal of information which may be used as a diagnostic tool for the early detection of diseases. Many metabolic disorders in man are accompanied by changes in the level of one or more trace elements in blood, McCall et al (1971). Blood is easy to obtain for analysis and many of the trace elements in blood occur at a concentration that can be detected using the present system. For example, the concentration of some of the trace elements like Ca, Zn and Rb in whole human blood are in the range (57.5-78.0), (4.8-9.3) and (1.17-5.98) ppm respectively, Iyengar et al (1978). To evaluate the present system for blood samples a specimen of whole blood was analysed. A fresh human specimen of whole blood was lyophilized (i.e. freeze-dried), pulverized and pressed into five pellets of 1.5 cm in diameter and 30 mg.cm^{-2}. The freeze-drying

process allows the preparation of thin uniform specimens and increases the trace element sensitivity due to the concentration factor of about five in the case of blood, Giauque and Jaklevic (1972). The results of analysing the above mentioned five blood pellets are shown in Table (6.1) for Zr, Cu and V excitation. A good agreement for the concentration of Ca and Fe respectively can be seen with Zr and Cu excitation energy. Also the concentration of Cl and K respectively are in good agreement with Zr, Cu and V excitation energy. Similar measurements obtained for a particular element with different exciting energies serves as a check for the results. The proton current used was 10 μA for Zr and 1 μA for each of Cu and V targets. The analysis time was about 18 minutes for Zr excitation and 10 minutes for each of the Cu and V excitations. Table (6.1) also compares the results obtained with those of Iyengar et al (1978) which represent a compilation of a large number of data. The results obtained do not disagree with Iyengar et al (1978) for most of the detected elements except in the case of Cu and Zn as is clear from Table (6.1). However, the copper concentration obtained here agrees very well with the value of 11 ppm reported by Giauque and Jaklevic (1972) for lyophilized human whole blood specimen analysed by a Mo transmission tube. Since the concentration factor obtained by lyophilizing the specimen was five, the concentrations of the elements in the original specimen are one-fifth the values shown. Figures (6.3), (6.4) and (6.5) compare

TABLE 6.1

A COMPARISON OF THE AVERAGE MASS CONCENTRATIONS IN (μg/g) OF LYOPHILIZED HUMAN WHOLE BLOOD OBTAINED FROM ANALYSING FIVE PELLETS USING THREE EXCITATIONS WITH THE COMPILATION OF IYENGAR ET AL (1978). CONCENTRATIONS OF THE ELEMENTS IN THE ORIGINAL SPECIMEN ARE ONE-FIFTH THE VALUES SHOWN.

Element	Excitation			Iyengar et al (1978)
	Zr	Cu	V	
S	-	-	9500 ± 800	8400-9650
Cl	13500 ± 1800	13650 ± 1100	13100 ± 980	12950-16450
K	9850 ± 800	9990 ± 750	9800 ± 700	7250-9600
Ca	480 ± 150	480 ± 70	-	287.5-390
Fe	2770 ± 200	2860 ± 210	-	1505-2650
Cu	11.8 ± 3.6	-	-	3.2-6.4
Zn	3.2 ± 0.3	-	-	24-47
Br	37 ± 7	-	-	6.5-40.5*
Rb	16.6 ± 1.4	-	-	5.85-29.9

* varies with drugs and diet.

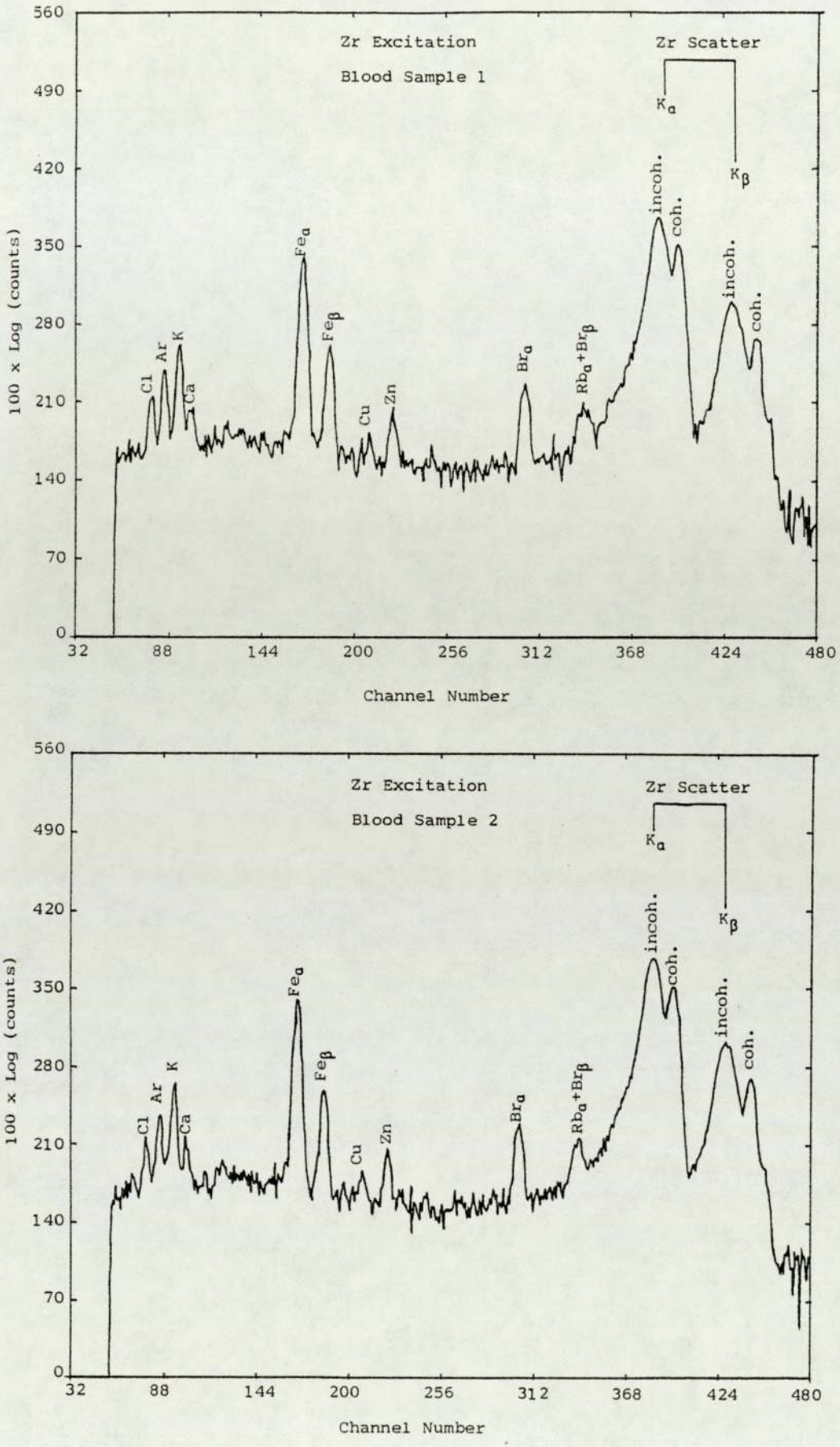

Figure (6.3) Comparison of spectra obtained from two blood pellets using Zr excitation illustrating the reproducibility achieved.

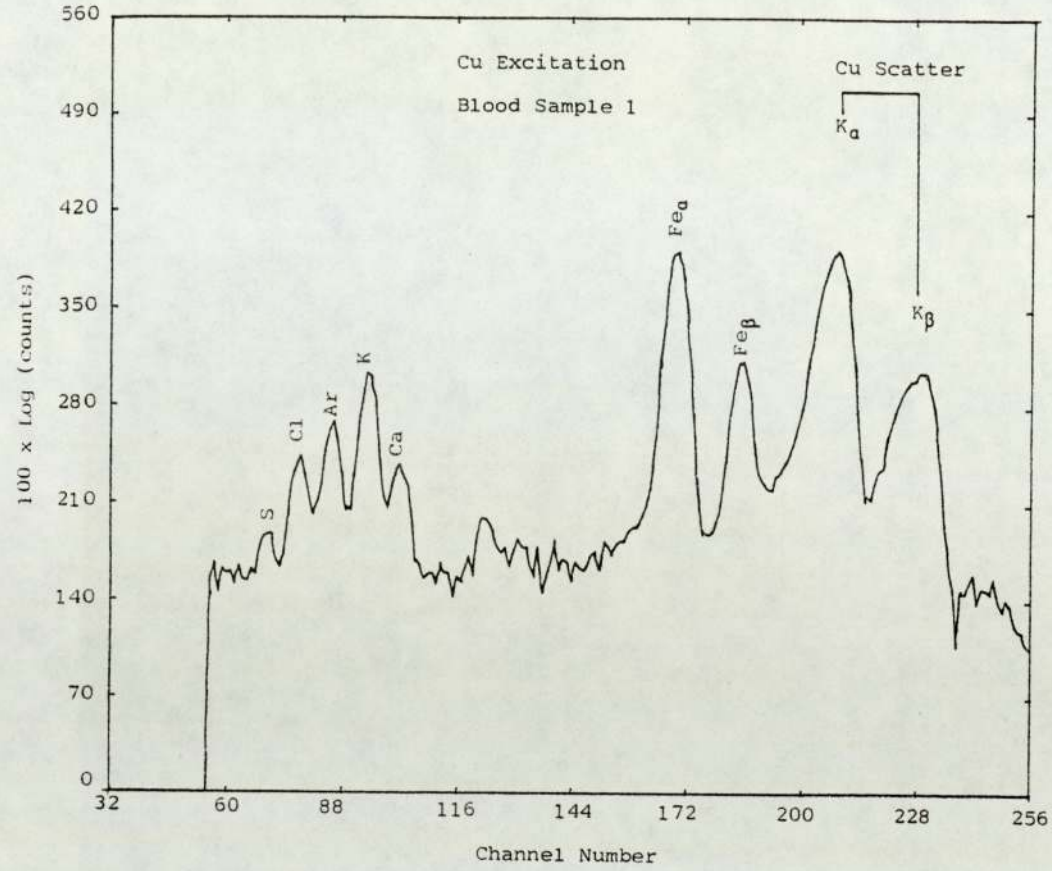

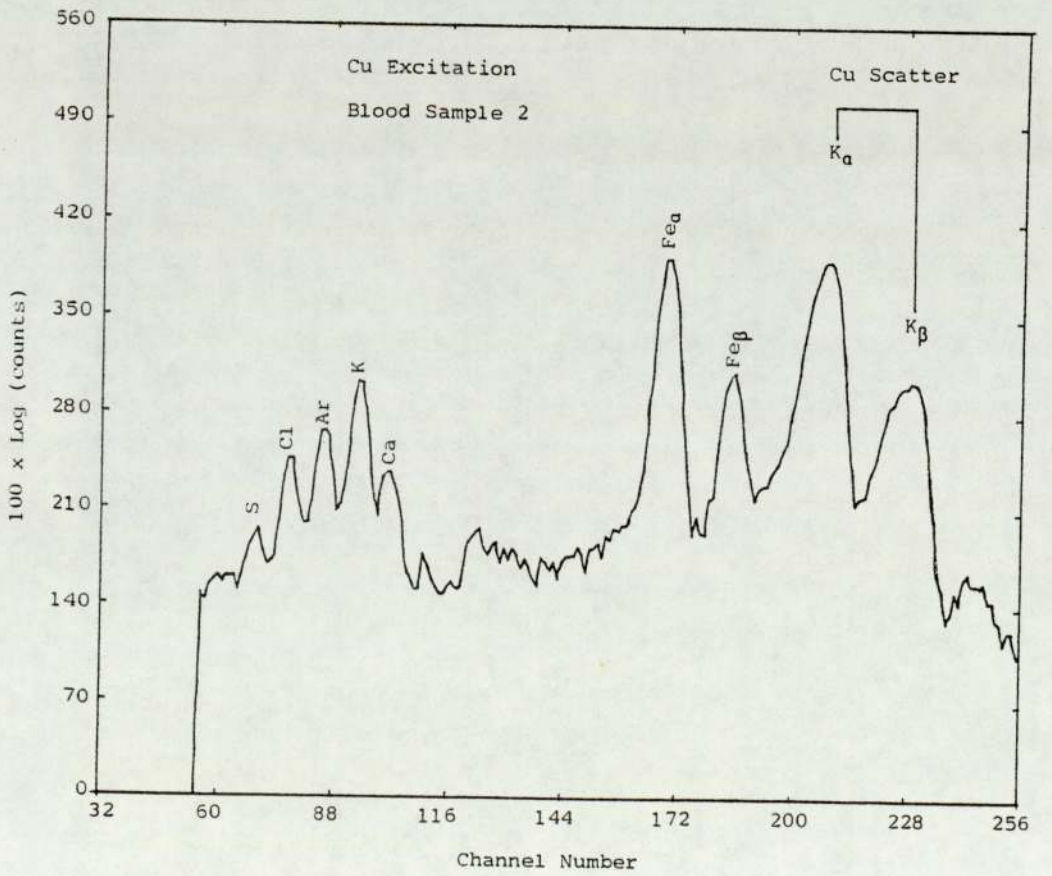

Figure (6.4) Comparison of spectra obtained from two blood pellets using Cu excitation illustrating the reproducibility achieved.

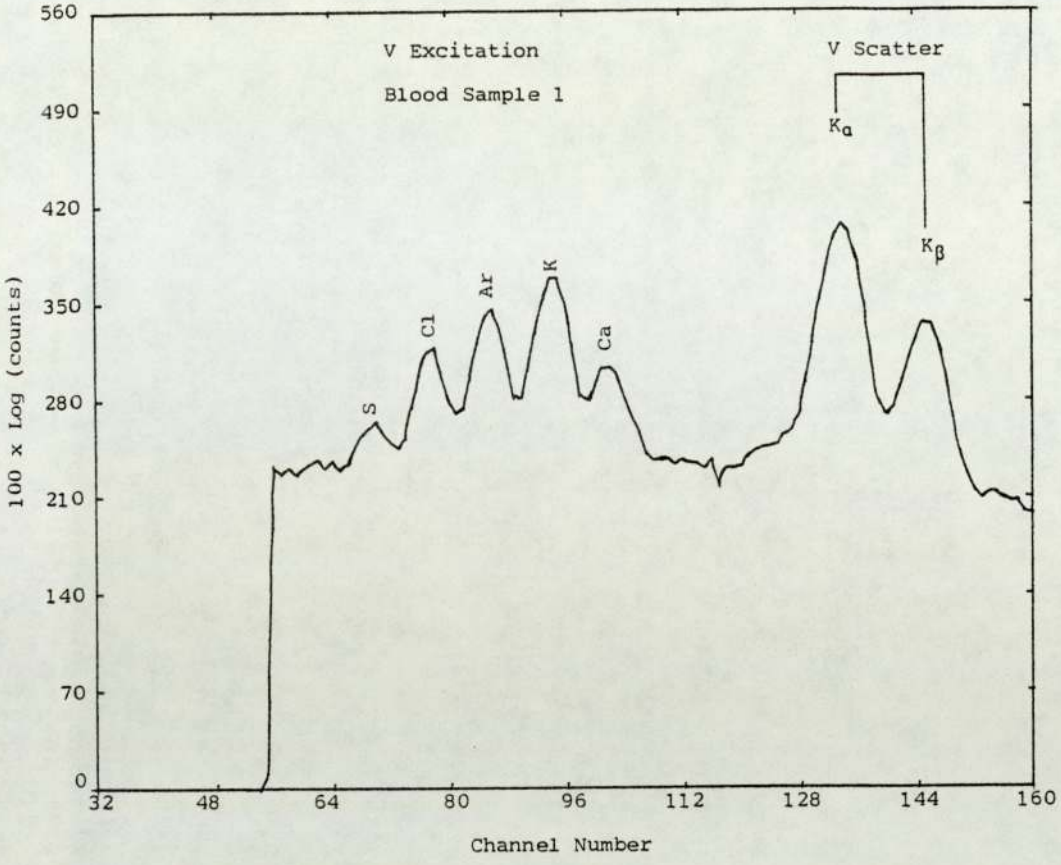

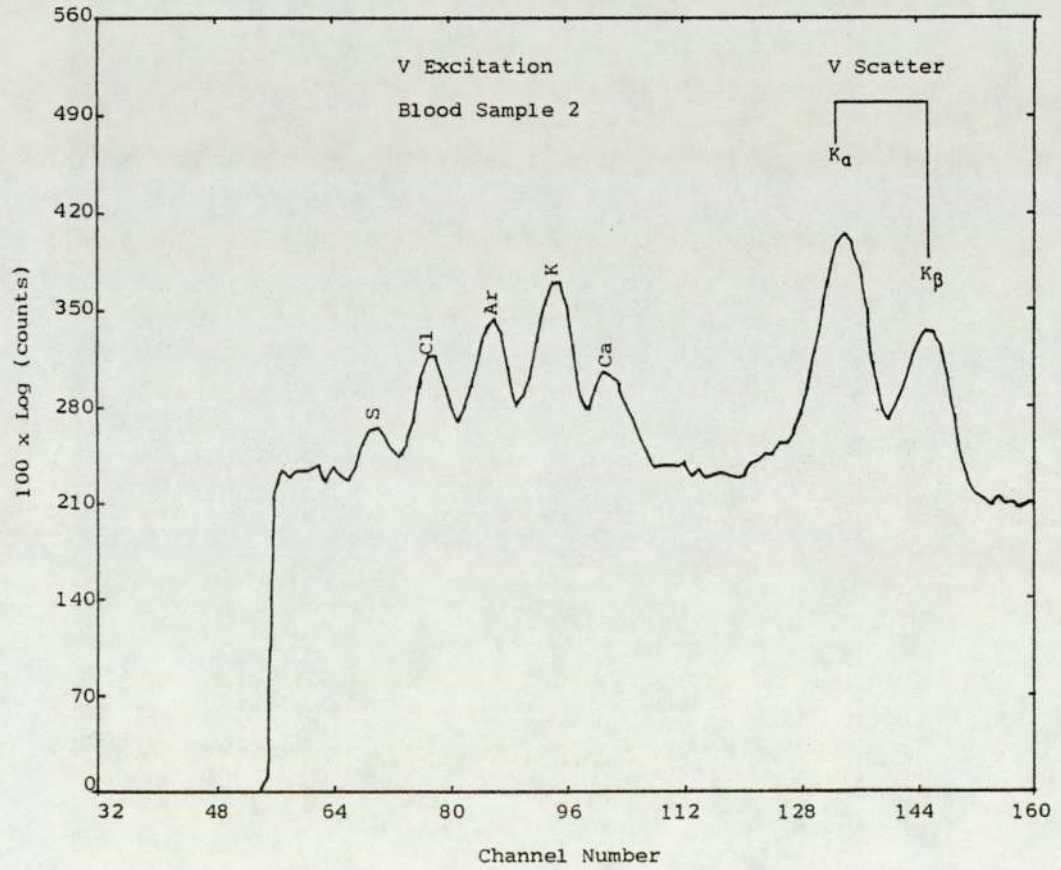

Figure (6.5) Comparison of spectra obtained from two blood pellets using V excitation illustrating the reproducibility achieved.

spectra obtained from two blood pellets using Zr, Cu and V excitation respectively and illustrate the reproducibility achieved.

From this pilot study, it can be concluded that the present system is capable of analysing blood samples and detecting nine elements with good reproducibility.

6.4 STUDIES ON HAIR SAMPLES

Since hair is readily available in fairly large quantities it has received considerable attention in recent years, Vir et al (1981), Ely et al (1981) and Chen et al (1981). Trace element analysis of human hair has potential value in clinical applications. Interest has centred on the trace element content of hair and on elemental ratios as indicators of the long term biological history and activity of the donor. In addition the bulk trace element content in hair may be diagnostic in certain conditions for instance in severe nutritional deficiencies and in environmental contamination. However, longitudinal scanning of hair strands with PIXE has been described by Campbell et al (1981) and with XRF by Toribara et al (1982).

Reported values for trace elements in human hair vary widely, Saied (1981). Some of this variation can be attributed to influences of nutritional status and geochemical environment, but the control of the analytical method may be the main factor responsible for the discrepancies.

6.4.1 Preparation of Hair Samples

Before any preparation for analysis, hair samples were washed in a 50-50 solution of acetone and ethanol to remove any dust or dirt. The washing solution contained negligible amounts of the trace elements. The transformation of hair to powder was achieved in two stages:

1) The hair was reduced to about 2 mm lengths using the brittle fracture technique at liquid nitrogen temperatures. A special PTFE mortar and pestle were made for this purpose. The PTFE material was selected because of its ability to stand liquid nitrogen temperatures as well as causing virtually no contamination and has the property of non-abrasive nature. The application of the brittle fracture technique to homogenize biological samples has been discussed by Iyengar and Kasparek (1977).

2) The hair was then transferred to an agate container containing two agate balls and vibrated at 3000 cycles per minute for a period of one hour. The resulting powder was compressed into a thin pellet as described in section (6.1). The pellets were then mounted between two layers of Kimfoil.

6.4.2 Hair Samples of Hyperactive Children

There has been considerable concern and controversy about the concentration of trace elements in hair and their changes in healthy and mentally subnormal children. The present system has been employed in another pilot

study to further demonstrate its versatility and capability to determine the trace element present in human hair. Samples from ten mentally subnormal children were prepared as discussed in section (6.4.1) and analysed using Zr excitation. The proton current used was 10 μA and each sample was analysed for about 15 minutes. Table (6.2) shows the result of analysing these ten samples denoted by A, B, C, D, E, F, G, H, I and R. Figures (6.6) to (6.15) show the spectra obtained from analysing these samples using Zr excitation. The elemental concentrations in human hair vary with many factors such as geographical location, diet, age, shampoos and cosmetics. Thus a meaningful conclusion may be made only when elemental concentrations of these children are compared with those from a normal group of children living under similar conditions.

This pilot study clearly demonstrates that the sensitivity and accuracy obtainable makes the approach ideally suited to the analysis of hair samples.

TABLE 6.2

MASS CONCENTRATION IN (μg/g) OF SOME OF THE ELEMENTS FOUND IN THE HAIR OF HYPERACTIVE CHILDREN ANALYSED USING Zr EXCITATION.

Patient	Ca	Cu	Zn	Br	Pb
A	1138 ± 165	51 ± 6	217 ± 17	8 ± 1	18 ± 3
B	657 ± 139	42 ± 5	177 ± 14	5 ± 1	17 ± 3
C	585 ± 182	53 ± 6	220 ± 17	11 ± 2	17 ± 3
D	599 ± 138	63 ± 6	139 ± 11	12 ± 2	18 ± 4
E	550 ± 148	23 ± 4	163 ± 13	7 ± 1	38 ± 5
F	692 ± 136	64 ± 6	98 ± 9	13 ± 2	20 ± 4
G	727 ± 144	78 ± 7	109 ± 9	11 ± 2	33 ± 5
H	577 ± 123	74 ± 7	110 ± 9	9 ± 1	24 ± 4
I	757 ± 132	83 ± 8	135 ± 11	9 ± 1	22 ± 3
R	884 ± 149	20 ± 3	165 ± 13	6 ± 1	17 ± 3
Normal range Iyengar et al (1978)	146-3190	11-34	99-450	0.65-53.3	3-70

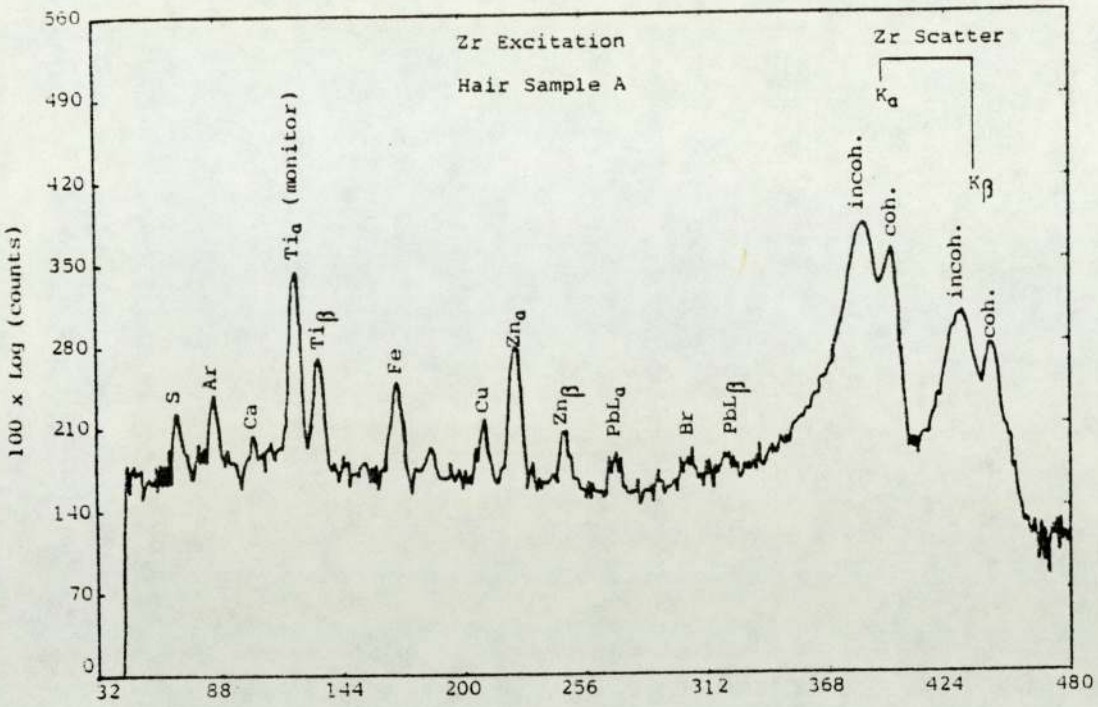

Figure (6.6)

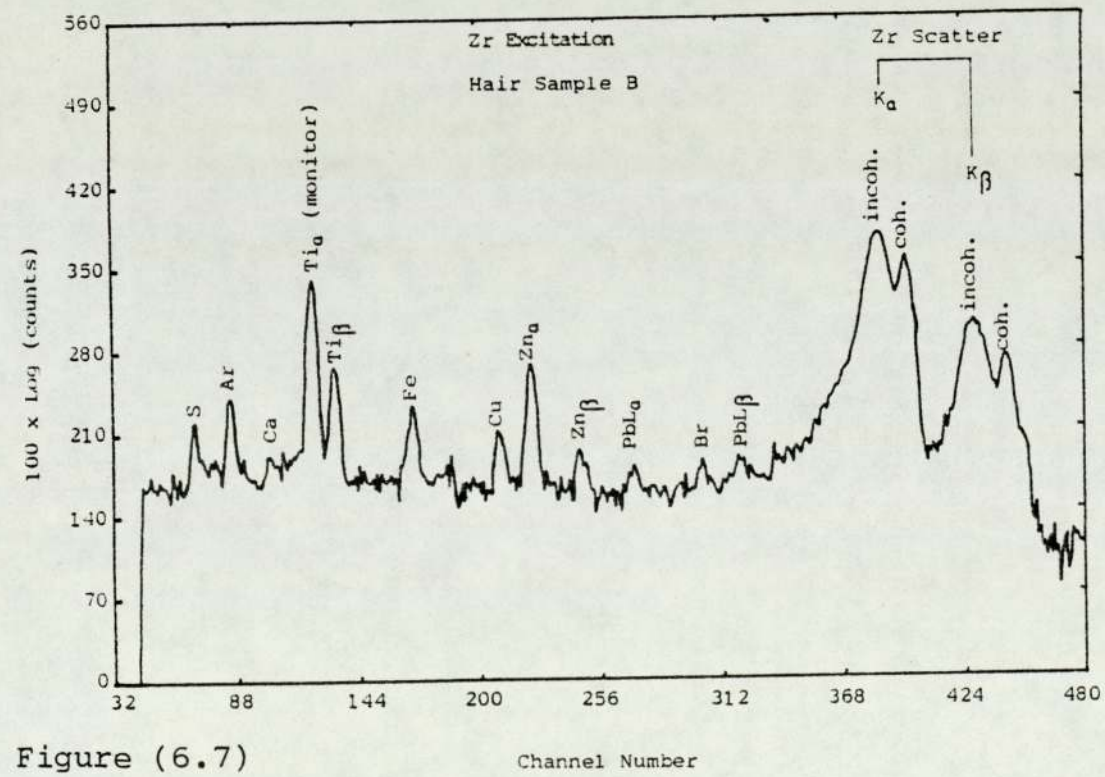

Figure (6.7)

Figures (6.6) to (6.15)
Spectra obtained from analysing ten samples from mentally subnormal children using Zr excitation and 10 μA proton current for 15 minutes.

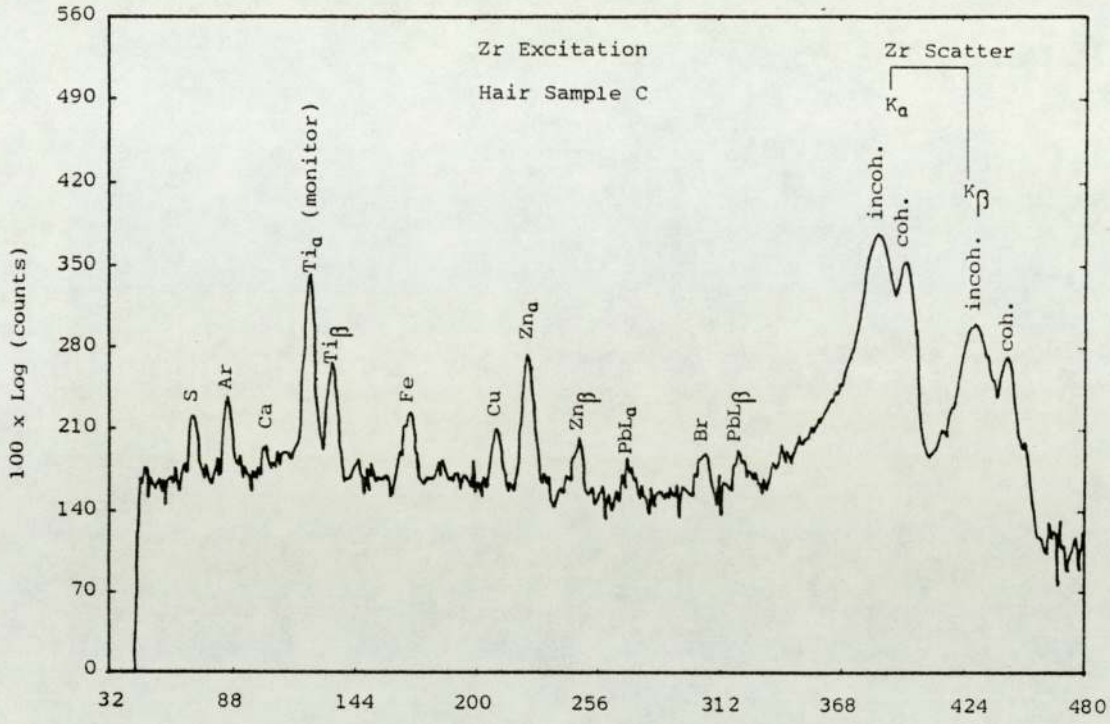

Figure (6.8)

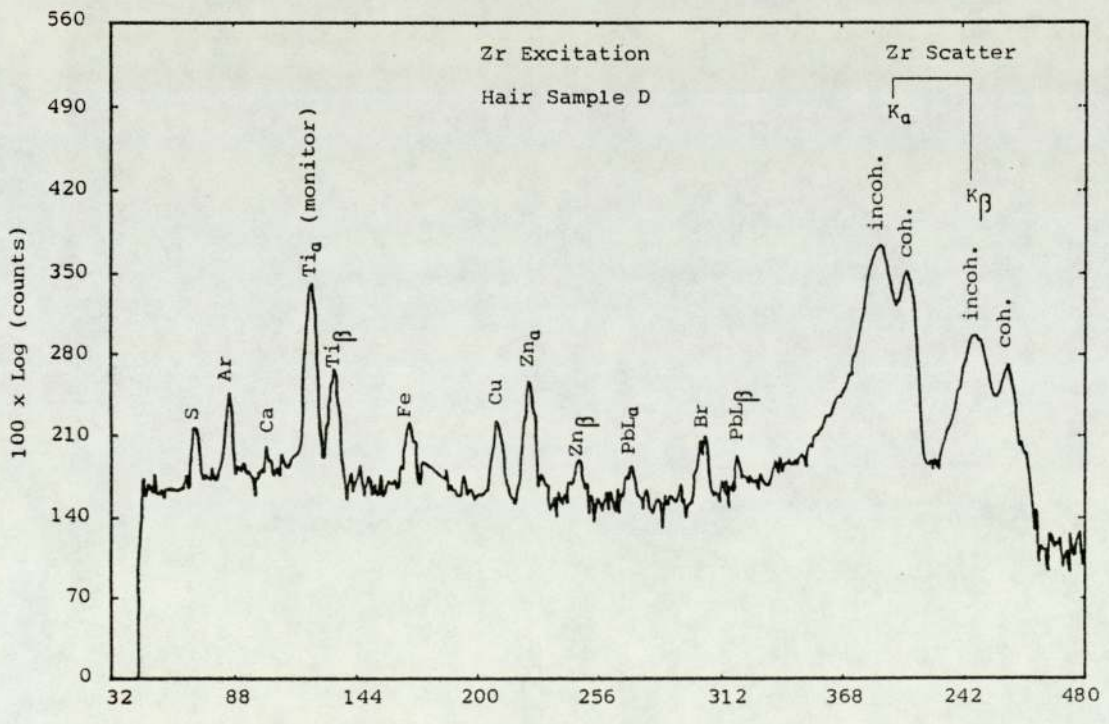

Figure (6.9)

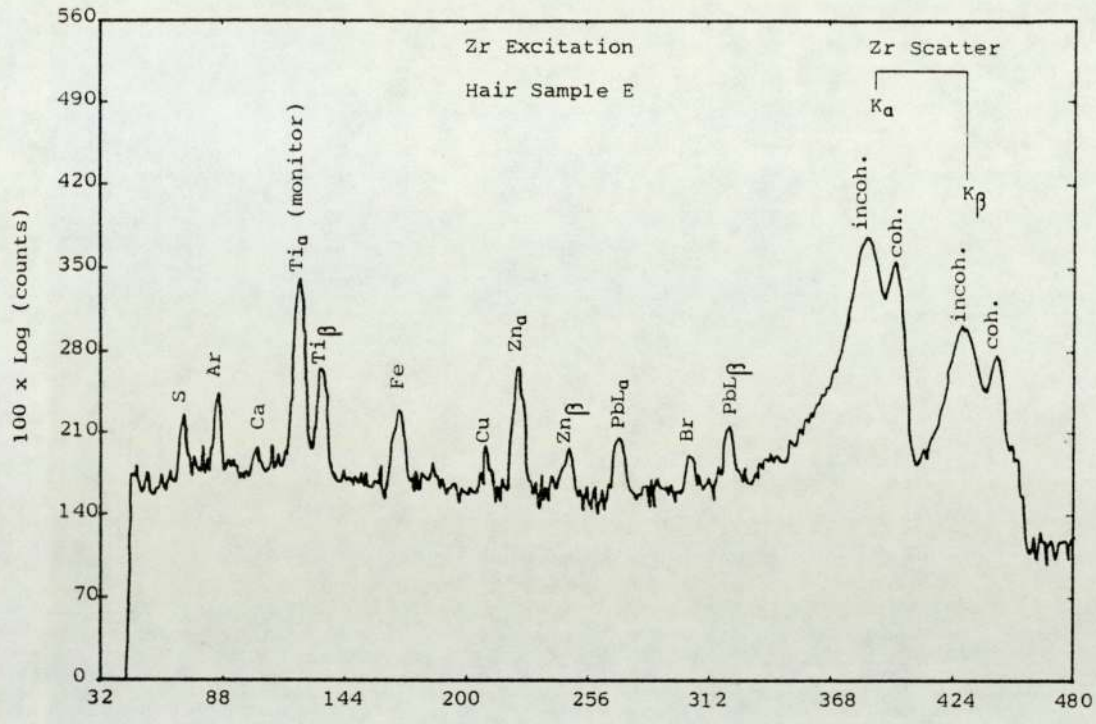

Figure (6.10)

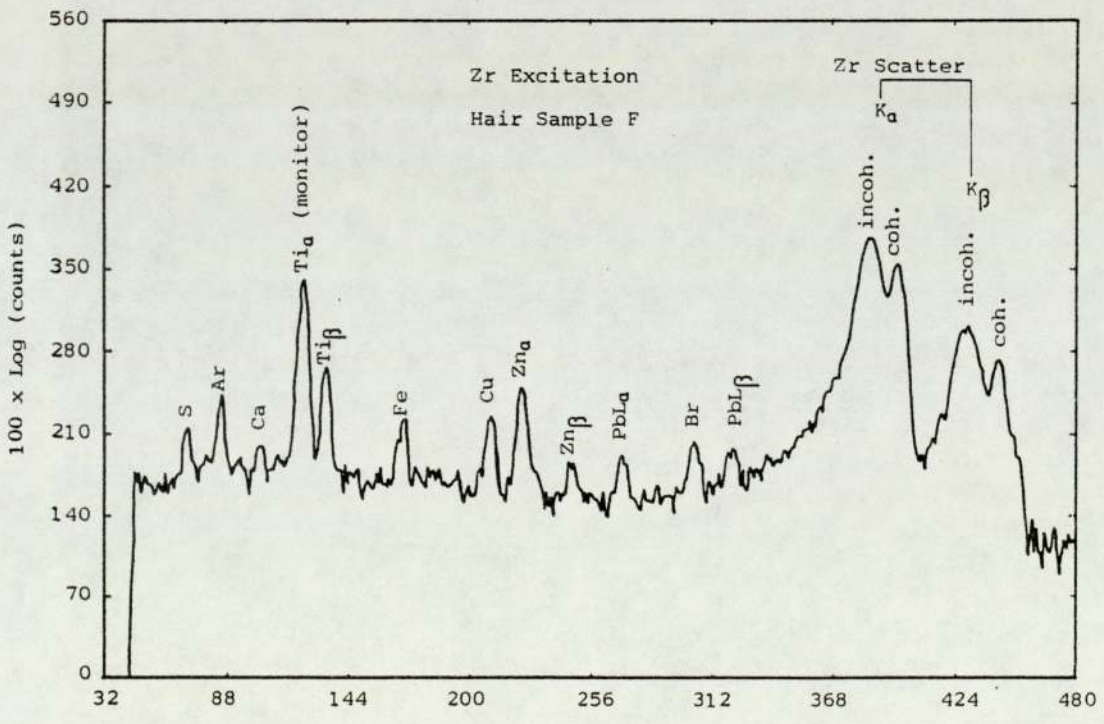

Figure (6.11)

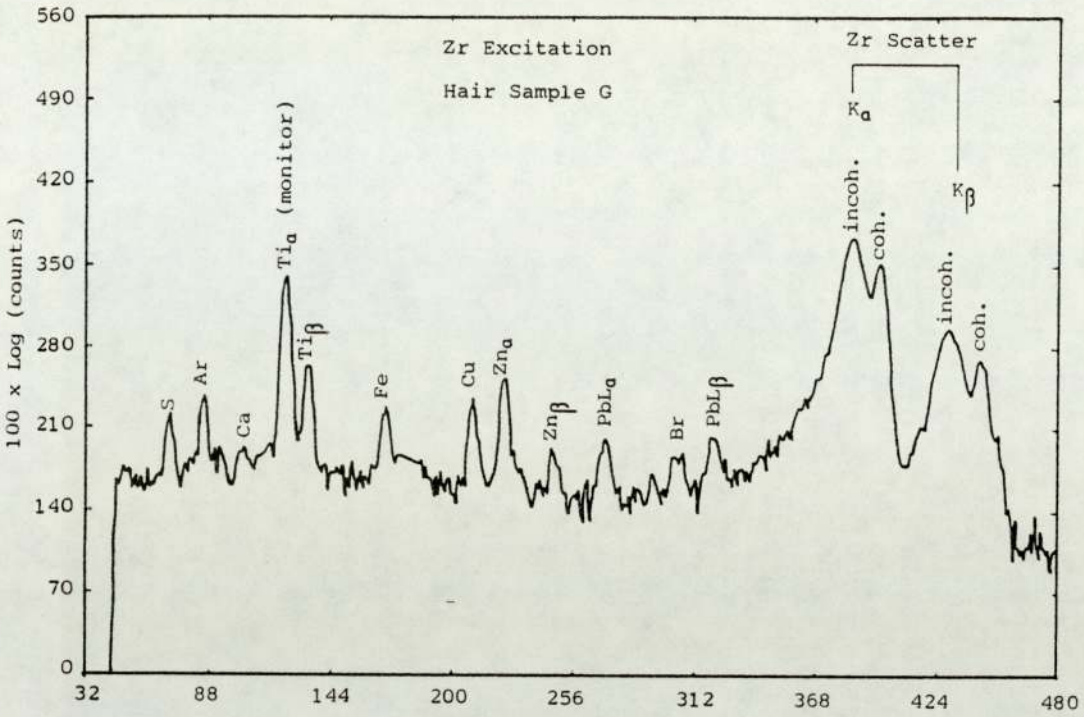

Figure (6.12)

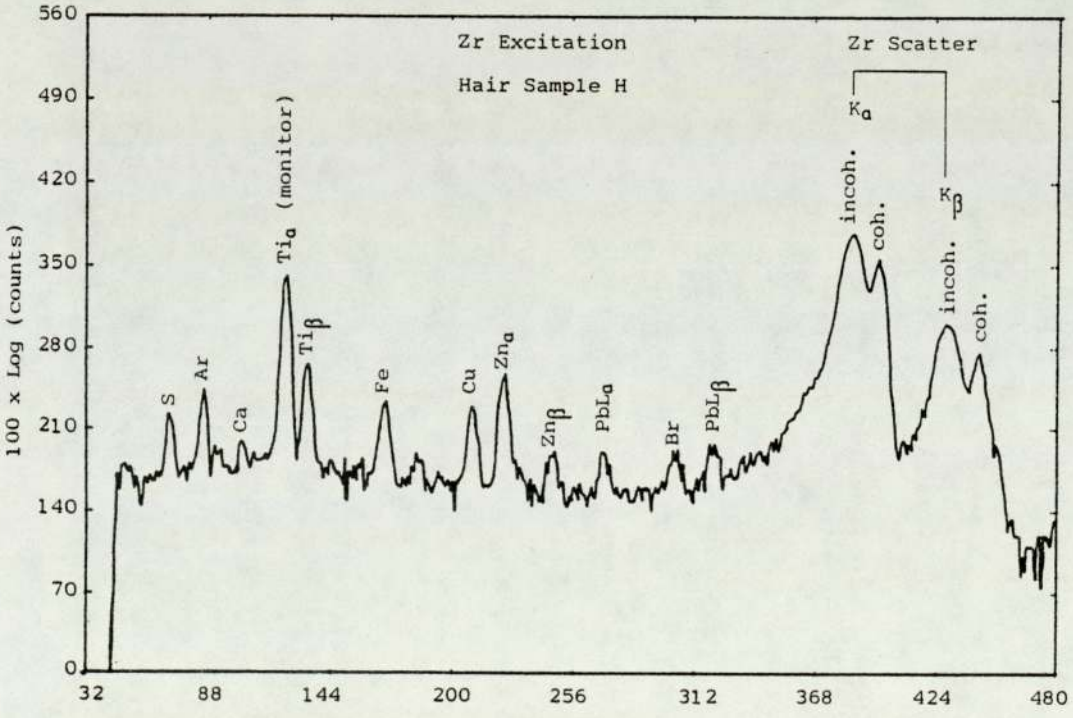

Figure (6.13)

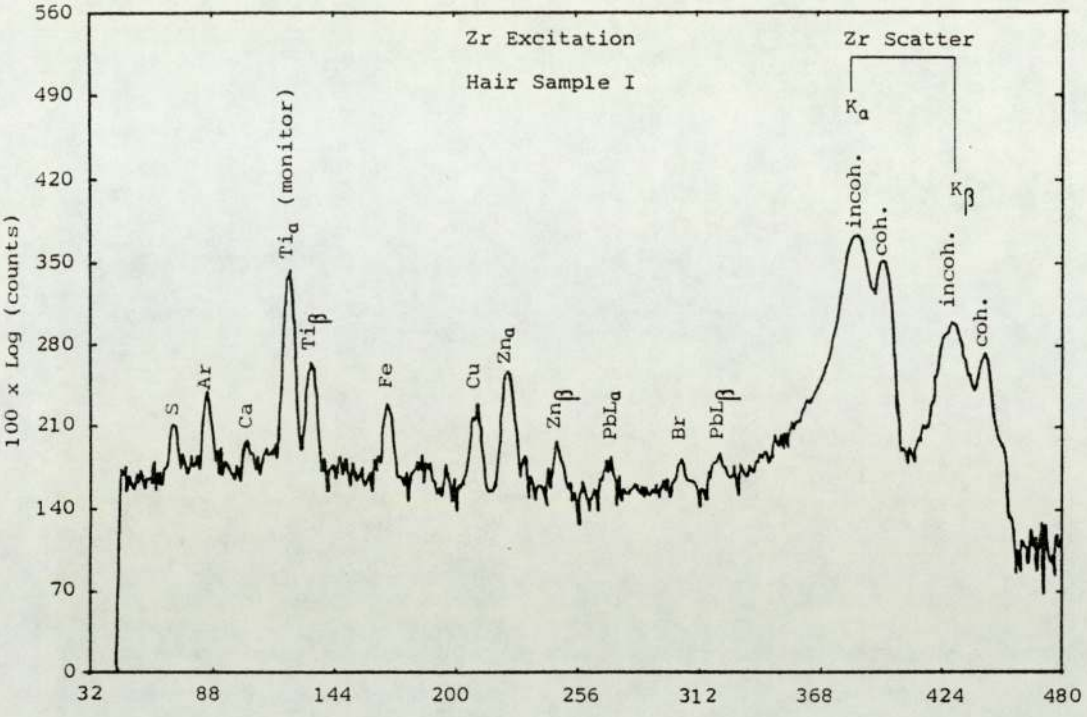

Figure (6.14)

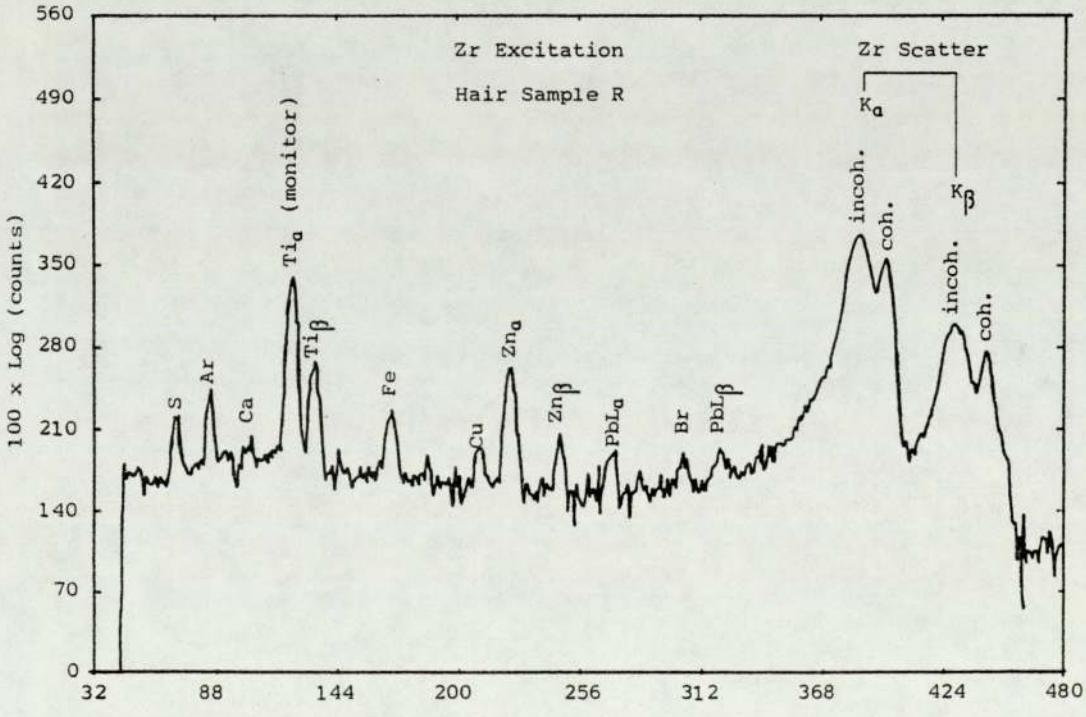

Figure (6.15)

CHAPTER SEVEN

CONCLUSIONS

It has been shown that characteristic X-rays induced by protons can be applied with advantage to radiography and fluorescence analysis. The utilization of the K X-rays of Ag to radiograph a test object of Cd and Mo foils placed side by side produced a high contrast which cannot be obtained with conventional radiography. Good agreement with the theoretical calculations was obtained. The radiography of the perspex phantom demonstrates the feasibility of the technique for thick soft tissue object radiography. The potential of applying these X-rays in radiography is that it could be used to complement conventional radiography especially when high contrast of a particular feature is needed. The technique is limited to a few centimeters thickness of perspex or equivalent material because of the decrease in flux of X-rays with high atomic number targets bombarded by protons.

X-ray fluorescence analysis is now widely accepted as a powerful tool for qualitative and quantitative analysis of different specimens. Its future advances depend, among other factors, upon the development of high intensity monoenergetic photon sources, Cooper (1973). The monoenergetic X-ray excitation, as developed in the present work, provides a new and useful tool for multi-

element analysis. The preferential excitation of trace elements by monoenergetic photons makes the technique appropriate for a wide range of samples. Although up to seven targets have been used to produce characteristic X-rays, a variety of other targets may be mounted instead in the target chamber for the excitation of particular samples. In order to solve a specific analytical problem, the availability of a single excitation energy may be adequate. However, a suitable choice of the incident X-ray energies allows one to minimize enhancement effects and reduce spectra complexity through selective ionization of the elements in most samples. The excitation of specimens by monoenergetic X-rays induced by protons has an obvious advantage, on the basis of excitation efficiency, when the primary X-ray energy is just above the absorption edge of the element to be analysed. As the absorption edge of the element concerned moves further away from the primary X-ray energy the efficiency falls. Detectabilities for a number of biologically important elements in bovine liver, blood and hair samples have been shown to be within practical limits for research purposes. In order to evaluate the overall accuracy of the present system, an NBS SRM-1577 bovine liver was analysed. Good agreements of the trace elements concentration with the certified values has been achieved. This implies that the technique as developed, is accurate and reliable. The introduction of a thin Ti wire as an X-ray beam monitor seems adequate to correct for the uncertainty due to proton beam energy and charge collecting system.

This technique may be used as a complementary tool to other analytical techniques such as PIXE and broad spectrum XRF analysis. It is non destructive in the sense that specimen composition does not change during analysis and hence specimens may be analysed several times.

In order not to reduce the sensitivity and detection limits obtainable, X-rays generated within the sample compartment must not be detected. The choice of material is hence important to eliminate stray X-ray lines. The sample holder and support were made of plastic and perspex and these materials have low fluorescence yields for low energy X-rays.

For future trends, the high purity monoenergetic X-rays induced by protons can be further increased by exploiting the anisotropic distribution of bremsstrahlung radiation. This can be achieved by observing the emitted X-rays at angles greater than 90^{o}, Ishii et al (1977) and Renan (1980). High purity primary targets are necessary for providing exciting spectra free from impurity peaks. The variation in primary X-ray intensity between the extreme edges of the sample, and the problem of sample non-uniformity can be removed by rotating the sample during analysis. Samples with Z=15 to 20 are efficiently analysed when they are made into thin pellets and placed in vacuum. The introduction of an automatic sample changer is essential if one is to analyse a large number of samples rapidly and economically. The application of an on-demand

beam pulsing system gives better sensitivity by minimising pile up effect for the analysed samples due to improved performance at high count rates. Detector improvements such as reducing incomplete charge collection, resolution and counting rate capabilities are useful.

The possible solution that this technique could provide to problems in industry and medicine is based primarily on its selective excitation character. The analysis of blood and hair samples demonstrates that the system is capable of analysing biomedical samples with acceptable accuracy. The method used for hair grinding, though time consuming, proved to yield a fine powder which could be easily pressed into a self supporting pellet. Irradiation times required in the present work were typically 10-18 minutes for analysing biomedical samples.

The limitation of any particular technique can be evaluated on the basis of the individual requirements of the user. System sensitivity cannot be expressed without referring to the sample form and method of presentation. Since about 53 mg of biomedical samples may be analysed with the present system in a single excitation, a preconcentration of the trace element in liquid and soft tissue samples by freeze drying or other technique is necessary if they are required to be analysed in a reasonable irradiation time. To obtain representative results, more than one sample is required to be analysed. Samples presented for analysis must be homogeneous and

uniform for efficient quantitative analysis. An added disadvantage is the availability of a well-equipped accelerator facility.

LIST OF REFERENCES

Ahlberg M., Akselsson R., Brune D. and Lorenzen J., "Proton-Induced X-Ray Analysis of Steel Surfaces for Microprobe Purposes" Nuclear Instruments and Methods 123 (1975) pp385-393

Ahlberg M. and Akselsson R., "Proton-Induced X-Ray Emission in the Trace Analysis of Human Tooth Enamel and Dentine" International Journal of Applied Radiation and Isotopes 27 (1976) pp279-290

Ahlberg M.S. and Adams F.C., "Experimental Comparison of Photon-and Particle-Induced X-Ray Emission Analysis of Air Particulate Matter" X-Ray Spectrometry, Vol.7, No.2 (1978) pp73-80

Alder K., Bohr A., Huss T., Mottleson B. and Winther A., "A Study of Nuclear Structure by Electromagnetic Excitation with Accelerated Ions" Reviews of Modern Physics 28 (1956) pp432-542

Andermann G. and Kemp J.W., "Scattered X-Rays as Internal Standards in X-Ray Emission Spectroscopy" Analytical Chemistry, Vol.30, No.8 (1958) pp1306-1309

Bador R., Vandrous J.C., Romand M. and Diaine C., "X-Ray Fluorescence Analysis in Medicine" European Spectroscopy News 27 (1979) pp41-43

Bambynek W., Crasemann B., Fink R.W., Freund H.H., Mark H., Swift C.D., Price R.E., Venugopala R., "X-Ray Fluorescence Yield, Auger and Coster-Kronig Probabilities" Review Modern Physics, 44 (1972) pp716-813

Bang J., Hansteen J.M. Kgl. Dansk. Videnskab. Selskab. Mat.-Fys. Medd 31 (1959) No.13

Barfoot K.M., PhD Thesis "Central Bureau for Nuclear Measurement" Geel (1980) pp76

Beaman S.A. and Lillicrap S.C., "Optimum X-ray Spectra for Mammography" Physics in Medicine and Biology, Vol.27, No.10 (1982) pp1209-1220

Bearse R.C., Close D.A., Malanify J.J. and Umbarger C.J., "Production of K_α and L_α X-rays by Protons of 1-3.7 MeV" Physical Review A7 (1973) pp 1269-1272

Bens J.R. and Delarue, "The Fundamentals of X-ray and Radium Physics", J.Selman, Thomas Publisher (1972) pp319

Bertin E.P., "Principles and Practice of X-Ray Spectrometric Analysis" Plenum Press, New York (1975)

Bertin E.P., "Introduction to X-ray Spectrometric Analysis" Plenum Press, New York (1978)

Betteridge W., "A Further Handbook of Industrial Radiology" ed. W.J.Wiltshire, Edward Arnold, London (1957) pp226

Birch R., Marshall M. and Ardran G.M., Catalogue of Spectral Data for Diagnostic X-Rays, Hospital Physicists' Association, Scientific Report Series-30, London (1979)

Birks L.S., "Fluorescent X-Ray Excitation Efficiencies" Spectrochim Acta 17 (1961) pp 148-154

Birks L.S., X-Ray Spectrochemical Analysis, Interscience Publishers, New York (1969) pp 21

Boster T.A. and Edwards J.E., "X-Ray K-Absorption Fine Structure of Niobium and Copper at Cryogenic Temperatures" Physical Review (USA) Vol.170, No.1 (1968) pp 12-16

Brandt W. and Lapicki G., "L-Shell Coulomb Ionization by Heavy Charged Particles" Physical Review A20 (1979) pp 465-480

Brown D.B., Gilfrich J.V. and Peckerar M.C., "Measurement and Calculation of Absolute Intensities of X-Ray Spectra" Journal of Applied Physics, 46, No.10 (1975) pp 4537-4540

Brown M.D., Simons D.G., Land D.J. and Brennan J.G., "K-shell ionization cross sections for Ti, Cr, Co, Ni, Cu and Zn targets induced by protons in the energy range 300-2400 keV" Physical Review A, Vol.25, No.6 (1982) pp 2935-2945

Burhop E.H.S. and Asaad W.N., "The Auger Effect" Advances in Atomic and Molecular Physics 8 (1972) pp 163-284

Burke W.E., Hinds L.S., Deodato G.E., Sager E.D,Jr. and Borup R.E., "Internal Standard X-Ray Spectrographic Procedure for the Determination of Calcium, Barium, Zinc and Lead in Hydrocarbons" Analytical Chemistry, Vol.36, No.13 (1964) pp 2404-2407

Cahill T.A., "Ion Excited X-ray Analysis of Environmental Sample" New Uses of Ion Accelerators ed. J.F.Ziegler (Plenum, New York, 1975) pp 1-71

Campbell J.L., "Specimen Preparation in PIXE Analysis" Nuclear Instrument and Methods 142 (1977) pp 263-273

Campbell J.L., Faiq S., Gibson R.S., Russell S.B. and Schulte C.W., "Determination of Trace Element Profiles and Concentrations in Human Hair by Proton-Induced X-ray Emission Spectrometry" Analytical Chemistry 53 (1981) pp 1249-1253

Carlson T.A., "Photoelectron and Auger Spectroscopy" Plenum Press, New York and London, (1975) Chapter 6

Chattarji D., "The Theory of Auger Transitions" Academic Press, London (1976) pp 27

Chen J.X., Guo Y.Z., Li H.K., Ren C.G., Tang G.H., Wand X.D. Yang F.C and Yao H.Y., "Trace Element Analysis of Human Hair by PIXE" Nuclear Instruments and Methods 181 (1981) pp 269-273

Christensen L.H., Rasmussen S.E., Pind N. and Henriksen K., "A Versatile Spectrometer For Secondary X-Ray Fluorescence Excitation" Analytica Chimica Acta 116 (1980) pp 7-17

Clark G.L. and Shafer W.M., "The Technique of Microradiography and Its Application to Metals" Transactions of American Society For Metals, 29 (1941) pp 732-754

Cookson J.A., Armitage B.H. and Ferguson A.T.G., "Proton Radiography" Non-Destructive Testing, August (1972) pp 225-228

Cooper J.A., "Comparison of Particle and Photon Excited X-Ray Fluorescence Applied to Trace Element Measurements of Environmental Samples" Nuclear Instruments and Methods 106 (1973) pp 525-538

Cooper J.A., "Interpretation of energy-dispersive X-ray spectra" American Laboratory, Vol.8, No.11 (1976) pp 35-48

Currie L.A., "Limits for Qualitative Detection and Quantitative Determination" Analytical Chemistry, Vol.40, No.3 (1968) pp 586-593

Currie L.A., "Detection and Quantitation in X-ray Fluorescence Spectrometry" X-ray Fluorescence Analysis of Environmental Samples, ed. T.G. Dzubay (1978), Pub. Ann Arbor Science, pp 289-306

Deconnink G., Demortier G. and Bodart F., "Application of X-ray Production by Charged Particles to Elemental Analysis" Atomic Energy Review 13, No.2 (1975) pp 367-412

Dick C.E. and Motz J.W., "Utilization of Monoenergetic X-Ray Beams to Examine the Properties of Radiographic Intensifying Screens" IEEE Transactions on Nuclear Science (USA), Vol.ns-28, No.2 (1981) pp 1554-1558

Drummond W.E. and Stewart W.D., "Automated energy-dispersive X-ray fluorescence analysis" American Laboratory, Vol.12, No.11 (1980) pp 71-80

Dyer G.R., Gedcke D.A. and Harris T.R. "Fluorescence Analysis Using An Si(Li) X-Ray Energy Analysis System with Low-Power X-Ray Tubes and Radioisotopes" Advances in X-Ray Analysis 15 (1972) pp 228-239

Dyson N.A., "X-rays in atomic and nuclear physics" Longman Group Limited, London (1973)

Dzubay T.G., ed., "X-ray fluorescence analysis of environmental samples", Ann Arbor Science, Ann Arbor (1977)

Ely D.L., Mostardi R.A., Woebkenberg N. and Worstell D., "Aerometric and Hair Trace Metal Content in Learning-Disabled Children" Environmental Research 25 (1981) pp 325-339

Fewell T.R. and Shuping M.S., "A Comparison of Mammographic X-Ray Spectra" Radiology 128 (1978) pp 211-216

Fink R.W., Jopson R.C., Mark H. and Swift C.D., "Atomic Fluorescence Yields" Reviews of Modern Physics 38 (1966) pp 513-540

Folkmann F., Graade C., Huss T. and Kemp K., "Proton Induced X-ray Emission as a Tool for Trace Element Analysis" Nuclear Instruments and Methods 116 (1974) pp 487-499

Folkmann F., "Analytical Use of Ion-Induced X-rays" Journal of Physics E: Scientific Instruments 8 (1975) pp 429-444

Garcia J.D., "Inner-Shell Ionization by Proton Impact" Physical Review A1 (1970a) pp 280-285

Garcia J.D., "X-Ray Production Cross-Section" Physical Review A1 (1970b) pp 1402-1403

Garcia J.D., Fortner R.J. and Kavanagh T.M., "Inner-Shell Vacancy Production in Ion-Atom Collision" Reviews of Modern Physics 45 (1973) 111-177

Gedcke D.A., Elad E. and Denee P.B., "An Intercomparison of Trace Element Excitation Methods for Energy-Dispersive Fluorescence Analyzers" X-Ray Spectrometry, Vol.6 No.1 (1977) pp 21-29

Giauque R.D. and Jaklevic J.M., "Rapid Quantitative Analysis by X-Ray Spectrometry" Advances in X-Ray Analysis 15 (1972) pp 164-175

Giauque R.D., Garrett R.B. and Goda L.Y., "Energy Dispersive X-ray Fluorescent Spectrometry for Determination of Twenty-Six Trace and Two major Elements in Geochemical Specimens" Analytical Chemistry, Vol.49, No.1 (1977) pp 62-67.

Giauque R.D., Garrett R.B. and Goda L.Y., "Determination of Trace Elements in Light Element Matrices by X-ray Fluorescence Spectrometry with Incoherent Scattered Radiation as an Internal Standard" Analytical Chemistry, Vol.51, No.4 (1979) pp 511-516

Gihwala D., Olivier C., Peisach M. and Pineda C.A., "The Determination of Chromium in Steels by PIXE-Induced XRF" Journal of Trace and Microprobe Techniques, Vol.1, No.2 (1982) pp 199-211

Gilfrich J.V. and Birks L.S., "Spectral Distribution of X-Ray Tubes for Quantitative X-Ray Fluorecence Analysis" Analytical Chemistry 40 (1968) pp 1077-1080

Goodfellow Metals Ltd., Cambridge Science Park, Milton Road, Cambridge CB4 4DJ, England

Gordon B.M. and Kraner H.W., "On the Development of a System for Trace Element Analysis in the Environment by Charged Particle X-ray Fluorescence" Journal of Radio-analytical Chemistry 12 (1972) pp 181-188

Gore J.C. and Hooker G.R., "A Method of Measuring the Radio-Opacity of Catheters" British Journal of Radiology 54 (1981) pp 289-295

Goulding F.S. and Jaklvic J.M., "Photon-Excited Energy-Dispersive X-Ray Fluorescence Analysis For Trace Elements" Annual Review of Nuclear Science 23 (1973) pp 45-74

Goulding F.S., "Some Aspects of Detectors and Electronics for X-ray Fluorescence Analysis" Nuclear Instruments and Methods 142 (1977) pp 213-223

Goulding F.S. and Jaklevic J.M., "XRF Analysis-Some Sensitivity Comparisons Between Charged Particle and Photon Excitation" Nuclear Instruments and Methods 142 (1977) pp 323-332

Gray A.L., "An Automatic X-Ray Analytical Instrument For The Chemical Laboratory" Advances in X-ray Analysis 15 (1972) pp 185-196

Grodstein G., (white),"National Bureau of Standard" 1957, NBS Circular, pp 583

Guffey J.A., Van Rinsvelt H.A., Adams W.R., Sarper R.M., Karcioglu Z. and Fink R.W., "Elemental Analysis of Biomedical Samples by PIXE" Advances in X-Ray Analysis 21 (1978) pp 261-266

Gunn E.L., "Determination of Lead in Gasoline by X-Ray Fluorescence Using an Internal Intensity Reference", Applied Spectroscopy, Vol. 19, No.3 (1965) pp 99-102

Hansen J.S., Freund H.U. and Fink R.W., "Relative X-Ray Transition Probabilities to the K-shell" Nuclear Physics A142 (1970) pp 604-608

Hansen J.S., McGeorge J.C., Nix D., Schmidt-Ott W.D., Unus I. and Fink R.W., "Accurate Efficiency Calibration and Properties of Semiconductor Detectors for Low-Energy Photons" Nuclear Instrument and Methods 106 (1973) pp 365-379

Hansteen J.M. and Mosebekk O.P., "Atomic Coulomb Excitation by Heavy Charged Particles" Nuclear Physics, A201 (1973) pp 541-560

Hansteen J.M., Advances in Atomic and Molecular Physics, eds. D.R.Bates and B.Bederson (Academic, New York, 1975) Vol.11 pp 299

Hettinger G. and Starfelt N., "Bremsstrahlung Spectra From Roentgen Tubes" Acta Radiological 50 (1958) pp 381-394

Hoffman E.J. and Phelps M.E., "Production of Monoenergetic X-rays from 8 to 87 keV" Physics in Medicine and Biology, Vol.19 No.1 (1974) pp 19-35

Hopkins J.I., "Low Energy X-Ray Attenuation Measurements for Elements of Low Atomic Number" Journal of Applied Physics (USA) Vol.30, No.2 (1959) pp 185-187

Hubbell J.H., "Photon Cross-Section, Attenuation Coefficients, and Energy Absorption Coefficients From 10 keV-100GeV" NBS-29, Washington (1969)

Irons R.D., Schenk E.A. and Giauque R.D., "Energy-Dispersive X-Ray Fluorescence Spectroscopy and Inductively Coupled Plasma Emission Spectrometry Evaluated for Multielement Analysis in Complex Biological Matrices" Clinical Chemistry, Vol.22, No.12 (1976) pp 2018-2024

Ishii K., Kamuya M., Sera K., Morita S. and Tawara H., "Directional Anisotropy of Secondary-Electron Bremsstrahlung Induced by Proton Bombardment of Thin Solid Target" Physical Review A15 (1977) pp 2126-2129

Iyengar G.V., "Homogenised sampling of bone and other biological materials" Radiochemical and Radioanalutical Letters, Vol.24, No.1 (1976) pp 35-42

Iyengar G.V. and Kasparek K., "Application of the brittle fracture technique (BFT) to homogenise biological samples and some observations regarding the distribution behaviour of the trace elements at different concentration levels in a biological matrix" Journal of Radioanalytical Chemistry, Vol.39 (1977) pp 301-316

Iyengar G.V., Kollmer W.E. and Bowen H.J.M., "The Elemental Composition of Human Tissues and Body Fluids. A Compilation of Values for Adults" Editor: Dr. Hans F. Ebel, Verlag Chemie. Weinheim, New York (1978)

Jaklevic J.M. and Goulding F.C., "Detection of Low Energy X-ray with Si(Li) Detectors", IEEE Transactions on Nuclear Science, NS-18, No.1 (1971) pp 187-189

Jaklevic J.M., Giauque R.D., Malone D.F. and Searles W.L., "Small X-Ray Tubes for Energy Dispersive Analysis Using Semi-Conductor Spectrometer" Advances in X-Ray Analysis 15 (1972) pp 266-275

Jaklevic J.M. and Thompson A.C., "X-Ray Methods For The Chemical Characterization of Atmospheric Aerosols" Nuclear Instruments and Methods 193 (1982) pp 309-314

Jenkins D.,"Radiographic Photography and Imaging Process" MTP Press Limited, Lancaster, England (1980) pp 132

Jenkins R., Gould R.W. and Gedcke D., "Quantitative X-Ray Spectrometry" Marcel Dekker Inc. (1981) pp 32

Johansson S.A.E. and Johansson T.B., "Analytical Application of Particle Induced X-ray Emission" Nuclear Instrument and Methods 137 (1976) pp 473-516

Johnson G.A. and O'Foghludha F., "An Experimental 'Transmolydenum' Tube for Mammography" Radiology, Vol.127 (1978) pp 511-516

Johnson G.A., Manson E.L. and O'Foghludha F., "Simple Method of Obtaining Si(Li) Detector Efficiency" Nuclear Instruments and Methods 151 (1978) pp 217-220

Johnson G.A. and O'Foghludha F., "Investigation of transmolybdenum fluorescent anodes for mammography" Proceeding of the Society of Photo-Optical Instrumentation Engineers 233 (1980) pp 158-163

Katsanos A. and Hadjiantoniou A., "Sensitivity of the External Beam PIXE Elemental Analysis Method" Nuclear Instruments and Methods 149 (1978) pp 469-473

Keith H.D. and Loomis T.C, "measurement of K-shell Fluorescence Yield and K_α/K_β Intensity Ratio for Nickel" X-Ray Spectrometry, Vol.7, No.4 (1978) pp 217-224

Khaliquzzaman M., Zaman M.B. and Khan A.H., "Trace Element Analysis in Biological Materials by External Beam PIXE" Nuclear Instruments and Methods 181 (1981) pp 209-215

Khan M.R., Crumpton D. and Francois P.E., "Proton-induced X-ray production in titanium, nickel, copper, molybdenum and silver" Journal of Physics B, Vol.9, No.3 (1976) pp 455-460

Khan M.R., Hopkins A.G. and Crumpton D., "Proceeding of the 8th International Conference on X-ray Optics and Microanalysis, Boston (1977) pp 287-290

Khan Md.R. and Crumpton D., "Proton Induced X-ray Emission Analysis" Critical Review in Analytical Chemistry Vol.2, Issue 2 (1981) pp 103-155; Vol.2, Issue 3 (1981) pp 161-193

Khan O.R., MPhil Thesis, University of Aston in Birmingham (1979)

Khan R., PhD Thesis, University of Aston in Birmingham (1975)

Khandelwale G.S., Choi B.H. and Merzbacher E., "Atomic Data" (1969) pp 103; Choi B.H., Merzbacher E. and Khandelwale G.S., "Atomic Data" 5 (1973) pp 291

Kieser R. and Mulligan T.J., "X-Ray Fluorescence Spectroscopy as a Tool for Fish Stock Discrimination" Advances in X-Ray Analysis 19 (1976) pp 487-495

Krause M.O., Atomic Radiative and Radiationless Yields for K and L Shell" Journal of Physical and Chemical Reference Data 8 (1979) pp 307-322

La Fleur P.D., "Biological Matrix Standard Reference Materials for Trace Element Determinations" Journal of Radioanalytical Chemistry 19 (1974) pp 277-232

Lander J.J., "Auger Peaks in the Energy Spectra of Secondary Electrons from Various Materials" Physical Review, Vol.91, No.6 (1953) pp 1382-1387

Lewis C.W., Watson R.L. and Natowitz J.B., "Projectile Z Dependence of K X-Ray Emission Induced by Alpha Particles and Deutrons" Physical Review A5 (1972) pp 1773-1784

Lin T.L., Luo C.S. and Chou J.C., "The (pX,X) Experiment-A New Approach For Partial Sensitivity Enhancement in Trace Element Analysis" Nuclear Instruments and Methods 151 (1978) pp 439-444

Madison D.H. and Merzbacher E., Atomic Inner-Shell Processes, ed. B.Crasemann (Academic, New York, 1975) Vol.1, pp 1

Mahrok M.F., Crumpton D. and Francois P.E., "The Application of Proton Induced X-Ray Emission to Radiography" Nuclear Instruments and Methods 181 (1981) pp 105-107

Marshall M., Peaple L.H.J., Ardran G.M. and Crooks H.E., "A comparison of X-ray spectra and outputs from molybdenum and tungsten targets" British Journal of Radiology, 48 (1975) pp 31-39

McCall J.T., Goldstein N.P. and Smith L.H., "Implication of trace metals in human diseases" Federation Proceedings, Vol.30, No.3 (1971) pp 1011-1015

Meredith W.J. and Massey J.B., "Fundamental Physics of Radiology" John Wright, Bristol (1977) pp 235

Merzbacher E. and Lewis H.W., Handbuch der Physik, ed. S.Flugge; Springer Verlage, Berlin 34 (1958) pp 166

Micromatter Co. Seattle, WA, U.S.A.

Millar R.H. and Greening J.R., "Experimental X-ray mass attenuation coefficients for materials of low atomic number in the energy range 4 to 25 keV" Journal of Physics B: Atomic and Molecular Physics, Vol.7, No.17 (1974) pp 2332-2344

Montenegro E.C., Baptista G.B. and Duarte P.W.E.P.", K and L X-Ray Mass Attenuation Coefficients For Low-Z Materials" Atomic Data and Nuclear Data Tables 22 (1978) pp 131-177

Moriya Y., Ato Y and Miyagawa S., "Sensitivity in Light Element Analysis by 2 MeV and 150 keV Proton and Photon Induced X-rays" Nuclear Instruments and Methods 150 (1978) pp 523-528

Morrison G.H., Trace Analysis, Interscience, New York, (1965)

Motz J.W., Dick C.E., Lucas A.C., Placious R.C. and Sparrow J.H., "Production of High-Intensity K X-Ray Beams" Journal of Applied Physics 42 (1971) pp 2131-2133

Musket R.G, "Detection of Proton-Induced Boron X-ray with a Si(Li) Detector", Nuclear Instruments and Methods 117 (1974) pp 385-389

Owers M.J. and Shalgosky H.I., "Use of X-ray Fluorescence for Chemical Analysis" Journal of Physics E7 (1974) pp 593-603

Perry S.K. and Brady F.P., "A Comparative Study of Alpha and X-ray Induced X-ray Emission for Elemental Analysis" Nuclear Instruments and Methods 108 (1973) pp 389-402

Phull J., Private Communication (1982)

Porter D.E., "High Intensity Excitation Sources for X-ray Energy Spectrometry" X-Ray Spectrometry 2 (1973) pp 85-89

Prasad A.S., Trace Elements Analysis, Academic Press, New York, Vol.1 and Vol.2 (1976)

Raith B., Roth M., Gollner K., Gonsior B., Ostermann H, and Uhlhorn C.D., "Trace Element Analysis by Ion Induced X-ray Emission Spectroscopy" Nuclear Instruments and Methods 142 (1977) pp 39-44

Renan M.J., "Optimisation of Trace Analysis by PIXE: Angular Dependence of the Background Continuum" X-ray Spectrometry 9 No.2 (1980) pp 90-94

Rhodes J.R., "Radiosotope X-Ray Spectrometry" The Analyst 91 (1966) pp 683-699

Saied S.O., PhD Thesis, University of Aston in Birmingham (1981)

Scofield J.H., "Exchange correction of K X-ray emission rates" Physical Review, A9, No.3 (1974) pp 1041-1049

Sioshansi P. and Lodhi A.S., "Escape Peak Losses in Si(Li) Detectors" X-Ray Spectrometry, Vol.8, No.2 (1979) pp 65-67

Smith R.L., "The Effect of Scattering on Contrast in Microfocus Projection X-Radiography" British Journal of Non-Destructive Testing, September (1980) pp 236-239

Sood B.S., Allawadhi K.L., Gandhi R., Batra O.P. and Singh N., "Sample Analysis Using Gamma Ray Induced Fluorescent X-Ray Emission" X-Ray Spectrometry, Vol.12, No.1 (1983) pp 19-22

Spiller E., "Recent Developments Towards High Resolution X-Ray Imaging" Nuclear Instruments and Methods 177 (1980) pp 187-192

Standzenieks P., Rindby A. and Selin E., "Development of a Low Power Monoenergetic X-Ray Tube For Trace Element Analysis" Nuclear Instruments and Methods 153 (1978) pp 269-276

Stewart P.A.E., "Advances in Radiology and Fluoroscopy" British Journal of Non-Destructive Testing, January (1982) pp 27-32

Storm E. and Israel H.I., "Photon Cross-Sections from 1 keV to 100 MeV for Elements Z=1 to Z=100" Nuclear Data Tables A7 (1970) pp 565-681

Tawara H., Ishii K. and Marita S., "Bremsstrahlung Induced by Proton and Helium-3 Ion Impact" Nuclear Instruments and Methods 132 (1976) pp 503-505

Toribara T.Y., Jackson D.A., French W.R., Thompson A.C. and Jaklevic J.M., "Nondestructive X-ray Fluorescence Spectrometry for Determination of Trace Elements Along a Single Strand of Hair" Analytical Chemistry, Vol.54, No.11 (1982) pp 1844-1849

Underwood E.J., Trace Elements in Human and Animal Nutrition, Academic Press, New York (1971)

Valkovic V., "Trace Element Analysis", (Taylor and Francis Ltd., London, 1975)

Valkovic V., "Proton-Induced X-ray Emission: Applications in Medicine" Nuclear Instruments and Methods 142 (1977) pp 151-158

Van Espen P.J. and Adams F.C., "External Reference Signal in X-ray Energy Spectrometry" Analytical Chemistry, Vol.48, No.12 (1976) pp 1823-1826

Vane R.A. and Stewart W.D., "The Effective Use of Filters with Direct Excitation of EDXRF" Advances in X-Ray Analysis 23 (1980) pp 231-239

Veigele WM.J., "Photon cross section from 0.1 keV to 1 MeV for elements Z=1 to Z=94" Atomic Data 5 (1973) pp 51-111

Vir S.C., Love A.H.G. and Thompson W., "Zinc concentration in hair and serum of pregnant women in Belfast" The American Journal of Clinical Nutrition 34 (1981) pp 2800-2807

Walter R.L., Willie R.D., Gutknecht W.F. and Joyce J.M., "Analysis of Biological, Clinical and Environmental Samples Using Proton-Induced X-Ray Emission" Analytical Chemistry 46 (1974) pp 843-855

Woldseth R., "X-ray Energy Spectrometry", Published by Kevex Corporation, Burlington, California (1973)

Young F.C., Roush M.L. and Bergman P.G., "Trace Element Analysis by Proton-Induced X-Ray Excitation" International Journal of Applied Radiation and Isotopes 24 (1973) pp 153-163

Zulliger H.R. and Aitken D.W., "Fano Factor Fact and Fallacy" IEEE Transactions on Nuclear Science, NS-17 No.3 (1970) pp 187-193